Titre: Title:	Mechanical and Functional Insights of the Biofilm Polymeric Matrix and its Role in the Antibacterial Resistance
Auteur: Author:	Clémence Abriat
Date:	2021
Type:	Mémoire ou thèse / Dissertation or Thesis
Référence: Citation:	Abriat, C. (2021). Mechanical and Functional Insights of the Biofilm Polymeric Matrix and its Role in the Antibacterial Resistance [Thèse de doctorat, Polytechnique Montréal]. PolyPublie. https://publications.polymtl.ca/6626/

POLYTECHNIQUE MONTRÉAL

affiliée à l'Université de Montréal

Mechanical and Functional Insights of the Biofilm Polymeric Matrix and its Role in the Antibacterial Resistance

CLÉMENCE ABRIAT

Département de génie chimique

Thèse présentée en vue de l'obtention du diplôme de *Philosophiæ Doctor*

Génie chimique

Juin 2021

POLYTECHNIQUE MONTRÉAL

affiliée à l'Université de Montréal

Cette thèse intitulée :

Mechanical and Functional Insights of the Biofilm Polymeric Matrix and its Role in the Antibacterial Resistance

présentée par **Clémence ABRIAT**

en vue de l'obtention du diplôme de *Philosophiæ Doctor*

a été dûment acceptée par le jury d'examen constitué de :

Pierre CARREAU, président
Marie-Claude HEUZEY, membre et directrice de recherche
Nick VIRGILIO, membre et codirecteur de recherche
France DAIGLE, membre et codirectrice de recherche
Marylise DUPERTHUY, membre
Peter FISCHER, membre externe

DEDICATION

To my parents,

ACKNOWLEDGEMENTS

I would like to thank the many people who shaped my PhD experience.

First and foremost I would like to express my gratitude to my supervisor Professor Marie-Claude Heuzey and my co-supervisors Professor Nick Virgilio and Professor France Daigle for their support, encouragement and guidance during my PhD thesis. They shared their multidisciplinary expertise and were always available to help and guide me through this project. I could not have had better mentors to help me to grow into an independent researcher.

I would like to thank the thesis committee for accepting to evaluate my thesis: Professor Pierre Carreau, Professor Marylise Duperthy and Professor Peter Fischer.

During this project, I was very fortunate to travel abroad as a visiting researcher at Stanford University, in two wonderful labs. I would like to thank Professor Gerald G. Fuller and Professor Lynette Cegelski for welcoming me and sharing their expertise with me. Thank you Gerry for first introducing me to research during my master and for your mentorship and guidance over the years. I would also like to thank Mary Fuller for her hospitality and welcoming me into the Fuller's house. I would like to express my gratitude to the people from the Fuller's and Cegelski's labs for their help and support during my time at Stanford, and contributing to this enriching and fun experience. I would also like to thank Dr. Emily Hollenbeck who first trained me on the interfacial rheology setup and application to biofilms during my master project. I am grateful to Kyle Enriquez for his help with the Western blot analysis.

I gratefully acknowledge the foundation Friends of Polytechnique Montréal and Mitacs for providing me the financial support for my internship at Stanford University.

I would like to thank Professor Jan Vermant for welcoming me in his lab at ETH Zurich and Dr. Bram Schroyen for training me on their innovative interfacial rheological exchange cell.

I would like to thank the technical and administrative staff from the Chemical Engineering department at Polytechnique Montréal for being a great help during my project, especially Matthieu Gauthier, Gino Robin and Martine Lamarche.

Many thanks to my colleagues in the rheology, interfaces and microbiology groups for sharing their knowledge and giving me feedback thorough this project. I was fortunate to be part of

interdisciplinary research teams which opened me to multiple scientific fields and encouraged me to learn new techniques. I am grateful to my colleagues Karine, Maud, Claudie, Julie, Camille, Tahiana, Arthur and Caroline for all the help and fruitful discussions over the years.

I would like to thank Olivier Gazil for his help during this project, especially with the nanoparticles synthesis. I really enjoyed our collaboration and learning new recipes. A special thanks also to my colleagues and friends Teodora and Helia for their guidance and help during this journey and the long discussions about the research and personal life.

Finally I would like to thank my family. To my parents for always encouraging my curiosity and for their constant love, encouragement and support in my life. And to Yann, thank you for your love and support during this journey.

RÉSUMÉ

Les bactéries sont des microorganismes sociaux qui vivent généralement au sein de communautés complexes appelées biofilms, entourées de substances polymériques qu'elles ont elles-mêmes produites. Le développement de biofilms bactériens sur différentes surfaces pose de nombreux problèmes dans les domaines industriel et sanitaire. La matrice polymérique protège les bactéries des stress extérieurs, les rendant extrêmement résistantes dans la nature ainsi que dans les infections, et difficiles à traiter avec les antibiotiques traditionnels. Dans les habitats naturels, plusieurs espèces bactériennes coexistent souvent dans des biofilms. Elles interagissent de manière synergique ou antagoniste et leurs interactions entre espèces peuvent influencer le développement et les propriétés des biofilms. Les connaissances actuelles sur les interactions entre les différentes espèces sont encore limitées malgré des progrès récents qui ont permis l'analyse de communautés microbiologiques complexes. L'objectif de ce travail est de comprendre le comportement viscoélastique et la composition des biofilms bi-espèces, et d'étudier le rôle de la matrice polymérique dans la résistance antibactérienne.

Dans un premier temps, le comportement viscoélastique et microbiologique d'un modèle de biofilm composé de deux bactéries environnementales, *Bacillus licheniformis* et *Pseudomonas fluorescens* a été étudié. L'évolution des propriétés viscoélastiques au cours du temps, et l'analyse microbiologique et microscopique de la pellicule, ont démontré que *P. fluorescens* contribuait principalement aux propriétés du biofilm bi-espèces. La croissance planctonique a également révélé que *P. fluorescens* se développait plus rapidement que *B. licheniformis*, sans mécanisme de compétition antimicrobien entre les deux espèces. Ces résultats ont lié l'influence de la cinétique de croissance à la composition et aux propriétés viscoélastiques du biofilm en fonction du temps de croissance du biofilm. En combinant des techniques quantitatives à l'échelle macroscopique - rhéologie interfaciale, biomasse et énumération bactérienne - avec une analyse microscopique, les changements viscoélastiques uniques observés dans ce biofilm bi-espèces ont été reliés à la croissance bactérienne.

Dans un second temps, un biofilm bi-espèce composé par le pathogène *Vibrio cholerae* et *Escherichia coli*, a été choisi pour établir une relation entre les propriétés viscoélastiques et la composition de la matrice extracellulaire. L'analyse quantitative en temps réel des propriétés

rhéologiques du biofilm pendant la croissance a été combinée à l'étude des principaux composants de la matrice et de la microstructure de la pellicule. Les résultats ont mis en évidence la compétition pour l'interface entre les deux espèces, due au taux de croissance de la formation du biofilm. La relation entre les propriétés viscoélastiques et la composition moléculaire du biofilm a suggéré que *V. cholerae* inhibait la production de fibres amyloïdes de *E. coli*, même lorsqu'il était initialement présent en petites quantités.

Enfin, une stratégie antibactérienne a été développée contre les biofilms matures à l'interface de *V. cholerae*. Des nanoparticules d'argent (AgNPs) ont été préparées par synthèse hydrothermale, en utilisant deux polysaccharides naturels de charges opposées: le chitosane et l'alginate. La matrice polymérique du biofilm a fourni une résistance accrue aux AgNPs, les biofilms matures étant quatre fois plus résistants que les souches ne formant pas de biofilms. De plus, les AgNPs ont interagi avec les composants de la matrice pour perturber, voire détruire, la microstructure. Deux protéines structurales, RbmA et Bap1, ont joué un rôle crucial dans la résistance aux AgNPs, mettant en évidence le rôle de la composition de la matrice sur la résistance aux AgNPs.

En combinant des outils innovants pour comprendre la formation de biofilms à l'interface air-liquide au fil du temps, cette recherche fournit des connaissances fondamentales sur les interactions entre-espèces et le rôle de la matrice extracellulaire, ce qui est d'une grande importance dans la conception de nouvelles stratégies antimicrobiennes pour détruire et supprimer les biofilms.

ABSTRACT

Bacteria are social microorganisms that tend to coexist in complex communities called biofilms, in which they are surrounded by self-produced extracellular polymeric substances. The development of bacterial biofilms on various surfaces raises important issues in the industrial and health domains. The polymeric matrix protects bacteria from external stresses making them extremely persistent in nature as well as in infections, and complicating the treatments with traditional antibiotics. In natural habitats, multiple bacterial species often coexist together in biofilms. They interact in synergetic or antagonistic ways and their interspecies interactions can influence the biofilms' development and properties. The current knowledge on interspecies interactions is still limited despite recent advances that have enabled analysis of complex microbiological communities.

The objective of this work is to understand the viscoelastic behavior and the composition of dual-species biofilms, and to investigate the role of the polymeric matrix in the antibacterial resistance.

In a first phase, the mechanical and microbiological behavior of a model biofilm composed of two environmental bacteria *Bacillus licheniformis* and *Pseudomonas fluorescens* was investigated. The time-resolved viscoelastic properties, microbiological and microscopic analysis of the pellicle demonstrated that *P. fluorescens* mainly contributed to the dual-species biofilm properties. Planktonic growth revealed that *P. fluorescens* grew faster than *B. licheniformis*, with no antimicrobial competitive mechanisms between the two species. Those results linked the influence of growth kinetics to the time-dependent composition and properties of dual-species biofilm. By combining macroscale quantitative techniques – interfacial rheology, biomass and bacterial counts – with microscopic analysis, the unique viscoelastic changes observed in dual-species biofilms were related to bacterial growth.

In a second phase, a dual-species biofilm composed by the pathogen *Vibrio cholerae* and *Escherichia coli* was chosen to establish a relationship between the viscoelastic properties and the extracellular matrix composition. Real-time quantitative analysis of the biofilm rheological properties during growth was combined with the investigation of major matrix components and the pellicle microstructure. The results highlighted the competition for the interface between the two species, driven by the biofilm formation growth rate. Relating the viscoelastic properties to the

molecular composition of the dual-species biofilm suggested that *V. cholerae* inhibited the production of *E. coli* amyloid fibers, even when initially present in small amounts.

Finally, an antibacterial strategy was developed against *V. cholerae* mature pellicle biofilms. Silver nanoparticles (AgNPs) were prepared via hydrothermal synthesis, using two natural polysaccharides with opposite charges: chitosan and alginate. The polymeric matrix provided an increase resistance to AgNPs, with mature pellicles being four times more resistant than non-biofilms formers. In addition, the AgNPs interacted with the matrix components to disrupt the microstructure. Two structural proteins RbmA and Bap1 played a crucial role in the resistance to AgNPs, highlighting the role of matrix composition in the resistance to AgNPs.

By combining innovative setups to understand biofilms formation at the air-liquid interface over time, this research provides fundamental knowledge about interspecies interactions and the role of the extracellular matrix, which is of great importance in the design of new antimicrobial strategies to destroy and remove biofilms.

TABLE OF CONTENTS

LIST OF TABLES

LIST OF FIGURES

LIST OF SYMBOLS AND ABBREVIATIONS

This list presents the symbols and abbreviations used in the thesis.

AgNP	Silver nanoparticle
BAM	Brewster angle microscope
Bo	Boussinesq number
CFU	Colony forming unit
CR	Congo red
CS	Chitosan
CV	Crystal violet
δ	Phase angle
DWR	Double-wall ring
ECM	Extracellular matrix
eDNA	Extracellular DNA
EPS	Extracellular polymeric substances
FWHM	Full width at half maximum
γ	Shear strain
G'	Elastic modulus
G''	Viscous modulus
ISR	Interfacial stress rheometer
LB	Luria-Bertani
LBNS	Luria-Bertani no salt
OD	Optical density
ω	Angular frequency

PBS	Phosphate-buffered saline
pEtN	Phosphoethanolamine
QS	Quorum sensing
ROS	Reactive oxygen species
SAED	Selected area electron diffraction
SDS-PAGE	Sodium dodecyl sulfate-polyacrylamide gel electrophoresis
SEM	Scanning electron microscopy
±SEM	±Standard error of the mean
σ	Stress
SP-ICPMS	Single-particle induced coupled plasma mass spectrometer
SPR	Surface plasmon resonance
TEM	Transmission electron microscopy
UV	Ultraviolet
YESCA	Yeast extract casamino acids

CHAPTER 1 INTRODUCTION

Biofilm is the dominant microbial form, comprising around 80% of the prokaryotic cells in nature apart for the oceans [1]. Bacteria predominantly exist within those microbial communities, embedded in a self-produced extracellular polymeric matrix. Biofilms were first observed on human tooth surfaces as early as 1684 by Antoni van Leeuwenhoek – the first to observe bacteria under the microscope, which he described as "animalcules"[2]. It is not until 1978 that J. W. Costerston and his colleagues formally described microorganisms assemblies colonizing their environment by adhering to surfaces [3]. The work and ideas of Costerston have brought into wide acceptance that bacteria predominantly exist and organize into biofilms.

In nature, hundreds of bacteria coexist in the same habitat, leading to interspecies interactions and the formation of multispecies biofilm structures [4]. Species cohabiting together can interact in synergetic or antagonistic ways, and those interspecies interactions influence the mechanical and physicochemical properties of biofilms [5]. Over the past years, a major work on biofilms has been achieved, providing information on how to fight them. However, most of the research has focused on single-specie biofilms, whereas mixed species biofilms is to be the dominant form [5]. Interspecies interactions within those multispecies biofilms might result in enhanced capabilities and resistance. The current knowledge of the interactions' effects on the extracellular matrix properties is limited despite its significant importance on the research of new strategies to fight biofilm formation.

Due to their ability to colonize multiple surfaces, biofilms are responsible for phenomena such as biofouling, water contamination and microbially influenced corrosion. In the health care system, the increased use of medical devices has provided a number of niches for the formation of bacterial biofilms, which accounts for up to 80% of bacterial infections according to governmental agencies [6]. Biofilm-related infections are among the most difficult diseases to treat because of their high resistance to antimicrobial agents compared to planktonic cells (i.e. free floating bacteria) [7]. The extracellular matrix, composed of extracellular polymeric substances (EPS), confers an undeniable advantage to bacteria against a wide range of external stresses. These EPS have been referred to as the "dark matter of biofilms" because of their complexity and relatively poorly understood physicochemical properties. The EPS account for 90% of most biofilm dry mass and they define the mechanical robustness of biofilms. This polymeric matrix consists of biopolymers such as

polysaccharides, proteins and nucleic acids, and works as a structural scaffold and protective barrier [8]. The complexity of a biofilm structure, mainly due to its heterogeneity and composition, makes it challenging to study, and to understand the mechanisms behind its resistance.

While the discovery of new antibiotics is slowing down, the number of deaths by antimicrobial resistant infection is increasing [9]. Biofilms account for 65 to 80% of microbial infections and are strongly implicated in the 1.7 million hospital-acquired annual infections in the United States, according to the Centers for Disease Control and Prevention (CDC) [10]. Over the past years, multiple approaches to fight biofilms have been investigated by elucidating the genetic pathways, physiological response and communication signals. However, the lack of information on the ECM composition, and its interactions with the environment, still limit the discovery of treatments against biofilm developments. In addition to the matrix complexity, most of biofilm studies are performed on single model species at specific time points and do not follow quantitatively the biofilm development over time. The nature of those inter-species interactions could influence the mechanical and physicochemical properties of biofilms as well as ECM components. Deeper knowledge of multispecies biofilms is required to find appropriate treatment against those structures.

This research aims to broaden the knowledge on biofilms, in order to ultimately develop solutions against them, by characterizing the interactions in a multispecies biofilm during its maturation, and understanding the role of the polymeric matrix composition in the antimicrobial resistance. The **main objective** of this work is to understand the viscoelastic behavior and composition of dual-species biofilms, and to investigate the role of the polymeric matrix in the antimicrobial resistance.

In this thesis, the viscoelastic properties of a dual-species model biofilm are quantified in real-time using for the first time interfacial rheology. Based on the rheological analysis and the unique viscoelastic profile for each single species, the interactions occurring between the bacterial species at the interface are unraveled. The molecular composition of the ECM is related to a pathogenic dual-species model biofilm viscoelastic profile, to apprehend the importance of the interspecies interactions on the final dual-species ECM composition. Finally, a model antibacterial strategy using silver nanoparticles is applied to evaluate the contributions of the individual ECM structural components on the antimicrobial resistance.

Organisation of the thesis

This thesis comprises three articles published or submitted to scientific journals, and consists of the following chapters:

- Chapter 2: Literature review and state-of-the-art
- Chapter 3: Objectives and coherence of the articles
- Chapter 4 to 6: Three articles reporting the main contributions and results from this work
- Chapter 7: General discussion
- Chapter 8: Conclusion and recommendations

CHAPTER 2 LITERATURE REVIEW

2.1 Bacterial Biofilms

2.1.1 Generalities

Biofilm is the dominant microbial form in nature, in which microorganisms are embedded in a self-produced matrix [1]. The process of biofilm formation is complex and can be modeled by specific steps (Figure 2-1). The biofilm lifecycle starts with the reversible initial adhesion of planktonic cells to a surface, driven by Brownian motion, gravitational and hydrodynamic forces [11]. Bacteria with a flagella have a competitive advantage for this first adhesion step, allowing them to overcome repulsive forces and attach more easily on the surface [12]. After this first reversible attachment, bacteria can irreversibly adhere to the surface using attachment organelles. Pili or fimbriae are filamentous adhesins composed of proteins used by many Gram-negative bacteria for irreversible attachment [13] - for example, type I pili for *Escherichia coli* or type IV pili for *Pseudomonas aeruginosa* [14, 15]. The adhered bacteria move along the surface, multiply and form clusters in two dimensions, also called microcolonies [16]. Those microcolonies grow and form the mushroom-shaped mature biofilm.

Extracellular polymeric substances (EPS) bind the cells together and are essential to maintain cohesion in the biofilm three-dimensional structure, as it was demonstrated in the *Vibrio cholerae* biofilm [17]. Biofilms are heterogeneous three-dimensional structures and each bacterial cell has to adapt to its microenvironment [18]. In the adhesion area, the bacterial cells are attached to the solid surface by external appendages such as pili or flagellum; in the biofilm, the bacterial cells form multilayers that gradually lead to the core of the biofilm; and finally in the detachment area bacteria are exposed to mechanical forces and nutrient changes which trigger the secretion of enzymes to degrade the ECM and the bacterial cells are dispersed to colonize other surfaces [19, 20]. The water channels inside the biofilm allow for the flow of nutrients, oxygen and microorganisms from one site to another through fluid circulation, and they also maintain the necessary hydrated conditions which provide a natural environment for the survival of the enclosed microbial community.

When stress-inducing conditions occur (i.e. nutrient limitations, oxygen fluctuations, etc.), the microorganisms detach from the biofilm structure. The dispersed bacteria can initiate the formation of a new biofilm on a suitable surface environment [21]. Many bacteria use cell-to-cell communication - called quorum-sensing (QS), which are mechanisms to coordinate this dispersal state [22].

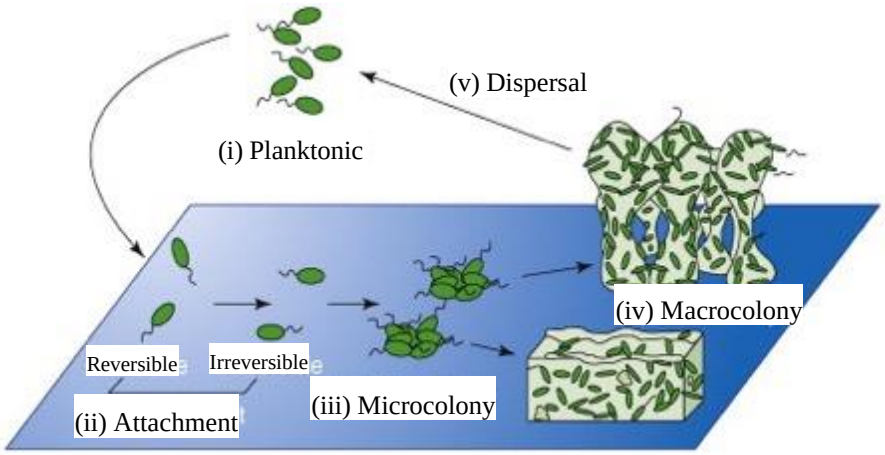

Figure 2-1 Biofilm life-cycle: (i) free-floating planktonic cells to the (ii) Attachment of planktonic cells to the surface. This step is characterized by a first reversible adhesion followed by the irreversible attachment of the cells to the surface. (iii) Formation of cell clusters also called microcolony. (iv) Development of a vertical structure and production of EPS to form the macrocolony corresponding to the mature biofilm. (v) Biofilm dispersal, bacteria can be released from the biofilm structure to colonize other surfaces [23]. Copyright (2009) Elsevier

Biofilms are heterogeneous structures due to local microenvironments and bacterial cells are in a wide range of physical states. Bacteria alter their gene expression and physiological properties to adapt to the local constraints of the environment [18]. Thus metabolically inactive or dormant-cells appear within the biofilm with antibiotic resistance [24]. Furthermore, bacterial cells within the biofilm community are protected by the extracellular matrix (ECM) from external stresses, for example oxidizing agents, ultraviolet radiation, predation, host immune response, etc. [20]. Those advantages contribute to the biofilm enhanced resistance to antibiotics - up to 1000 times more resistant compared to planktonic cells, making biofilm-related infections extremely complicated to treat [25].

2.1.2 The extracellular matrix

One of the main features of biofilms is the self-produced extracellular matrix (ECM) composed of extracellular polymeric substances (EPS). It accounts for almost 90 percent of the dry biomass, whereas the bacterial cells account for less than 10 percent [20]. The matrix immobilizes the bacteria and brings them closer, encouraging cell-cell interactions and communications by chemical signalling between species. It forms a scaffold for the three-dimensional architecture of the biofilm and provides mechanical stability. EPS biopolymers vary between species, nutrients availability or the environmental conditions, and have been called "the dark matter of the matrix" due to the difficulty in analyzing them [26]. In general, EPS are composed of polysaccharides like cellulose or alginate, proteins and nucleic acids (eDNA) [8]. Their roles depend on their localization within the matrix, and stage of the biofilm development. Due to the heterogeneity of the matrix components and distributions, their respective contributions to the matrix integrity are still poorly understood. Several functions of the EPS have been identified, highlighting the matrix versatility (Table 2-1).

Table 2-1 Main functions of the ECM. Adapted from [20]

Function	EPS component involved
Adhesion	Polysaccharides, proteins, DNA and amphiphilic molecules
Cohesion	Neutral and charged polysaccharides, proteins (such as amyloids and lectins), and DNA
Protective barrier	Polysaccharides and proteins
Nutrient source	Potentially all EPS components
Retention of water	Hydrophilic polysaccharides and, possibly, proteins
Exchange of genetic information	Extracellular DNA (eDNA)

EPS are essential to maintain the cohesion of the biofilm structure, and they influence the biofilm architecture. Removing some EPS have shown to alter the biofilm morphology and integrity. For example, cellulose is an architectural component in *Escherichia coli* macrocolony morphology, while the protein TasA and an exopolysaccharide are required for *Bacillus subtilis* biofilm structural integrity [27, 28]. Exopolysaccharides in most biofilms represent a major fraction of EPS components [29, 30]. While some exopolysaccharides are homopolysaccharides - such as cellulose present in *E. coli* or *Salmonella* biofilms for example, the vast majority are heteropolysaccharides formed by neutral and charged residues. In many bacterial biofilms, exopolysaccharides are necessary to promote attachment to surfaces and other cells, to build and to provide a scaffold to maintain the biofilm structure, and to protect cells from microbial and host defenses, as well as environmental constraints [17, 31, 32].

Proteins account for a large portion of the extracellular matrix mass as well. Among them, enzymes act as a digestive system by breaking down biopolymers and give the biofilm carbon and energy sources [20]. Non-enzymatic proteins are implicated in the biofilm formation and in maintaining the cohesion within the biofilm matrix. For example, biofilm surface associated proteins (Bap) are required for biofilm formation of various bacterial species such as *V. cholerae, S. aureus*, etc. [33]. Amyloid fibers are insoluble extracellular protein fibers that have been identified in various habitats and implicated in the adhesion of the biofilm [34]. Another component playing a major role during the first step of the biofilm formation is extracellular DNA (eDNA). eDNA helps to maintain the 3D structure of the biofilm by acting as a cell-cell interconnecting compound. For *Pseudomonas aeruginosa* biofilms, eDNA is necessary to keep the mushroom-shaped structure and is mainly found at the basis of the biofilm [35]. The origin of eDNA has not been exactly determined, but it could come from direct secretion, lysis of sub- population by prophage, or release of small membrane vesicles [36]. eDNA has multiple roles in biofilm formation such as nutrient, scaffold, antibiotics resistance, major proinflammatory component and promoting self-organization of bacterial biofilms [37].

The extracellular matrix is thus a heterogeneous structure and the EPS components are also able to interact with each other, which contributes to the network cohesion and biofilm strength (Figure 2-2). Hydrophobic interactions and entanglements of the biopolymers with eDNA provide the

mechanical stability of the matrix, while forces such as hydrogen bonding and van der Waals interactions keep the network together [38].

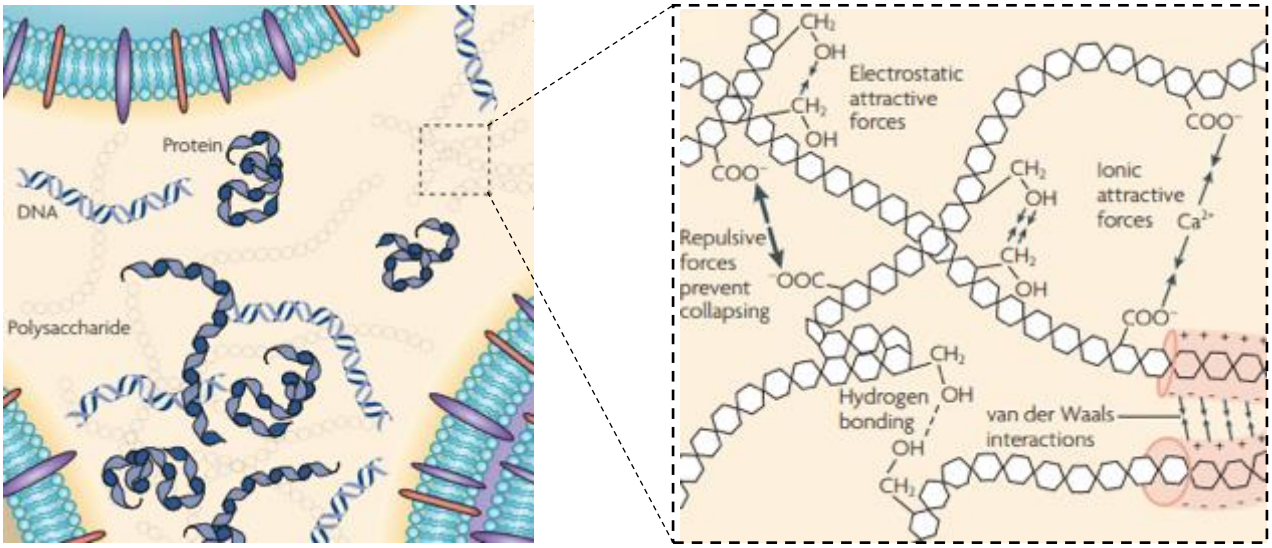

Figure 2-2 Schematic representation of extracellular polymeric substances at different scales: (a) major EPS components dispersed in the matrix and (b) principal forces keeping the matrix together. Figure adapted from *Flemming H.* et al (2010) [20]. Copyright (2010) Springer Nature

The extracellular matrix is an extremely complex structure – with a variable composition among bacterial species, that protects bacterial cells encased in its network. An in-depth understanding of the EPS composition and regulation is still unknown, especially in mixed-species biofilms.

2.1.3 Pellicle biofilms

Biofilms can grow on a variety of biotic or abiotic surfaces. When they are located at the air-liquid interface they are called pellicles. This type of interface is a rich environment, providing access to both the nutrients from the liquid medium and oxygen from the air. Despite the presence of air-liquid interfaces in the environment and the advantageous conditions for aerobic microorganisms, pellicle biofilms have been less studied [39]. Compared to solid surface-associated biofilms, bacteria have used different strategies to form floating pellicle biofilms. Flagellum - a protein appendage that allows bacterial motility - has been found to be essential in the pellicle development

with, for example, an *E. coli* flagellum-deficient mutant being unable to form a pellicle [40]. There are two possible mechanisms for the pellicle formation: either the bacteria attach to the wall and then develop the pellicle, or bacteria aggregate at the air-liquid interface and those clusters spread at the interface, forming the film.

Aerobic bacteria secrete their extracellular matrix and build the pellicle biofilm using either mechanisms depending on the strain and environmental conditions. For example, it appears that a solid surface is required for *Dickeya dadantii* to build a pellicle biofilm [41]. In contrast, *V. fischeri* forms its pellicle first on the surface of the liquid rather than attach to the plastic well, in the presence of arabinose [42]. In another study, Brewster-angle microscopy (BAM) was used to assess the formation of aggregates at the air-liquid interface by *E. coli* UTI89 growing in treated and untreated medium, which eventually lead to a film [43]. The Gram-positive bacteria *Bacillus subtilis* has been extensively studied for its ability to produce a wrinkled and robust pellicle biofilm, although many Gram-negative bacteria including pathogens are able to form a pellicle at the air-liquid interface (Figure 2-3). Among those Gram-negative bacteria, the most common identified exopolysaccharide in the pellicle matrix is cellulose [44]. This polysaccharide has been identified as an essential component to the development of the pellicle biofilm for different species such as *E. coli, Salmonella* Typhimurium, and *Pseudomonas fluorescens* [40, 45, 46]. Exopolysaccharides appear to be critical for the pellicle formation of other bacterial species. For example, the overproduction of the *V. cholerae* polysaccharide VPS in the rugose variant leads to the development of a strong wrinkled pellicle [47]. Some bacteria require amyloid fibers to form a pellicle. For example, *B. subtilis* secretes a protein component, TasA, that assembles into amyloid-like fibers, while *E. coli* requires the amyloid fibers curli for the pellicle formation [28, 40]. eDNA have also been identified as a major component in solid surface-associated biofilm, however its role is still unclear in most pellicle biofilms [44].

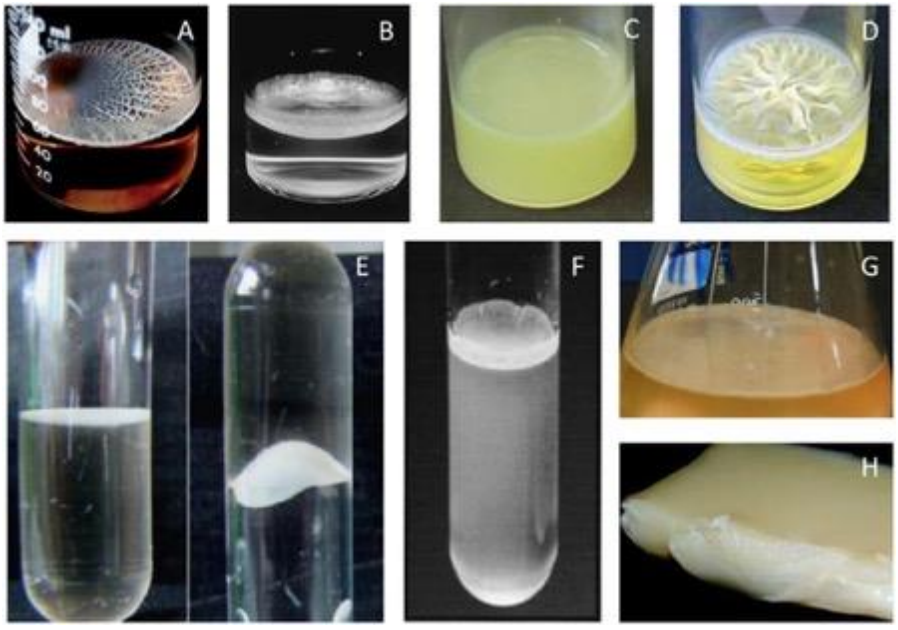

Figure 2-3 Mature pellicle morphology of bacterial species formed under various conditions: (a) *Bacillus subtilis* (b) *Pseudomonas fluorescens* SBW25 rugose variant (c-d) *Pseudomonas* species (e) *Acinetobacter baumannii* (tube hanging upside down to illustrate the strength of the pellicle) (f) *Salmonella* Enteritidis (g) *Shewanella oneidensis* (h) *Gluconacetobacter xylinus* [44]. Copyright (2014) Wiley

Bacteria tend to adapt their behavior in response to their environment. For example, *S.* Typhimurium switch from a surface associated-biofilm to a pellicle with a change in nutrient composition [48]. The air-liquid interface is a favorable niche for many bacterial species with its high oxygen concentration. However, there are only a few studies on the behavior of multi-species pellicle biofilm and their interactions at the interface.

2.1.4 Multispecies biofilms

In natural habitats, multiple bacterial species coexist together within biofilms (Table 2-2) [4]. Over the past few years, major breakthroughs on biofilms have been achieved, providing information on how to fight them. However, most of the researches have focused on single-specie biofilms, whereas mixed species biofilms appear to be the dominant form [5].

Table 2-2 Examples of distributions of multiple-species biofilm [4].

Localization	Species
Marine sediments	*Desulfosarcina variabilis, Desulfocapsa sulfoexigens, Nitrospina gracilis, Vibrio splendidus, Pseudoalteromonas* sp., *Arhodomonas aquaeolei, Anodontia phillipiana, Lucina pectinate, Riftia pachyptila, Alvinella pompejana, Verrucomicrobium* sp.
Chronic wounds	*Corynebacterium* sp., *Bacteroides, Peptoniphilus, Fingoldia, Anaerococcus, Peptostreptococcus* sp., *Streptococcus, Serratia, Staphylococcus, Enterococcus* sp.
Urinary catheter	*Staphylococcus epidermidis, Enterococcus faecalis, Escherichia coli, Proteus mirabilis, Pseudomonas aeruginosa, Klebsiella pneumoniae*
Dental plaque	*Streptococcus, Peptostreptococcis, Neisseria, Veillonella, Actinomyces, Bifidobacterium, Corynebacterium, Eubacterium, Lactobacillus, Propionibacterium, Rothia, Campylobacter, Eikenella, Fusobacterium, Haemophilus, Leptotrichia, Prevotella, Porphyromonas, Selenomonas, Treponema*

The interactions between the different species influence the development of biofilms and their properties. It can result in emergent properties such as an increased tolerance to antimicrobials or an increased virulence in infections [49, 50]. Species cohabiting together can also interact in synergetic or antagonistic ways. Oral multispecies biofilms are frequently found since hundreds of different bacteria live in this environment. A study from Filoche et al. showed that *S. mutans* first colonize the tooth surface, and with the cooperation of *Actinomyces*, promotes the growth of *Lactobacillus* in an oral mixed species biofilm [51].

The ability of some species to cooperate and coexist is not limited to oral bacteria. Medical devices are very often infected by *Staphylococcus* biofilms. *Staphylococcus aureus* and *Staphylococcus epidermidis* form multispecies biofilm that have different properties when exposed to various environmental factors, as it was demonstrated in a recent study by Stewart et al. [52]. Bacteria also interact in an antagonistic manner and competition can be observed within a biofilm. Recent studies have shown for example that *P. aeruginosa* can inhibit *E. coli* growth [53]. *E. coli* bacterial cells were grown in the presence of various percentages of *P. aeruginosa* spent media and the final cell density was measured. This study demonstrated that *P. aeruginosa* secretes molecules that are

antagonistic in nature to *E. coli* growth. Those interactions between mono- and mixed species are governed by cell-cell communication. The communication is realized via a system called quorum-sensing, which enables bacteria to express specific genes in a coordinated fashion, according to the density of their local populations [54]. Quorum-sensing enables bacteria to coordinate their response to the environment through production of signaling molecules called autoinducers. Some quorum-sensing systems are used for interspecies communication and can be required for mixed species biofilm formation [5].

Since multispecies biofilms are very complex structures, the knowledge of how species interact with each other and affect biofilm properties is still very limited.

2.2 Mechanical properties of bacterial biofilms

2.2.1 Biofilms viscoelasticity

As mentioned previously, the ECM polymeric network accounts for 90 percent of a biofilm dry mass, and is responsible for the physical properties of the biofilm. From a biophysical point of view, the ECM is considered as a cross-linked (both physically and chemically) polymer gel, providing strong mechanical stability to the biofilm [55]. While biofilms are heterogenous structures with a wide range of properties, they have been recognized as viscoelastic materials [56]. A viscoelastic material exhibits both elastic and viscous properties – the permanent viscous deformation under stress and the reversible deformation (memory) from the elastic part. Shear stress has an impact on the biofilm structure and morphology due to its viscoelasticity. Biofilms grown under high shear flow tend to be stronger, thinner and denser with large cellular clusters and ripples [55, 57-59]. Under weak to moderate laminar flow, the biofilm is an heterogeneous structure with water channels [59]. The interactions between the polymeric components – binding proteins, entanglements or crosslinks – inside the matrix allow the biofilm to withstand environmental shear forces. The matrix composition dictates the biofilm mechanical response to shear stresses. The stress response of biofilms was modeled for various bacterial strains, and multiple relaxation times were attributed to EPS components [60]. The two shorter relaxation times (< 0.75 s and 0.75 to 3 s) were respectively attributed to water and soluble polysaccharides, which account for the heaviest

mass in the biofilm. A distinguishably narrow relaxation time (10 to 25 s) was attributed to the interaction of intact eDNA with other matrix components in response to mechanical stresses. In *Pseudomonas aeruginosa* biofilm - a model organism in biofilm studies - , Psl polysaccharides have been shown to increase the elasticity and stiffen the biofilm in the presence of the protein CdrA, while the polysaccharides Pel or alginate are responsible for the biofilm ability to withstand high deformation [61]. For *V. cholerae*, the biofilm strong mechanical properties have been shown to depend on the proteins RbmA, Bap1 and RbmC cross-linking (covalent) with the polysaccharide VPS (*Vibrio* polysaccharide) [62].

2.2.2 Interfacial rheology

Over the past two decades, rheology has emerged as a useful technique to investigate biofilm mechanical properties [63]. Rheology can be defined as the study of the flow/deformation of soft materials such as polymers, colloidal suspensions, gels, hydrogels, slurries, biomaterials, biopolymers, biological fluids, etc. It is the quantitative study of the manner in which materials deform and flow. When a material is deformed, the mechanical stresses and strains - which correspond to the gradient of displacements of particles when applying an external force on a body, are measured. The relationship between the stress and strain is then used to calculate the material rheological/mechanical properties. Three types of shear rheometry tests are usually performed on viscoelastic materials: stress relaxation, creep-recovery and dynamic oscillation. In an oscillatory test, a small sinusoidal oscillatory strain is applied to the sample and the resulting stress is measured. For a pure solid, the strain and stress response are perfectly in phase, while for a pure viscous liquid they have a 90° phase lag due to the energy dissipation. A viscoelastic fluid exhibits a phase lag between the stress and strain since the stress is directly proportional to the strain for the elastic response, while it is proportional to the derivative of the strain for the viscous part. When the viscoelastic material is deformed through oscillations (at a deformation amplitude γ_0) at a certain frequency ω, a phase angle δ between 0 and 90° is added to the stress σ. From the measured stress, the storage modulus *G'* that quantifies the elasticity, and the loss modulus *G"* that quantifies the viscous contribution, can be calculated (2-1).

$$\sigma(t) = \gamma_0[G' \sin(\omega t) + G'' \cos(\omega t)] \qquad (2\text{-}1)$$

Determining the elastic and viscous moduli is necessary to understand the material's viscoelastic behavior in response to a given stress.

If a material is located at an air-liquid or liquid-liquid interface, its viscoelastic properties can be quantified using interfacial rheology – the equivalent in 2D of 3D bulk rheology. When studying interfacial rheology – shear or dilatational, the same principles described above can be applied. Shear interfacial rheological properties can be obtained by measuring the response of the viscoelastic material when a torque is applied to the interface directly. A variety of measuring techniques and geometries have been proposed in the literature to measure the displacement within this two-dimensional interface. The most common geometries used for interfacial shear rheology are the interfacial stress rheometer (ISR), which uses a magnetic needle at the interface in a glass chamber (Figure 2-4.A), the double-wall ring (DWR) (Figure 2-4.B) and the bicone (Figure 2-4.C) that are both fixed to a rotational rheometer [64]. The (DWR) setup first described by Vandebril et al. measures the viscoelastic properties of the interface by positioning a platinum-iridium ring at the interface, which is analog to a two-dimensional double wall Couette setup [65]. The other geometry used for interfacial measurements that can be fixed to a rotational rheometer is the bicone geometry, which can be considered as a two-dimensional Couette device. A flow field analysis was developed for the bicone geometry, allowing the calculation of the absolute interfacial properties [66]. To obtain the interfacial mechanical properties, the interface has to be decoupled from the bulk flow. The influence of the surface drag due to the bulk flow on the interface is described by a dimensionless number called the Boussinesq number (Bo) (2-2):

$$Bo = \frac{surface\ drag}{subphase\ drag} = \frac{\eta_i}{\eta_b L} \tag{2-2}$$

with η_i and η_b the viscosities of the interface and subphase, and L the characteristic length scale which depends on the geometry used. When $|Bo| >> 1$, the interfacial properties dominate the response, while when $|Bo| \leq 1$ the measured properties are dominated by the bulk subphase.

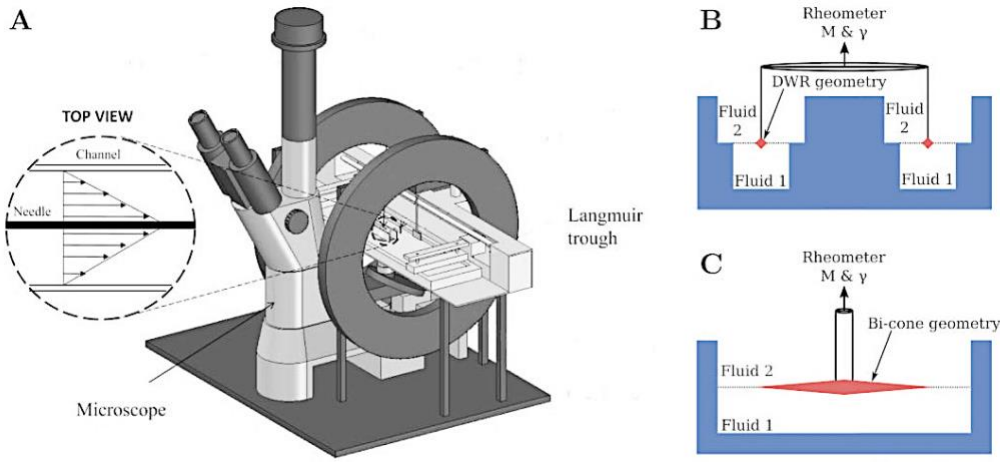

Figure 2-4 Schematic representation of the main experimental setups for interfacial shear rheology: (A) Interfacial stress rheometer (ISR); (B) Double-wall ring (DWR) setup; (C) Bicone geometry. Copyright (2020) The Society of Rheology [64].

Interfacial shear rheology is challenging since the thin interface signal is often much weaker compared to the one from bulk materials and the measurements are often close to the instrument limits. Recently, the operating limits for the various interfacial rheometers were determined, highlighting the high sensitivity of the ISR and DWR setup, while the bicone setup appears to be more suitable for interfaces with high interfacial moduli and viscosities [64]. Interfacial rheology geometries have to combine high sensitivity with large Bo values to reliably measure the viscoelastic properties of a material at the interface.

2.2.3 Interfacial rheological measurements of biofilms

Monitoring the biofilm evolution over time can provide important knowledge on its formation. However, most techniques in microbiology allow the analysis only after several hours of bacterial growth. Interfacial shear rheology is a useful technique to quantify the biofilms mechanical properties at the air/liquid interface and monitor changes over time. The double-wall ring (DWR) interfacial setup has been used to evaluate the impact of EPS on the biofilm viscoelastic properties. For example, *Escherichia coli* is widely known for forming resilient biofilms, and the major

components of its extracellular matrix are bacterial amyloid fibers named curli and cellulose [27]. Interfacial shear rheology brought quantitative data and supported the hypothesis that curli enhance the viscoelasticity of *E. coli* biofilms formed at the air-liquid interface [43]. Another example of the DWR interfacial rheology setup used to quantify the mechanical properties of biofilm formation at the air-liquid interface is with *Vibrio cholerae* (Figure 2-5) [67]. Interfacial rheology, combined with techniques that determine the pellicle morphology, its chemical composition and microscale architecture, highlighted the role of the protein Bap1 to maintain the biofilm's matrix over time. More recently, the role of bacterial appendages and EPS on *P. aeruginosa* pellicle formation was evaluated with the DWR geometry, combined with the analysis of pellicle microscale architecture [68].

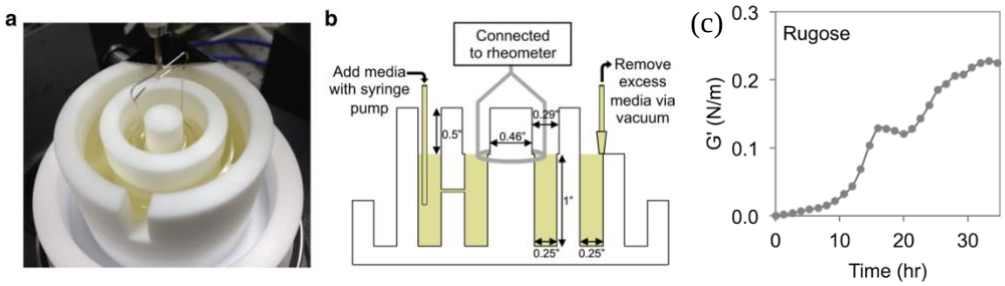

Figure 2-5 Double-wall ring interfacial rheology setup modified for biofilm studies: (a) Teflon flow chamber with a du Noüy ring positioned at the air-liquid interface; (b) Schematic representation of the setup, with evaporation control through a syringe pump to inject media, and vacuum to remove the excess media; (c) Evolution of the elastic modulus of *V. cholerae* rugose pellicle. Copyright (2014) Elsevier [67].

The influence of environmental stimuli on single-specie biofilms was studied using the bicone geometry combined with an exchange flow chamber (Figure 2-6) [69]. Interfacial rheology demonstrated that biofilms have different growth profiles depending on the media composition and changes of pH could disrupt it. After a change in pH, the elastic modulus of a *E. coli* mature biofilm decreased and the biofilm network was completely disintegrated around pH 4. This study assessed the impact of the environment composition on biofilm growth and mature biofilms through interfacial rheology.

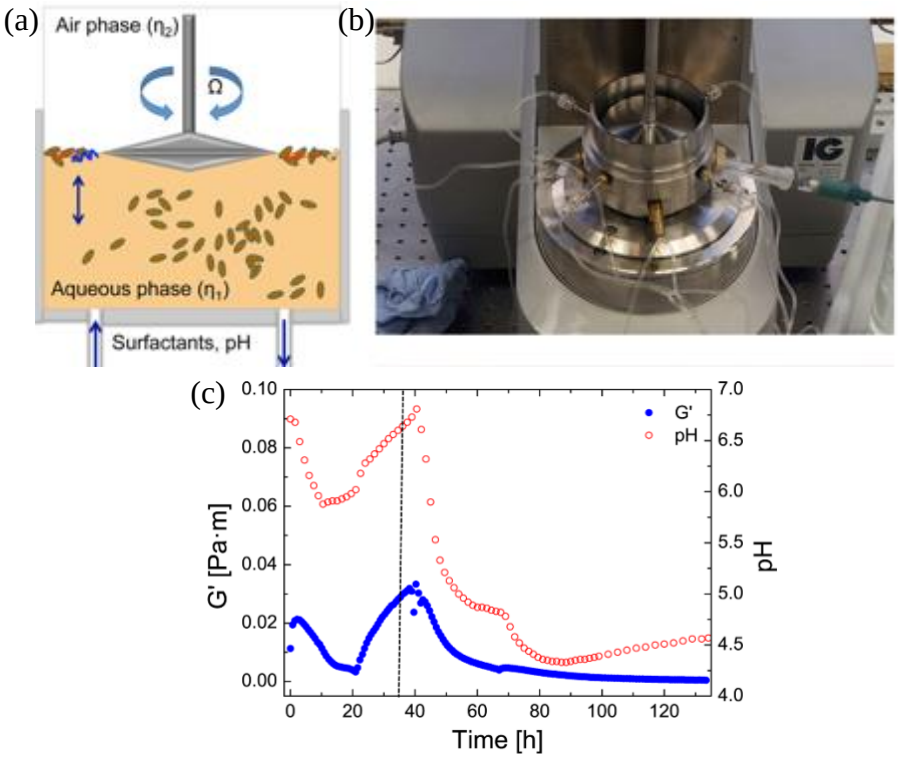

Figure 2-6 Bicone setup adapted to study the effect of an environmental change on biofilm growth: (a) Schematic side view of the flow chamber with the bicone; (b) Interfacial rheology experimental setup with the bicone positioned at the air-liquid interface; (c) Effect of pH change on *E. coli* biofilm elastic modulus *G'*. *Rühs et al.* (2013) [69].

In addition to interfacial rheology, various techniques have been developed over the past two decades to characterize the biofilms viscoelastic properties, from both macroscopic and microscopic perspectives. Since biofilms are heterogeneous materials, active or passive micro-rheology are useful techniques to measure local mechanical properties by the displacement of tracers visualized under a microscope. Active micro-rheology uses magnetic or optical tweezer to move the beads within the extracellular matrix and measures the local mechanics of the biofilm [70]. Bacteria were successfully used as passive tracers to measure the viscoelasticity of *S. aureus* and *P. aeruginosa* biofilms [71]. Bulk rheology is also a classic rheological method to quantify solid surface-associated biofilms mechanical properties [72, 73]. For example, *P. aeruginosa* biofilms grown on agar plate were collected and a plate-plate geometry was used to assess the effect of various treatments on the biofilms viscoelasticity [74].

Most rheological studies on biofilms focus on single-species and despite their omnipresence in the environment, there are very few studies on the rheological properties of multi-species biofilms. Recently, Yannarell et al. used bulk rheology to characterize the mechanical properties of *Pantoea agglomerans* and *Bacillus subtilis* mature dual-species biofilm [75]. They demonstrated that the rheological properties of the dual-species biofilm were a combination of the single-species biofilm. Additional analysis will help to further understand the biofilms mechanical behavior in multispecies communities and in their natural environment, in order to design efficient strategies to eradicate them.

2.2.4 Biofilms mechanical response to external stresses

Biofilms in the environment are exposed to various environmental stresses and they often experience high shear flows. Biofilms grown under high shear stresses tend to be more elastic and more resistant to detachment compared to biofilms exposed to low shear rates [76]. When they are exposed to different molecules and chemicals, their mechanical response also varies. For example, changing the nutrient composition influences the EPS production and thus the biofilm mechanical properties [77, 78]. *P. fluorescens* biofilms grown under low nutrient media had a higher Young's modulus and were more adhesive [79].

Exposure of biofilms to a variety of ions appears to trigger different mechanical responses specific to the ions involved. When a *P. aeruginosa* nonmucoid biofilm was exposed to the cations Ca^{2+} or $Cu^{2+,}$ the mechanical properties did not change, while in the presence of Fe^{2+}, the storage modulus decreased [74]. This behavior was attributed to the interactions between the polysaccharide Psl and Fe^{2+} [80]. *P. aeruginosa* mucoid biofilms, however, displayed an increased shear modulus after treatment with the cations Ca^{2+}, Mg^{2+} and Fe^{2+}, which could be due to the production of the negatively charged alginate [81].

Biofilms are extremely difficult to treat and to remove compared to planktonic bacteria. They tend to be mechanically resistant to a wide range of external chemicals such as ethanol, bleach, urea, etc. While a number of biocides and antimicrobials are able to reduce bacteria viability, they usually do not destroy the biofilm mechanical integrity - they might weaken or strengthen it, but

the biofilm recovers its mechanical properties with the surviving bacteria when the chemical treatment is stopped [55]. Thus, following the addition of $FeCl_3$ and $Al_2(SO_4)_3$, *P. aeruginosa* biofilms acquired a granular aspect that was attributed to ionic interactions with the EPS negatively charged components (Figure 2-7. A). The biofilms had a higher elasticity in the presence of $FeCl_3$ and $Al_2(SO_4)_3$, and were able to fully regain their elasticity after being subjected to high deformation, despite taking 1 min instead of 20 seconds to recover without chemicals (Figure 2-7. B) [74].

Similarly, the mechanical properties of *E. coli* biofilms were affected by the addition of the biocide chlorohexidine: the elasticity increased with increased chlorohexidine concentration due to the destruction of the intracellular material [82].

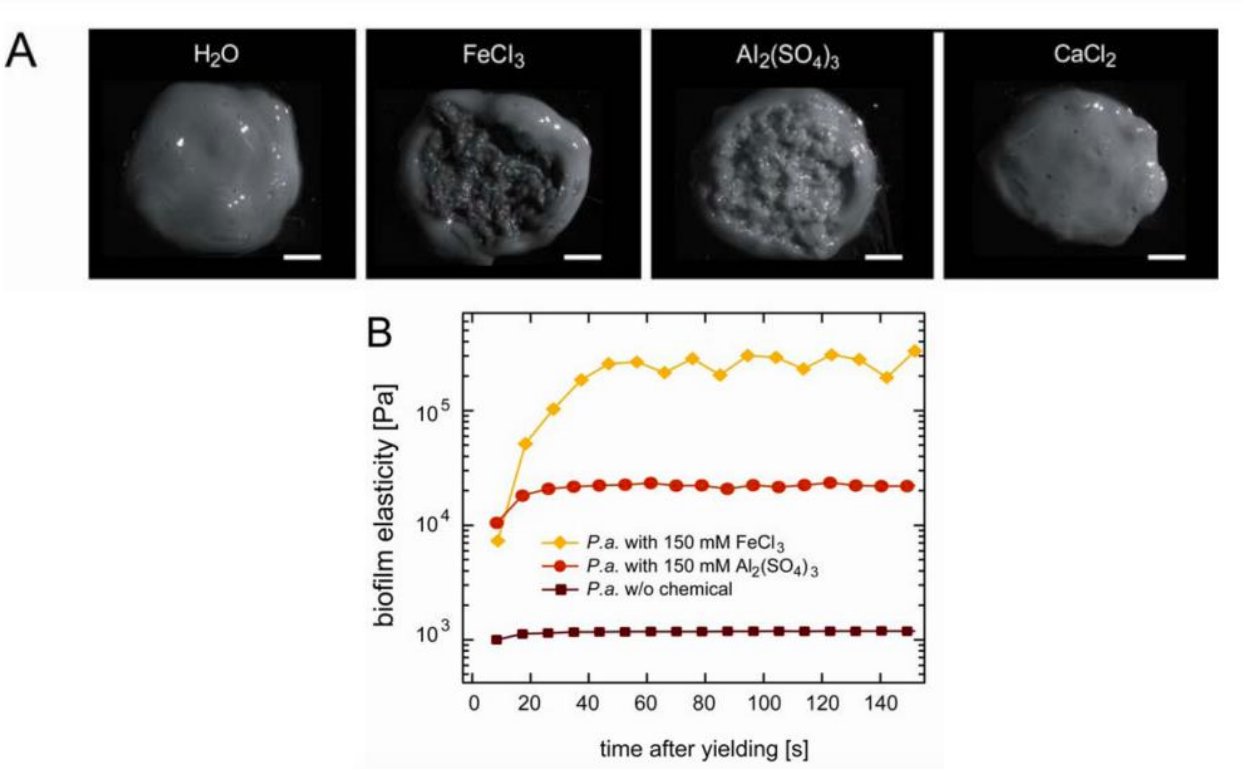

Figure 2-7 (A) *P. aeruginosa* biofilm macroscopic morphology after the addition of a drop of chemical solution (B) Time required for the biofilm to recover its elasticity in the presence of ions. Copyright (2011) Royal Society of Chemistry [74].

Despite an increase in the study of biofilm mechanical properties over the past few years, there is still a limited understanding on how the biofilm mechanical robustness and composition influences its survival to antimicrobials.

2.3 Anti-biofilm strategy: nanoparticles

2.3.1 Antimicrobial activity of metallic nanoparticles

The extensive use of traditional antibiotics has led to an increased emergence of bacteria resistant to all existing antibiotics. These multi-drug resistant bacterial strains represent a major threat to human health and leads to an increased mortality rate [83]. Over time, bacteria have developed multiple mechanisms to acquire resistance against antibiotics, for example by modifying their target site or inactivate the drug with a cellular enzyme [84]. Since very few new antimicrobials has been discover over the past decades, nanotechnological strategies have been extensively explored to treat microbial infection [85]. Several types of nanoparticles have been successfully used as antimicrobial agents or drug carriers. In particular, metallic nanoparticles have attracted a lot of attention due to their exceptional antimicrobial properties and multiple advantages. Metallic nanoparticles target multiple biomolecules, which considerably reduces the development of resistance mechanisms from bacteria, although some bacteria have started to develop resistance mechanisms [86]. Various types of metallic nanoparticles have demonstrated high antimicrobial activity against bacteria and other microorganisms. For example, synthesized zinc oxide nanoparticles (ZnO-NPs) have shown bactericidal properties on Gram-positive and Gram-negative bacteria as well as fungi [87, 88]. Zhang et al. demonstrated that gold nanoparticles (AuNPs) inhibited *S. aureus* growth, however much higher concentration where required to have an inhibition effect compared to silver nanoparticles (AgNPs) since their antimicrobial mechanism is different [89]. The potential antimicrobial mechanisms of some well-known metallic nanoparticles are described in Table 2-3 although future research is needed to fully understand them.

Table 2-3 Metallic nanoparticles and their potential antimicrobial mechanism. Adapted from [90].

Nanoparticles type	Antimicrobial mechanisms	References
Gold	Strong electrostatic interactions, accumulation at cell surfaces and interaction with cell membrane	[91, 92]
Silver	Interferences with cell membrane, DNA and electron transport damages, release of toxic Ag^{+} ions	[93]
Zinc oxide	Disruption of cell integrity, reactive oxygen species (ROS) production, release of toxic Zn^{2+} ions	[94, 95]
Titanium dioxide	Photo-dependent, ROS release	[96-98]
Copper and Copper oxide	Bacterial cell wall adhesion, ROS generation, membrane cell damage	[93]

2.3.2 Silver nanoparticles (AgNPs) as antimicrobial agents

Silver has been used for its antimicrobial properties to prevent wound-related infections [99]. Silver nanoparticles (AgNPs) are among the most studied nanoparticles nowadays. Their general formation mechanism was shown to consist of four main steps: the silver precursor is reduced within 5 seconds into dimers and trimers that then form 2-3 nm seeds. These particles remain stable for 5-10 min before coalescing and forming larger nanoparticles of 5-8 nm, as presented in Figure 2-8 [100].

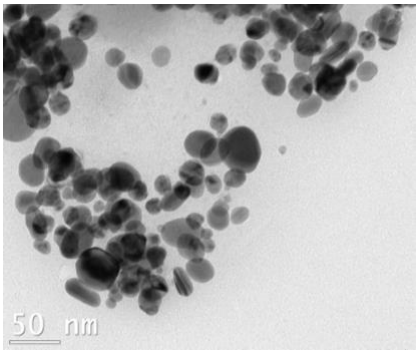

Figure 2-8 TEM image of AgNPs synthesized with alginate in our lab (Polytechnique Montreal).

Various chemical, physical or biological strategies have been used to synthesize AgNPs. Chemical synthesis of AgNPs has been predominantly explored due to the good morphology control it provides, and is usually low cost and easy to implement [101]. The stability and polydispersity of the nanoparticles suspension can be modified by tuning parameters such as the pH, temperature, precursor, reducing agents and their concentrations [102]. Green chemistry has become increasingly popular to replace the use of harmful reagents for AgNPs synthesis. For example, multiple research groups have successfully used natural polysaccharides such as glucose, starch, alginate or chitosan as both reductors and stabilizing agents [103-106]. These green chemistry synthesis methods are usually simple and low cost and lead to AgNPs with good antimicrobial properties. The antimicrobial properties of AgNPs depend strongly on their size, shape and charge and thus their synthesis process [107, 108]. AgNPs continuously release high concentrations of Ag^+ cations that are extremely toxic for cells. The general antimicrobial mechanism of AgNPs is described below (Figure 2-9) [93]. First, the AgNPs adhere to the bacterial cell wall [93]. This adhesion is mediated by the size of the AgNPs, but also electrostatic interactions, since the bacterial surface carries a negative charge [109]. AgNPs can have a positive, neutral or negative charge depending on their synthesis process. After the initial adhesion, AgNPs destabilise the membrane functions, structure and permeability. Once there are inside the bacterial cell, they can inactivate proteins, damage DNA and induce oxidative stresses by generating reactive oxygen species (ROS).

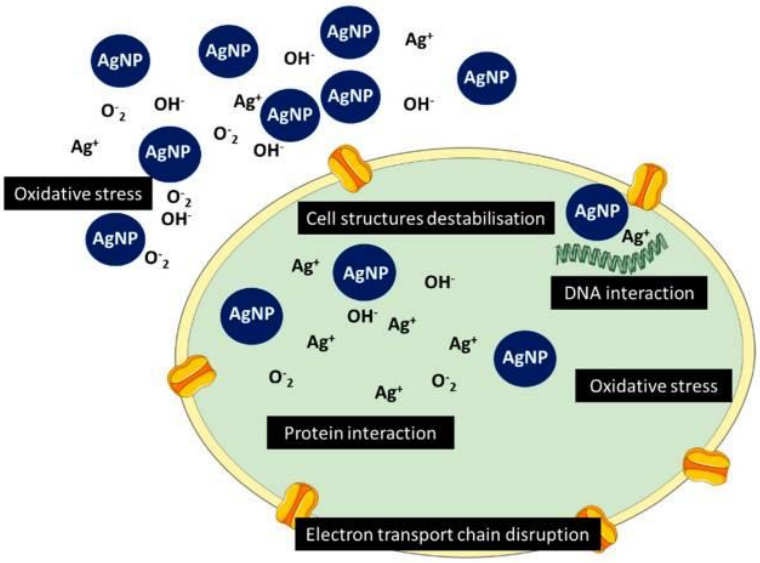

Figure 2-9 AgNPs general antimicrobial mechanism [93].

2.3.3 AgNPs-biofilms interactions

Bacteria within biofilms are embedded in a self-produced polymeric matrix and thus nanoparticles will interact with the components in this complex material. In contact with the biofilm matrix components (proteins, polysaccharides, lipids and nucleic acids), a corona of mono- or multiple layers is formed around the nanoparticles surface and it affects their physical properties [110]. This corona has been extensively studied when involving biological media such as blood plasma. However the corona formation inside a biofilm has not been fully investigated despite its importance in mediating the interactions between nanoparticles and the biofilm. Those interactions are mainly physical, either electrostatic, hydrophobic or steric (Figure 2-10). Electrostatic interactions contribute the most to the antimicrobial activity [111]. For example, the impact of electrostatic interactions in AgNPs antibiofilm activity was demonstrated by Badawy et al., who synthesized uncoated, neutral, cationic and anionic AgNPs [112]. Cationic AgNPs exhibited the highest antibiofilm activity against *Bacillus* species, while anionic AgNPs had the weakest antibacterial activity, most probably due to electrostatic repulsion. In another study, Mitzel and Tufenkji hypothesized that repulsive electrostatic forces between PVP-capped AgNPs and EPS led to low adsorption on *P. aeruginosa* biofilms [113]. These interactions can be modulated by

engineering AgNPs, for example by making them highly selective against a key biofilm component [111].

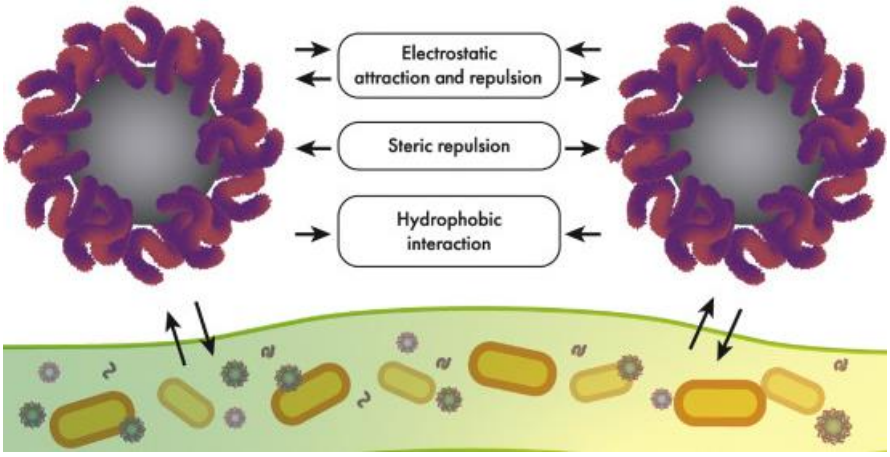

Figure 2-10 Schematic diagram of the multiple physicochemical interactions between nanoparticles and biofilm components. Copyright (2019) Elsevier [110].

While it has been established that the physicochemical properties of AgNPs play a significant role in the interactions with biofilms, a deeper characterization of the influence of the biofilm matrix chemical composition on AgNPs antimicrobial activity is still needed.

2.4 Summary

With the emergence of multi-resistant bacterial strains and the increased resistance of biofilms to existing antibiotics, there is a crucial need to develop new antimicrobial strategies. Bacteria within biofilm communities are protected by extracellular polymeric substances (EPS) which confers them an increased tolerance to external mechanical and chemical stresses. While there have been significant progresses in the biofilms knowledge, the extracellular matrix remains poorly understood. Its composition varies depending on the bacterial species as well as the environmental conditions, making it difficult to have a detailed knowledge of the polymers presents as well as their role in the biofilm viscoelastic and antibacterial resistance properties. Furthermore, while most studies focused on single bacterial biofilms, multiple bacterial species coexist together and

multi-species biofilms are the dominant form. Interspecies interactions are likely to influence the viscoelastic and physicochemical properties of biofilms as well as EPS composition.

The interfacial rheological properties of multi-species pellicle biofilms have not been studied before. A deeper understanding of the impact of interspecies interactions on the biofilm rheological behavior is required to find appropriate treatments. Moreover the interactions between antibacterial substances, such as nanoparticles, and the polymeric matrix are also not fully understood, although they are crucial to design efficient antibacterial treatments to remove biofilms. Thus enhanced knowledge of the role of interspecies interactions on the biofilms' mechanical and molecular properties, as well as the role EPS composition on the increased tolerance to antimicrobials, is required to unlock new strategies to disrupt and remove unwanted biofilms.

CHAPTER 3 OUTLINE OF DISSERTATION

3.1 Research objectives

As established in the literature review in Chapter 2, in order to design appropriate antimicrobial strategies to control and remove harmful biofilms, a better understanding of the biofilm matrix and its properties in multispecies biofilms is required. **The main objective** of this work is to understand the viscoelastic behavior and composition of dual-species biofilms, and to elucidate the role of the polymeric matrix in the antimicrobial resistance.

The specific objectives of this work are:

1. To quantify the bacterial interactions in a dual-species biofilm model with its rheological properties in real-time and its microbiological composition
2. To establish the interdependence between the viscoelastic properties and molecular biofilm matrix composition of a dual-species biofilm pathogenic model
3. To evaluate the role of the biofilm matrix composition in antimicrobial resistance

3.2 Organization of the articles

The following three chapters (Chapter 4 to 6) represent the main scientific findings of this thesis and are presented in the form of three peer-reviewed journal articles that respectively address the specific objectives.

Chapter 4 presents the first article entitled "*Microbiological and real-time mechanical analysis of Bacillus licheniformis and Pseudomonas fluorescens dual-species biofilm*" and was published in the journal *Microbiology* on July 1st, 2019. In this work, interactions within a model dual-species biofilm were characterized by quantifying the biofilm viscoelastic properties in real-time using interfacial rheology. The rheological properties were related to the microbiological composition of

the dual-species biofilm. It demonstrates the importance of growth kinetics in *Pseudomonas fluorescens* and *Bacillus licheniformis* competition for the interface in this dual-species biofilm.

Chapter 5 presents the results of the second article entitled "*Mechanical and microstructural insights of Vibrio cholerae and Escherichia coli dual-species biofilm at the air-liquid interface*" and was published in the journal "*Colloids and Surfaces B: Biointerfaces*" on January 11th, 2020. This work focuses on the viscoelastic and molecular properties of a pathogenic dual-species biofilm to demonstrate antagonistic interactions between the two pathogens. The biofilm formation rate was the major factor impacting the bacterial interactions. It modulated the polymeric matrix composition of the dual-species biofilm, with *Vibrio cholerae* inhibiting the production of amyloid fibers (curli) from *Escherichia coli*.

Chapter 6 presents the third article entitled "*The polymeric matrix composition in Vibrio cholerae biofilm mediates the resistance to silver nanoparticles prepared by hydrothermal synthesis*" and was submitted in the journal "*ACS Applied Materials and Interfaces*" on April 22nd, 2021. In this work, silver nanoparticles (AgNPs) were used against the pathogen *Vibrio cholerae* biofilm to evaluate the role of the polymeric matrix composition on the biofilm resistance to AgNPs. The biofilm polymeric matrix offered an increased protection to bacteria against AgNPs, and the interactions between EPS components and the nanoparticles modulated the antibacterial activity.

CHAPTER 4 ARTICLE 1: MICROBIOLOGICAL AND REAL-TIME MECHANICAL ANALYSIS OF *BACILLUS LICHENIFORMIS* AND *PSEUDOMONAS FLUORESCENS* DUAL-SPECIES BIOFILM

Authors: Clémence Abriat,[a,b] Nick Virgilio,[a] Marie-Claude Heuzey,[a#] France Daigle[b#]

[a]CREPEC, Department of Chemical Engineering, Polytechnique Montréal, Montréal, Québec, Canada

[b]Department of Microbiology, Infection and Immunology, Université de Montréal, Montréal, Québec, Canada

#Corresponding authors: marie-claude.heuzey@polymtl.ca and france.daigle@umontreal.ca

Published in *Microbiology*, 2019 Jul;165(7):747-756.

ABSTRACT : In natural habitats, bacterial species often coexist in biofilms. They interact in synergetic or antagonistic ways and their interactions can influence the biofilm development and properties. Still, very little is known about how the coexistence of multiple organisms impact the multispecies biofilm properties. In this study, we examined the behavior of a dual-species biofilm at the air-liquid interface composed by two environmental bacteria: *Bacillus licheniformis* and a phenazine mutant of *Pseudomonas fluorescens*. Study of the planktonic and biofilm growths for each species revealed that *P. fluorescens* grew faster than *B. licheniformis* and no bactericidal effect from *P. fluorescens* was detected, suggesting that the growth kinetics could be the main factor in the dual-species biofilm composition. To validate this hypothesis, the single and dual-species biofilm were characterized by biomass quantification, microscopy and rheology. Bacterial counts and microscale architecture analysis showed that both bacterial populations coexist in the mature pellicle, with a dominance of *P. fluorescens*. Real-time measurement of the dual species biofilms viscoelastic (i.e. mechanical) properties using interfacial rheology confirmed that *P. fluorescens*

was the main contributor of the biofilm properties. Evaluation of the dual-species pellicle viscoelasticity at longer time revealed that the biofilm, after reaching a first equilibrium, created a stronger and more cohesive network. Interfacial rheology proves to be a unique quantitative technique, which combined to microscale imaging, contributes to understand the time-dependent properties within a polymicrobial community at various stages of biofilm development. This work demonstrates the importance of growth kinetics in the bacteria competition for the interface in a model dual-species biofilm.

4.1 Introduction

Bacterial biofilms are communities omnipresent in the environment in which microorganisms are embedded within an extracellular matrix (ECM). This matrix consists of polysaccharides, proteins, nucleic acids and lipids, and works both as a structural scaffold and a protective barrier [114]. When pathogenic bacteria form biofilms, the resulting infections are complicated to treat since bacteria are protected within the ECM [115, 116]. Biofilms are frequently associated with chronic infections [117], such as urinary tract [118], chronic wound [119] or chronic airways infections in cystic fibrosis [120]. On the other hand, biofilms properties can also be beneficial to human activities, especially in the biotechnology industrial sector. Environmental bacterial biofilms have been used as filters for wastewater treatment to remove pollutants such as ammonia or nitrobenzene [121, 122], for example. Biofilm reactors have demonstrated their efficiency to convert organic wastes into alcohols and organic acids [123, 124].

Bacillus sp. are Gram-positive soil bacteria commonly isolated from biofilms. *B. subtilis* has been extensively studied for its ability to form resilient biofilms at the air-liquid interface [125, 126]. The ECM matrix of *B. subtilis* is mainly composed of extracellular polysaccharides and proteins, making this biofilm wrinkled and hydrophobic [127, 128]. Recently, another *Bacillus – B. licheniformis –* has attracted a lot of attention in the medical field over the past years for its probiotic effect [129], but has also been found to cause problems in industrial setups due to its ability to form very robust and resistant biofilms [130]. More specifically, in the dairy industry, *Bacillus sp.* are among the most common contaminants isolated from raw milk [131]. While *B. subtilis* biofilm formation has been well documented, not much is known about the ability of *B. licheniformis* to form such strong pellicles. A recent study on the mechanical resistance of *B.*

licheniformis and its matrix components revealed that its ECM is mainly composed of amyloid-like polymers and eDNA [132].

Another common bacterium found in soil and water habitats also known to form biofilms at the air-liquid interface is *Pseudomonas fluorescens*, a motile Gram-negative bacterium. *P. fluorescens* is well-known for causing food spoilage, contaminated drinking water and nosocomial infections [133]. In the dairy industry, *Pseudomonas* are important spoilage organisms and their ability to form biofilms make them resistant to environmental stresses [134]. The chemical composition of *P. fluorescens* ECM was analyzed for various strains. A cellulose-like polymer was found to be a key matrix component linked to the physical properties of the air-liquid pellicle [45].

Since biofilms contain viscoelastic materials, interfacial shear rheology is a useful technique to probe and quantify their mechanical properties at the air/liquid interface and to observe their evolution and changes in real time [43, 69]. When applying a small amplitude sinusoidal shear strain on a material – like biofilms – a dynamic sinusoidal stress response, usually not in phase with the input strain, is measured. The stress wave is then split into two contributions, and from the strain-stress relationship the elastic modulus *G'* modulus (in phase with strain) and viscous modulus *G"* are obtained. These dynamic moduli can be measured in the bulk phase (most common), or at the interface like done here. The continuous monitoring of biofilm evolution provides important knowledge on its formation and dynamic properties, especially since most of the other techniques currently used provide data at specific times only. Interfacial rheology was previously used to quantify the mechanical properties of *Vibrio cholerae* (the causative agent of cholera), which develops biofilms at the air-liquid interface [67]. Bacterial biofilms tend to exhibit unique mechanical properties due to the variation of their extracellular matrix composition. To our knowledge, interfacial rheology has never been applied to quantify multispecies biofilms viscoelastic properties in real-time, in correlation with microbiological analysis in a dual-species biofilm.

In natural habitats, multiple bacterial species coexist. The interactions between different species influence the development of biofilms and their properties [135, 136]. In order to develop strategies to interfere with biofilm formation, a deeper knowledge of the impact of interspecies interactions on the biofilm macroscopic and microscopic properties is required. Species cohabiting can interact in synergetic or antagonistic ways. Oral biofilms perfectly illustrate interspecies interactions, with

hundreds of species coexisting within a biofilm [51]. Bacteria also interact in an antagonistic manner and competition can be observed within a biofilm. Recent studies have shown for example that *P. aeruginosa* secretes molecules that can inhibit *Escherichia coli* growth [53]. *Staphylococcus aureus* and *Staphylococcus epidermidis* form a multispecies biofilm that have different properties when exposed to various environmental factors, such as the formation of a porous network by *S. aureus* at higher temperatures [52]. Moreover, the planktonic growth rate of each species has a major impact on the biofilm composition since *S. aureus* is the most prevalent species under unstressed conditions in the multispecies biofilm due to its faster growth rate [52].

In this work, we characterize the interactions within a multispecies biofilm model at the air-liquid interface, composed of two common contaminants in the dairy industry that [137-139] - *B. licheniformis* and a phenazine mutant of *P. fluorescens* to focus on the competition for the interface- using different approaches: (i) quantifying biofilm interfacial viscoelastic properties in real-time; (ii) characterizing biofilm biological compositions; and (iii) assessing the importance of growth factors on bacterial interactions within our dual-species model biofilm at the air-liquid interface, based on the acquired data. We hypothesize that the planktonic and biofilm growth rate is a major factor influencing the dual-species biofilm composition, as previously observed for *Staphylococcus* [52]. To validate this hypothesis, we combine the rheological results with biological parameters – biomass and bacterial content – to characterize the mature biofilm composition, and microscopic imaging, in order to better understand the bacterial interactions within the dual-species biofilm.

4.2 Material and methods

4.2.1 Bacterial strains

For all experiments, an environmental strain of *Bacillus licheniformis* and a phenazine mutant strain of *Pseudomonas fluorescens* (C5-10) [140] were used. A phenazine mutant was used to study the competition for the interface between the two bacteria and to remove the bactericidal effect from the phenazine production. This phenazine mutant strain will be referred simply as *P. fluorescens* in the text. Overnight cultures were grown in 5 ml of Luria-Bertani (LB) broth from

Bio Basic Canada Inc. at 37 °C under shaking in a New Brunswick Scientific G24 environmental incubator shaker at 200 rpm. Unless mentioned otherwise, overnight cultures were diluted to 0.5 OD_{600} measured with a Spectronic™ 200 from ThermoFischer Scientific. Single and dual-species biofilms at the air-liquid interface were grown in LBNS (LB-no salt) at 30 °C. For the dual-species biofilms, two initial ratios were tested. Ratio "1:1" means each species diluted to the same OD_{600}=0.5 was in equal quantity initially, while for ratio "100:1" there was only 1% of *P. fluorescens* to start with.

4.2.2 Planktonic and biofilm growths

Overnight cultures were diluted (1:100) in fresh LBNS media. The bacterial growth was monitored by reading the optical density at 600 nm (OD_{600}) during 48 h at 30 °C in both standing and shaking culture conditions. At specific time points, serial dilutions were performed and plated on LB agar and incubated overnight at 30 °C for the enumeration of viable bacteria (CFU/ml). Measurements were done on biological duplicates and technical triplicates and the mean ± SEM (standard error of the mean) was represented.

4.2.3 Congo Red agar tests

Overnight cultures were diluted to 0.5 OD_{600} and for dual-species biofilms, the diluted bacterial suspensions were mixed before spotting 10 µl onto Congo Red (CR) agar plates – composed of 1% tryptone (Difco), 1% agar (Difco), 40 µg/ml Congo Red (Sigma) and 1.5 µg/ml Brilliant Blue R (Sigma). The plates were incubated at 30 °C for 7 days.

4.2.4 Evaluation of *B. licheniformis* sensitivity to *P. fluorescens*

Sensitivity of *B. licheniformis* to *P. fluorescens* was evaluated by comparing single cultures to co-cultures of each bacteria in LBNS and by measuring bacterial population (CFU/ml) after 24 h.

The effect of *P. fluorescens* spent media on *B. licheniformis* growth was assessed using the protocol previously described by Khare et al. [53]. Briefly, *P. fluorescens* was grown overnight at 37 °C and diluted to 1:100 in LBNS for another 22 h at 37 °C under shaking. After centrifugation during 20 min at 5000 g, the supernatant was then filtered through a 0.20 µm filter Filtropur S (Sarstedt) and stored at -20 °C. *B. licheniformis* was diluted to 1:10 and grown with 50% of *P. fluorescens* spent media and 50% fresh LBNS at 30 °C under shaking. The bacterial growth was monitored by reading the optical density at 600 nm. Measurements were done on biological and technical triplicates.

4.2.5 Biomass quantitative analysis

The total biomass of biofilm formed in LBNS at 30 °C for 48 h was measured by staining the pellicle with crystal violet (CV), using a modified protocol from Ma et al. [141]. Non-adhering cells were carefully removed from the glass tubes, leaving only the pellicle. After two washes with sterile water, 1 ml of 0.1% CV was added. After 15 min of staining, the CV was removed, the tube was washed with water and 3 ml of 70% aqueous ethanol were added. The optical density of the eluted crystal violet was measured with a BioTek EL800 microplate reader at 595 nm.

To assess the number of viable bacteria within the biofilm, the non-adhering cells were again carefully removed and the pellicle biofilm was rinsed with PBS. The biofilm was treated by sonication to retrieve bacteria, using the method previously described by Brandi et al. [142]. The biofilm was subjected to two rounds of 12 one-second pulses at 20% power using an UltraSonics Sonicator cell disrupter Vibra-cell, equipped with a small-tip probe from Sonics & Materials Inc. Serial dilutions were plated and incubated at 30 °C overnight for bacterial counts. Sonication did not affect cell viability, as assessed by bacterial count on overnight cultures before and after sonication (**Fig. S1 in Supporting Information)**.

All tests were carried out in biological and technical triplicates. Measurements were done on biological duplicates and technical triplicates and the mean ± SEM was represented.

4.2.6 Fluorescence microscopy

To visualize bacteria within the biofilm formed at the air-liquid interface, biofilms were grown in 3 ml LBNS in glass tubes for 48 h or 72 h at 30 °C, at an initial dilution of 1:100 (**Fig. S2**). The media was then carefully removed and the pellicle washed with sterile water. The LIVE BacLight™ Bacterial Gram Stain Kit (ThermoFischer Scientific) was used to stain the bacteria and differentiate between Gram positive and negative bacteria. This kit is composed of two dyes - Syto 9 that stains both types of bacteria in green and hexidium iodide that stains only Gram positive bacteria in red - added in equal quantity to the pellicle. After 15 min in the dark at room temperature, part of the pellicle was placed on a glass slide and visualized under an inverted Nikon Eclipse Ti2 fluorescent microscope.

4.2.7 Interfacial rheology

To measure the viscoelastic properties of the biofilm at the air-liquid interface, a rotational rheometer (Physica MCR 501, Anton-Paar) combined with the bicone flow geometry was used (**Fig. S3)**. The interfacial bicone shear cell is made of glass and surrounded by a stainless steel external cover to keep the temperature constant. The temperature was maintained at 30 °C with a Peltier plate. A detailed methodology to obtain the interfacial properties was explained by Erni et al. [66] and was employed by Rühs et al. to quantify the response of bacterial biofilms at the air-liquid interface [69]. Briefly, an electrical current is applied to oscillate the rotating bicone at a constant deformation amplitude and a stress-response is measured. The elastic and viscous moduli quantifying the biofilm strength are calculated through the shear-strain relationship. The bulk and interface are assumed to be decoupled – with the Boussinesq number Bo between 50 and 40,000 (Bo = interface drag/subphase drag). Since the Boussinesq number is low during the first hours of the biofilm development ($50<B<100$), a flow field analysis was applied for the bicone geometry to remove the bulk influence and allowing the calculation of the absolute interfacial properties.

For our experiments, 115 ml of liquid media LBNS was introduced with a syringe in the shear cell geometry and 1 ml of bacterial suspension previously diluted to 0.5 OD_{600} was added. The rotating geometry, i.e. the bicone, was positioned at the air-liquid interface by using the normal force-

assisted surface detection test. Once the disk exactly pinned the interface, a time sweep test was started with the bicone oscillating at a strain (deformation) amplitude γ_0 = 1% and frequency ω = 0.5 rad/s for 48 h and 72 h to monitor the biofilm growth. When *B. licheniformis* was given a lead time, *P. fluorescens* suspension was carefully introduced through a syringe needle into the shear cell geometry at a given time.

To validate the viscoelastic behavior and verify that the tests were performed in the linear regime and did not perturb the biofilm, frequency and strain amplitude sweeps were respectively carried out at the end of the time sweep test. The graphs are representative of three to four different assays.

4.2.8 Scanning electron microscopy (SEM)

To perform SEM on mature biofilms, pellicles were transferred on glass cover slips coated with 0.1% poly-l-lysine. Biofilms were then fixed overnight at 4 °C with a solution of 2.5% glutaraldehyde and 4% formaldehyde in 1X PBS. The pellicles were then washed three times with 1X PBS and a solution of 0.1% osmium tetroxide was added, followed by 1 h incubation at 4 °C. Three washes of 1X PBS (5 min each) were performed to remove the osmium solution. Pellicles were dehydrated with a series of 30%, 50%, 70%, 80%, 90%, 95% and 100% ethanol treatments of 15 min each. Finally, the samples were dried using a critical point dryer (CPD) and coated with a thin layer of conductive carbon. They were imaged using a JEOL JSM 7400 field emission scanning microscope.

4.3 Results

4.3.1 Planktonic and biofilm growth rates in single and co-cultures

The growth curve of each species under shaking condition at 30 °C was evaluated in LBNS (**Fig. 4-1a**). After 24 h, the optical density (OD) of the *B. licheniformis* culture was half of that of *P. fluorescens*, but both cultures were similar after 48 h. The CFU/ml was determined at 24 h for

single and co-cultures - each species was added in equal quantity initially for the co-culture (**Fig. 4-1b**). The CFU/ml values for *B. licheniformis* in mono-culture (9.11×10^7 CFU/ml) were significantly lower than *P. fluorescens* (3.65×10^9 CFU/ml), indicating that *P. fluorescens* grew faster than *B. licheniformis* under these conditions. The optical density and CFU/ml were also measured in static conditions at 30°C. *B. licheniformis* growth was again slower than *P. fluorescens* reaching 7.67×10^7 CFU/ml, while *P. fluorescens* was 1.43×10^9 CFU/ml.

No significant decrease was found when *B. licheniformis* was co-cultured with *P. fluorescens*, showing that the presence of *P. fluorescens* did not have an impact on *B. licheniformis* growth and no bactericidal effect was observed. Additional measurements were made to verify that *P. fluorescens* did not produce molecules impacting *B. licheniformis* growth by monitoring the bacterial concentration of *B. licheniformis* in presence of *P. fluorescens* spent media (**Fig. S4)**.

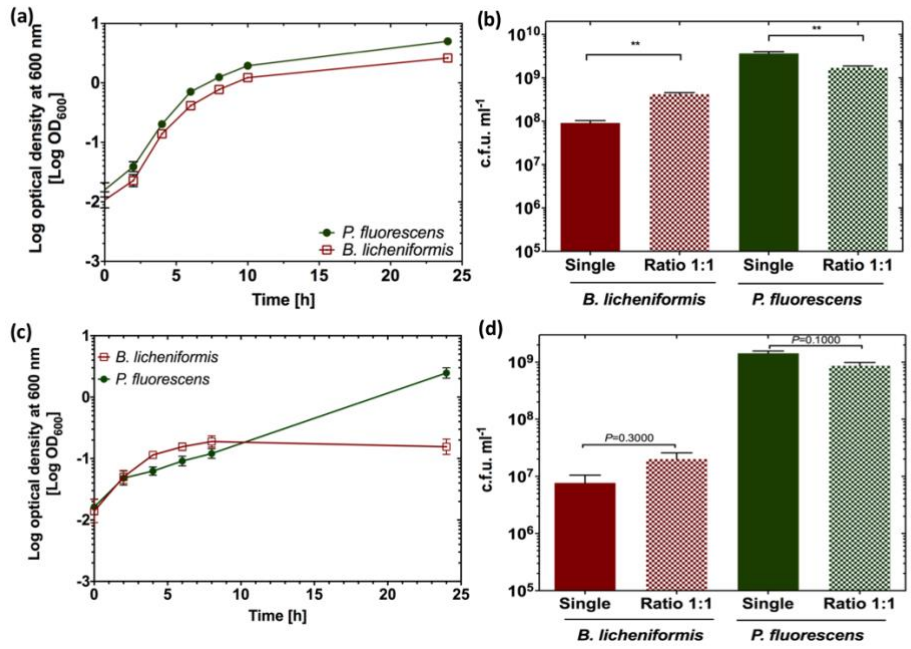

Figure 4-1 Planktonic (a and b) and biofilm (c and d) growths of *B. licheniformis* (•) and *Pseudomonas fluorescens* (O). Overnight cultures were grown for 48 h under shaking culture conditions at 30 °C for (a) and (b). The optical density was measured at selected times for (a) and (c), and the CFU/ml at 24 h for single and co-cultured bacteria at an initial ratio 1:1 in (b) and (d).

** statistically significant difference, $p < 0.0001$

4.3.2 Evaluation of biofilm formation with Congo Red agar

Biofilm formation was first analyzed on Congo Red (CR) agar to provide an initial qualitative understanding of the biofilm composition. Colony biofilms were evaluated after 7 days of growth at 30 °C (**Fig. 4-2**). *B. licheniformis* developed a wrinkled and rough colony biofilm, indicating a strong biofilm with the probable presence of amyloid-like polymers, as previously reported [132]. For *P. fluorescens*, only the center of the colony showed a wrinkled morphology, with a smooth white outer ring. The dual-species biofilm containing an equal amount of each bacteria initially, i.e. the ratio 1:1, exhibited a similar morphology to *P. fluorescens* alone, with a white outer ring. As the *P. fluorescens* initial content decreased to 1%, i.e. the ratio 100:1, this white outer ring became thinner. This first analysis on CR plates indicated that *P. fluorescens* seemed to be the most prominent species in the dual-species biofilm since the morphology of the ratio 1:1 colony after 7 days was comparable to *P. fluorescens* alone.

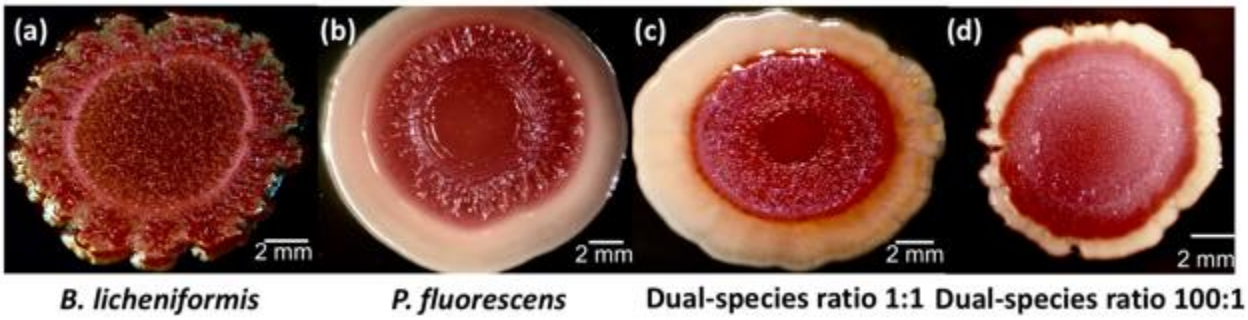

Figure 4-2 Colony biofilms grown on CR agar plates at 30 °C during 7 days: (a) *B. licheniformis*, (b) *P. fluorescens*, (c) dual-species biofilm ratio 1:1, and (d) dual-species biofilm ratio 100:1.

4.3.3 Quantitative analysis of the mature biofilm composition

The composition of the mature pellicle at 48 h was evaluated by quantifying the total biomass content and the number of viable bacteria. The biofilms biomass was quantified by measuring the OD after staining the pellicle with crystal violet (CV). The results indicated that the biomass of *B. licheniformis* biofilms was significantly higher than that of *P. fluorescens* (**Fig. 4-3a**). The OD_{595} values for *B. licheniformis* and *P. fluorescens* single-biofilms were 5.7 and 3.4 respectively. The

biomass was similar to the *P. fluorescens* value in the dual-species biofilms at a 1:1 ratio. However, when *P. fluorescens* content was decreased to 1% (ratio 1:100), the dual-species biofilm biomass increased to a level similar to *B. licheniformis*.

The bacterial content in single and dual-species biofilms was assessed by bacterial counts on the washed and sonicated pellicles (**Fig. 4-3b**). In single-species biofilms, the bacterial content was significantly higher for *P. fluorescens* (8.4×10^8 CFU/ml) compared to *B. licheniformis* (5.7×10^7 CFU/ml). The majority of bacteria present in the dual-species with an initial ratio 1:1 was *P. fluorescens* with 8.1×10^8 CFU/ml and only 1.2×10^7 CFU/ml of *B. licheniformis*. With only 1% of *P. fluorescens* initially present, the final bacterial content was still higher for *P. fluorescens* with 5.9×10^8 CFU/ml, indicating a strong presence of *P. fluorescens* despites its low initial concentration. However, the contribution of *B. licheniformis* significantly increased at 4.0×10^7 CFU/ml.

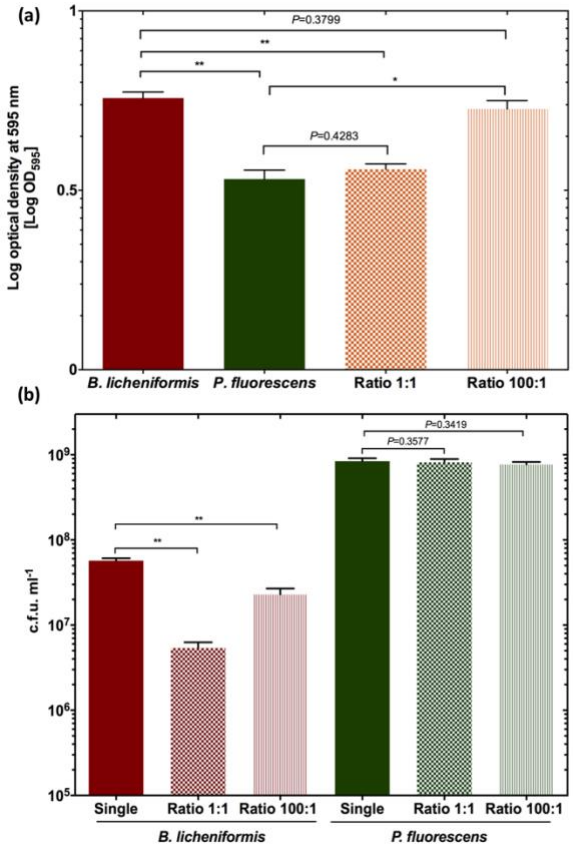

Figure 4-3 Biofilm composition after 48 h for single-species *Bacillus* and *Pseudomonas* biofilms, and dual-species biofilms (*Bacillus*:*Pseudomonas*) at ratio 1:1 and ratio 100:1. (a) Biomass of the total biofilms quantified by measuring the OD595 of crystal violet (CV) stained biofilms; (b) CFU/ml of each species within the sonicated biofilms.

* statistically significant difference, $p = 0.0003$

** statistically significant difference, $p < 0.0001$

4.3.4 Imaging of bacterial populations within single and dual-species biofilms

To visualize and assess the presence of bacterial population within the single and dual-species biofilms, the mature pellicles were stained after 48 h with a Gram fluorescent kit (**Fig. 4-4**). This kit was previously successfully applied to stain Gram (+) and Gram (-) bacteria [143]. The combination of two dyes allowed the simultaneous imaging of all bacteria in green and only the

Gram-positive bacteria *B. licheniformis* in red. *B. licheniformis* assembled in a well-organized network with the rod-shaped bacteria arranged in chains (Fig. 4-4a), an organization also observed for the pathogen *Bacillus anthracis* [144]. The organization within the *P. fluorescens* biofilm was quite different, with a higher concentration of bacterial cells packed together rather than aligned (Fig. 4-4b). In the dual-species biofilms, when the initial ratio was 1:1, the dominant bacteria was *P. fluorescens* with very few bacterial cells of *B. licheniformis* in red (Fig. 4-4c). Once the initial content of *B. licheniformis* was increased in the ratio 100:1, the Gram-positive bacterial cells were able to connect and form a structured network in the mature dual-species biofilm (Fig. 4-4d). The microscopic images supported the quantitative analysis of the mature biofilm, as the number of *B. licheniformis* bacteria increased when the initial content was increased from 50% to 99% (ratio 1:1 to 100:1). As expected for the biomass data, *P. fluorescens* was still present in great amount in the mature biofilm despite adding only 1% initially.

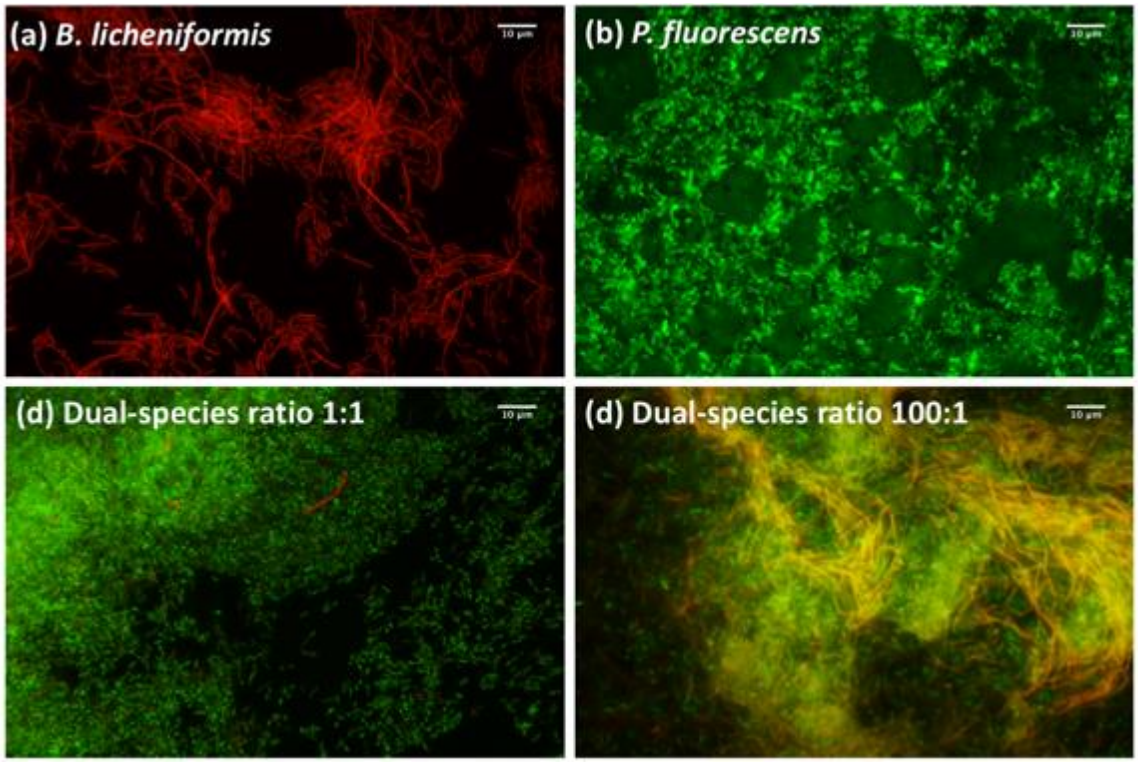

Figure 4-4 Fluorescence microscopy images: biofilms were stained with Syto 9 and hexidium iodide to visualize Gram + and Gram – bacteria: (a) *B. licheniformis*, (b) *P. fluorescens*, (c) dual-species biofilm ratio 1:1, (d) dual-species biofilm ratio 100:1 (scale bar: 10µm).

4.3.5 Evolution of biofilms viscoelasticity during pellicle formation

To probe and understand the interactions occurring in our dual-species biofilm model, we measured the viscoelastic properties of the pellicle during its formation at the air-liquid interface in real-time. We monitored the elastic and viscous moduli for each single species biofilm and the two ratios for the dual-species biofilms (**Fig. 4-5**).

The results showed that the single and dual-species biofilms forming at the air-liquid interface were elastic networks with a significantly higher interfacial elastic modulus G'_i compared to the interfacial viscous modulus G''_i, since the ratio G"/G' was around 0.2 (**Table S1**), as previously reported for other biofilms [43, 67, 69]. A higher value for the elastic modulus G'_i indicates a solid-like structure, thus strong biofilms at the air-liquid interface. The elasticity observed for the media alone (LBNS) was most probably due to proteins unfolding at the interface. *B. licheniformis* formed a stronger viscoelastic pellicle, compared to *P. fluorescens*, reaching a G'_i value of 0.60 ± 0.15 Pa·m after 48 h. In comparison, the elastic modulus of *P. fluorescens* was 30 times lower, but it formed its mature pellicle faster than *B. licheniformis,* with a characteristic sharp decrease at 20 h just before reaching its G'_i plateau value of 0.02 ± 0.01 Pa·m, 10 h before *B. licheniformis.*

In the dual-species biofilm, at a ratio 1:1, the biofilm viscoelastic characteristics were similar to *P. fluorescens*. It reached its plateau value after 24 h with a G'_i value of 0.01 ± 0.007 Pa·m, similar to *P. fluorescens* alone. The sharp decrease at about 20 h observed for the *P. fluorescens* biofilm formation was still present, although it was attenuated. This indicates that *P. fluorescens* is the main bacteria contributing to the biofilm strength in the dual-species biofilm.

When the initial content of *P. fluorescens* was decreased to only 1% (ratio 100:1), the dual-species biofilm viscoelasticity increased with G'_i, reaching 0.06 ± 0.02 Pa·m. However, despite the low initial content of *P. fluorescens*, this biofilm was unable to regain the full elasticity of *B. licheniformis* alone, since G'_i remained about 10 times lower.

By monitoring the viscoelastic properties over an extended period of 72h, an increase in the elastic modulus is observed for *P. fluorescens* and dual-species biofilms. Indeed, after reaching a first plateau at 35 h (G'_i = 0.02 Pa·m), the viscoelastic properties of the dual-species biofilm started to increase again until it reached a mature state at 72 h with an elastic modulus of G'_i = 0.48 Pa·m

(Fig. 4-5). In comparison, the single *P. fluorescens* biofilm displayed similar rheological behavior and final value over 72 h - the elasticity increased again after 48 h, until it reached a second plateau at 72 h (G'_i = 0.57 Pa·m). For the single *B. licheniformis* biofilm, the mature state was reached at 48 h and no significant increase in the rheological properties was observed between 48h and 72 h.

To summarize, *B. licheniformis* formed a stronger pellicle that was mature at 48 h, but in the dual-species biofilm, when the initial ratio of the two species was 1:1, *P. fluorescens* was the dominant bacteria and contributed the most to the viscoelastic properties during the first 48 h. A second equilibrium was reached when the viscoelastic properties increased for *P. fluorescens* single and the dual-species ratio 1:1 after 72 h.

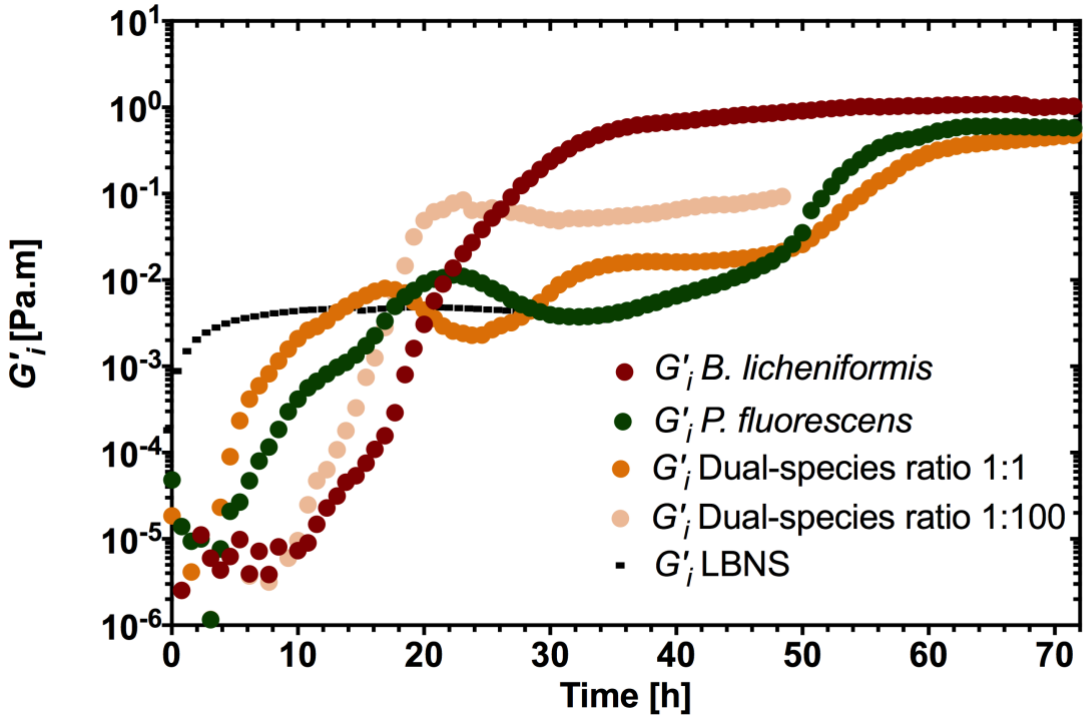

Figure 4-5 Development of the interfacial viscoelastic properties of biofilms formed at the air-liquid interface by media alone (black), *B. licheniformis* (red), *P. fluorescens* (green) and dual species ratio 1:1 (orange) and ratio 100:1 (beige).

4.3.6 Effect of time on the dual-species biofilm composition

Based on the results obtained from the microscopic and quantitative analyses of the dual-species biofilm – bacterial content and viscoelastic properties – and of planktonic and biofilm growths, we conclude that *P. fluorescens* is the dominant species in the biofilm during the first 48 h even when inoculated at 1% initially, due to its faster growth compared to *B. licheniformis*. To support this conclusion, we delayed the addition of *P. fluorescens* to give *B. licheniformis* time to colonize the interface and to form a biofilm with properties comparable to the single *B. licheniformis* film **(results presented in Fig S5)**.

The biofilm composition was analyzed by bacterial count at 72 h (**Fig. 4-6a**), showing that *B. licheniformis* and *P. fluorescens* were present in equal amount in the 1:1 dual-species biofilm (8×10^7 CFU/ml), which indicated some mortality from *P. fluorescens* and a stronger presence of *B. licheniformis* within the biofilm. These results at 72h were compared with the CFU/ml at 48h, showing the increase in bacterial content of *B. licheniformis* in the dual-species biofilm, while *P. fluorescens* decreased (**Fig. S6**). Microscopic fluorescence showed the presence of *B. licheniformis* arranged in chains surrounded by *P. fluorescens* (**Fig. 4-6b**). Thus two stable states were observed in our dual-species biofilm, the first corresponding to *P. fluorescens* dominance during the first 48 h and the second with the presence of both bacteria at 72 h in the mature dual-species biofilm.

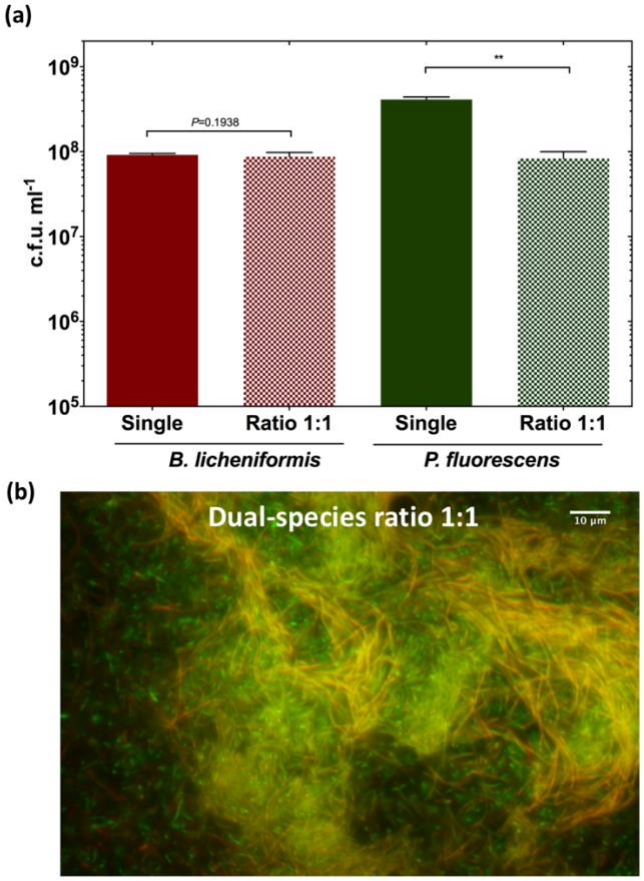

Figure 4-6 Composition of the dual-species at 72 h: (a) CFU/ml of the dual-species biofilm ratio 1:1; (b) fluorescence microscopic image of the dual-species biofilm ratio 1:1 (scale bar: 10 µm).

** statistically significant difference, $p < 0.0001$

4.3.7 Single and dual-species biofilm microstructure

To further characterize the single and dual-species biofilms, their microstructure was examined by SEM at 48 h and 72 h, respectively (**Fig. 4-7**). *B. licheniformis* bacterial cells are arranged in chains embedded in a thick extracellular matrix (Fig. 4-7a), as revealed also by fluorescence microscopy (Fig. 4-4a). A different architecture was observed for the *P. fluorescens* biofilm at 48 h with a thinner ECM structure (Fig. 4-7b). The *P. fluorescens'* microstructure was conserved in the 1:1 dual-species biofilm where the two bacterial populations were also observed, supporting our previous observation indicating that *P. fluorescens* contributed the most to the biofilm properties

at 48 h. While both bacterial populations were observed at 72 h, SEM revealed that the biofilm network appeared denser in the *P. fluorescens* and dual-species biofilms (Fig. 4-7b-c bottom).

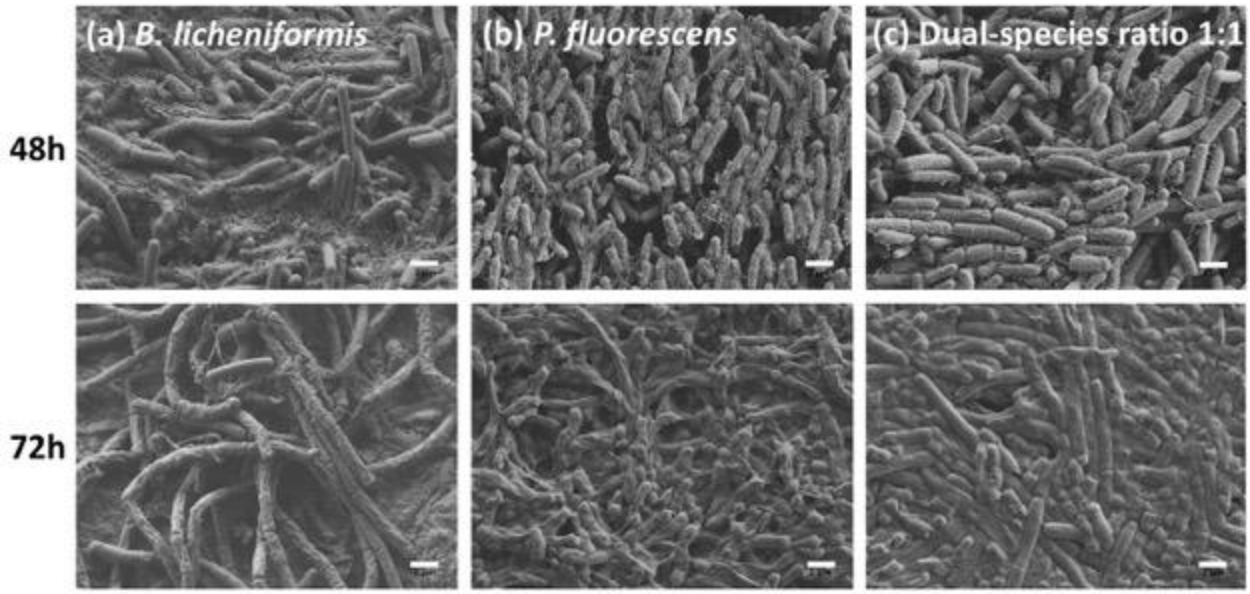

Figure 4-7 SEM images of the single and dual-species biofilms of (a) *B. licheniformis*, (b) *P. fluorescens*, and (c) dual-species ratio 1:1, at 48 h (top) and 72 h (bottom).

4.4 Discussion

The impact of bacterial interactions on the multispecies biofilms properties is very complex to unravel. In this work we studied a dual-species biofilm model formed by *B. licheniformis* and *P. fluorescens* – two common contaminants in the dairy industry – at the air-liquid interface. We hypothesized that growth kinetics is the major factor contributing to the dual-species biofilm composition. During biofilm growth, we observed that *P. fluorescens* was growing faster than *B. licheniformis* (Fig. 4-1a). This is consistent with previous research linking growth rates in *Staphylococcus* multispecies biofilms **[52]**. The CR colonial morphology of the dual-species biofilm was alike *P. fluorescens* colony biofilm. The quantitative analysis of the mature pellicle also showed that the dual-species biofilm composition was indeed similar to the *P. fluorescens*

biofilm with a low biomass content and an important *P. fluorescens* bacterial content. Fluorescence microscopic images were showing a dense and packed structure formed by *P. fluorescens* in the dual-species biofilm with equal initial amount of each bacteria. By using interfacial rheology, we observed that the viscoelastic profile of the dual-species biofilm (1:1 initial relative bacteria contents) at the air-liquid interface was almost identical to the *P. fluorescens* single species biofilm after 48 h. The macroscale rheological properties were supported by the biofilm microscale architecture that revealed that *P. fluorescens* single and the dual-species pellicles showed less extracellular matrix compared to the single *B. licheniformis* biofilm, where bacterial cells were embedded in a denser extracellular matrix. .

When the *P. fluorescens* initial content was decreased to 1%, the dual-species biofilm partially regained the *B. licheniformis* biofilm elasticity profile and biomass. The dominance of *P. fluorescens* in the dual-species biofilm even at very low initial content was explained by its faster growth during biofilm culture. In the biofilm state, the quantitative analysis of the pellicle indicated that the major contribution in *P. fluorescens* biofilm came from a high number of bacterial cells, while in *B. licheniformis* biofilm, there were less bacteria but they organized in chains and may secrete a stronger extracellular matrix that contributed to the biofilm biomass. No bactericidal effect of *P. fluorescens* on *B. licheniformis* was observed, either by direct contact or by secreted proteins. When *B. licheniformis* was given a 24 h head start, *P. fluorescens* was not able to interfere in the biofilm formation.

These findings supported our initial hypothesis stating that the biofilm growth rate was the major factor in the model dual-species biofilm composition after 48 h, with *P. fluorescens* colonizing faster the interface and being the dominant specie at 48 h. By monitoring the biofilm viscoelastic properties for longer period, a second equilibrium was reached after 72 h for both *P. fluorescens* single and the dual-species biofilms. Note that an increase in the wet weight between 48 and 72 h was also previously observed for a *P. fluorescens* biofilm at the air-liquid interface [45]. The quantitative and microscopic analysis revealed a denser extracellular matrix with an increase in *B. licheniformis* contribution to the dual-species biofilm at its mature state, i.e. 72 h. However, we were unable to determine whether *B. licheniformis* was also contributing to the viscoelastic properties since both single-species biofilms reached similar values at 72 h.

By relating the mechanical properties to the microscale structures during the biofilm formation, we were able to understand the growth competition within our model dual-species biofilm and distinguish two equilibriums in the dual-species biofilm: *P. fluorescens* was the dominant species during 48 h, then the biofilm became denser with an apparent increase in the ECM material and the coexistence of the two bacterial species together. These findings highlight the importance of real-time analysis which allows relating the planktonic growth factor to the competition within our dual-species biofilm system.

Because these bacteria are commonly found in the environment, it would be relevant to also study the impact of environmental changes and different surfaces on the biofilm composition and mechanical properties to find the appropriate treatment to disperse them. For example, the competition observed for the interface in our model could implicate that the bacteria are competing for the oxygen at the interface - it was previously demonstrated that oxygen triggers movements toward the air-liquid interface for *P. aeruginosa* and *B. subtilis* pellicles [145]. Finally, this work characterized a model non-pathogenic dual-species biofilm, it would be of interest to incorporate a pathogenic bacteria to this study to examine the impact of environmental bacteria - especially the probiotic *B. licheniformis* - against pathogens.

ACKNOWLEDGMENTS: We thank Martin Clément (Department of Microbiology, Infection and Immunology, Université de Montréal) for kindly providing *P. fluorescens* C5-10. We also thank the Electronic Microscopy Platform at Université de Montréal (Dr. Antonio Nanci) for their assistance in electron microscopy analyses.

4.5 Supporting information

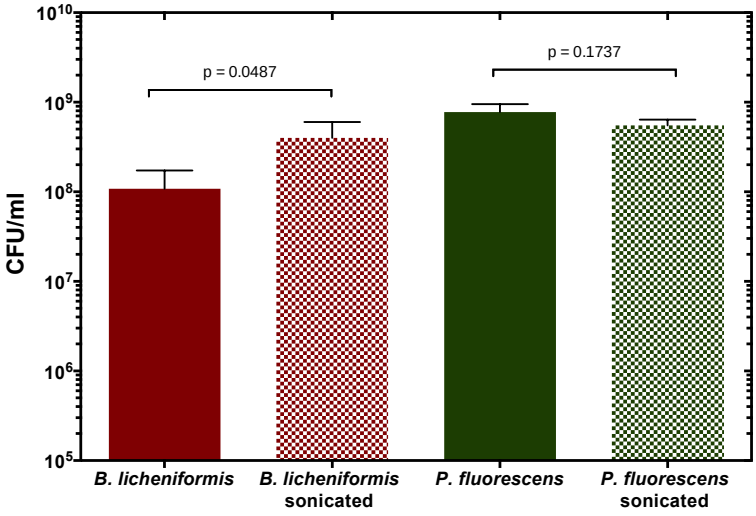

Figure S1 Colony forming units (CFU/ml) before and after sonication of bacterial suspensions for *B. licheniformis* and *P. fluorescens* overnight cultures.

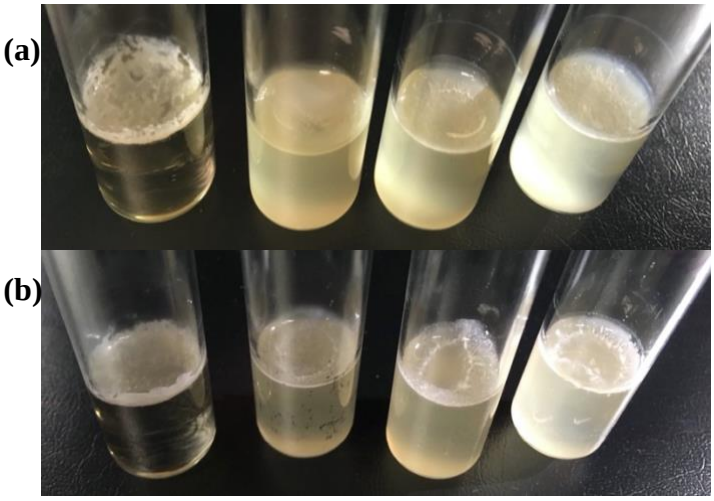

Figure S2 Biofilms of from left to right *B. licheniformis*, *P. fluorescens*, dual-species ratio 1:1 and 100:1, grown at the air-liquid interface in glass tubes at 30 °C for (a) 48 h and (b) 72 h.

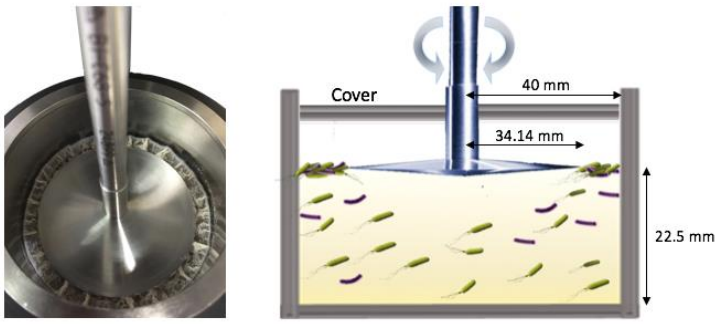

Figure S3 Interfacial rheology experimental setup: (a) Top view of the interfacial rheology system (IRS) with *B. licheniformis* mature biofilm attached to the bicone and (b) schematic of the interfacial rheology flow cell with the bicone (adapted from Rühs et al. [69]).

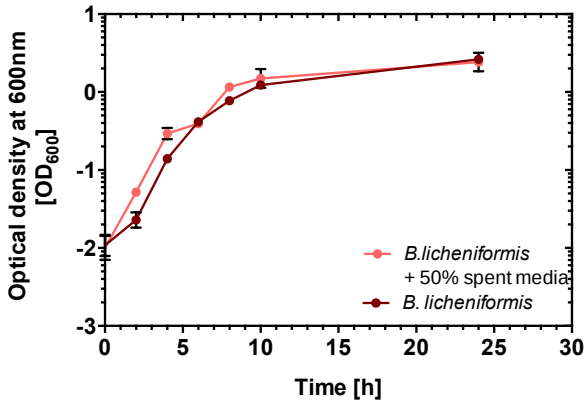

Figure S4 Optical density of B. licheniformis as a function of time (single culture), or in the presence of *P. fluorescens* spent media.

Table S1 Values for G"/G', the damping factor, at 72h for the single and dual-species biofilms.

Sample	***B. licheniformis***	***P. fluorescens***	**Dual-Species Ratio 1:1**
G_i"/G_i' at 72h	0.232	0.215	0.238

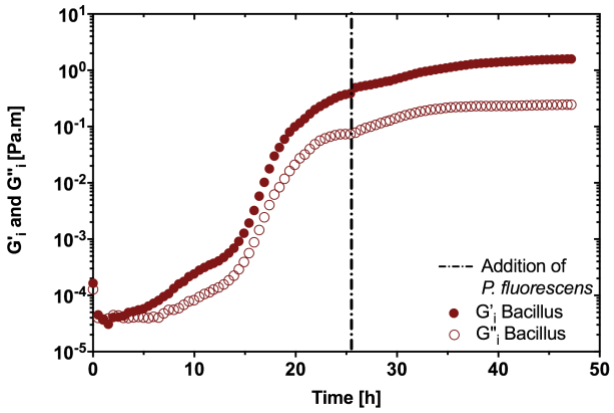

Figure S5 Viscoelastic moduli of *B. licheniformis* biofilm after delayed addition of *P. fluorescens* at 24 h.

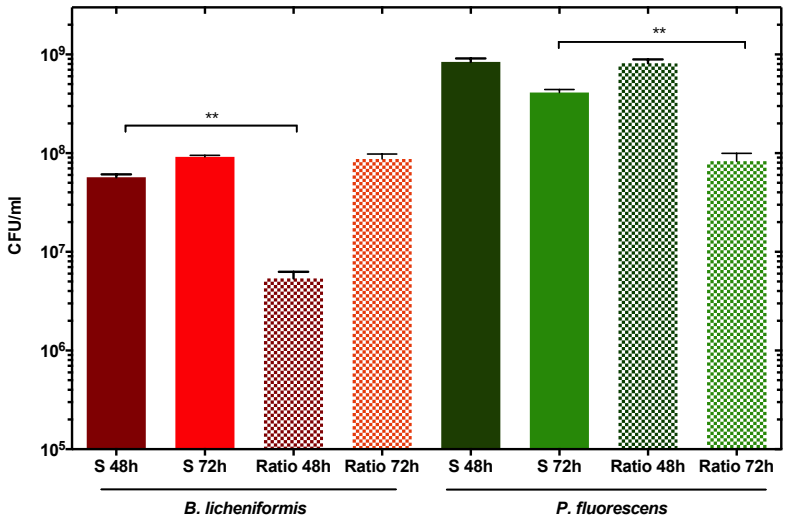

Figure S6 Comparison of the pellicle bacterial composition CFU/ml at 48h and 72h.

** statistically difference $p < 0.0001$

CHAPTER 5 ARTICLE 2: MECHANICAL AND MICROSTRUCTURAL INSIGHTS OF VIBRIO CHOLERAE AND ESCHERICHIA COLI DUAL-SPECIES BIOFILM AT THE AIR-LIQUID INTERFACE

Authors: Clémence Abriat,[a,b] Kyle Enriquez,[c] Nick Virgilio,[a] Lynette Cegelski,[c] Gerald G. Fuller,[d] France Daigle,[b] Marie-Claude Heuzey[a#]

[a]CREPEC, Department of Chemical Engineering, Polytechnique Montréal, Montréal, Québec, Canada

[b]Department of Microbiology, Infection and Immunology, Université de Montréal, Montréal, Québec, Canada

[c]Department of Chemistry, Stanford University, Stanford, California, United States

[d]Department of Chemical Engineering, Stanford University, Stanford, California, United States

#Corresponding author: marie-claude.heuzey@polymtl.ca

Published in *Colloids and Surfaces B: Biointerfaces* 2020 Apr;188:110786

GRAPHICAL ABSTRACT

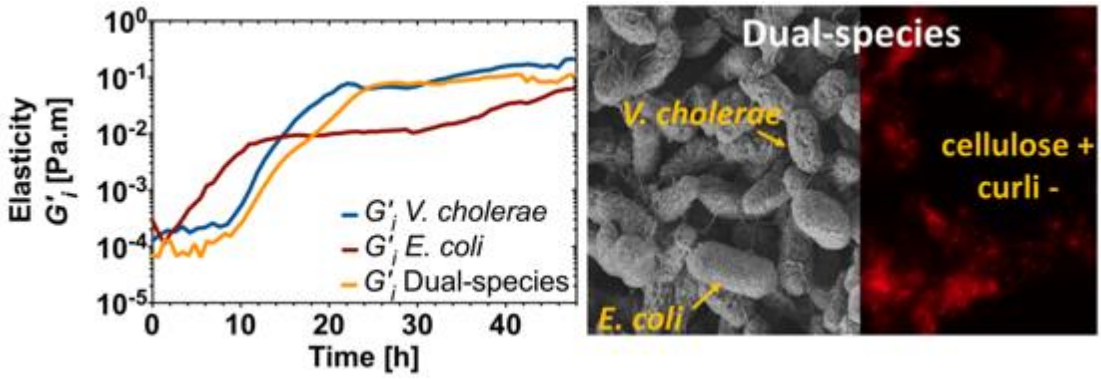

ABSTRACT : Biofilm is the dominant microbial form found in nature, in which bacterial species are embedded in a self-produced extracellular matrix (ECM). These complex microbial communities are responsible for several infections when they involve multispecies pathogenic bacteria. In previous studies, interfacial rheology proved to be a unique quantitative technique to follow in real-time the biofilm formation at the air-liquid interface. In this work, we studied a model system composed of two bacteria pathogenic capable of forming a pellicle biofilm, *V. cholerae* and *E. coli.* We used an integrated approach by combining a real-time quantitative analysis of the biofilm rheological properties, with the investigation of major matrix components and the pellicle microstructure. The results highlight the competition for the interface between the two species, driven by the biofilm formation growth rate. In the dual-species biofilm, the viscoelastic properties were dominated by *V. cholerae,* which formed a mature biofilm 18 hours faster than *E. coli*. The microstructure of the dual-species biofilm revealed a similar morphology to *V. cholerae* alone when both bacteria were initially added at the same amount. The analysis of some major ECM components showed that *E. coli* was not able to produce curli in the presence of *V. cholerae,* unless enough time was given for *E. coli* to colonize the air-liquid interface first. *E. coli* secreted phosphoethanolamine (pEtN) cellulose in the dual-species biofilm, but did not form a filamentous structure. Our pathogenic model system demonstrated the importance of the biofilm growth rate for multispecies biofilm composition at the air-liquid interface.

5.1 Introduction

Biofilms are the dominant microbial form in many environments used by bacteria as a survival strategy [1, 146]. These microbial communities are bacteria embedded in a self-produced extracellular matrix (ECM). The ECM comprises polysaccharides, proteins and extracellular DNA, and acts as a protective barrier, making biofilms extremely resilient to antimicrobial treatments in case of pathogenic infections [114, 116, 117].

The pathogen *Vibrio cholerae* is the causative agent of cholera [147, 148]. This Gram-negative bacteria is found predominantly in aquatic environments and when it invades the human host – through contaminated food or water – it colonizes the small intestine and can then cause severe diarrhea [149-152]. *V. cholerae* is capable of forming resilient biofilms resistant to stresses from

the environment and the host [153, 154]. It has been previously established that the major components from the extracellular matrix are the Vps polysaccharide and three proteins: RbmA, Bap1 and RbmC [155]. Hollenbeck et al. provided a mechanical insight of the *V. cholerae* pellicle by interfacial rheology correlated to microscale insights and they determined that Bap1 was an essential component of the matrix strength [67]. Although this pathogen has been extensively studied over the past year, little is still known about its interactions with other bacterial species. For example, some strains of *V. cholerae* use a type VI secretion system (T6SS) under certain conditions to kill species such as *E. coli* and *S.* typhimurium [156].

E. coli is a well-studied Gram-negative bacteria often used as a model organism for biofilm formation studies [157]. Recently, Thongsomboon et al. established that the cellulose produced naturally by commensal and pathogenic *E. coli* strains is a modified phosphoethanolamine (pEtN) cellulose [158]. pEtN cellulose and amyloid curli fibers are essential structural components of the extracellular matrix in *E. coli* biofilms, with pEtN cellulose contributing to the cohesion and elasticity [27], while curli mediates the adhesion to surfaces or cells. Curli fibers contribute to the biofilm's mechanical properties and are required for the biofilm formation at the air-liquid interface (pellicle) [43] .

The mechanical strength of biofilms depends on the ECM molecular composition and structural organization. Interfacial shear rheology is a powerful technique to measure the viscoelastic changes within complex fluids such as polymers, proteins or surfactants. As biofilms are viscoelastic materials, interfacial rheology has previously been successfully applied to track changes in the mechanical properties as the biofilm forms at the air-liquid interface, in real-time [43, 67, 69, 159]. Studies showed that bacterial species exhibited unique viscoelastic changes and that their mechanical properties were dependent on the environmental conditions such as pH, temperature or media [69]. By correlating the rheological analysis with the molecular composition of the biofilms, some key components – for example Bap1 for *V. cholerae* and curli for *E. coli* biofilms - were highlighted for their role in the pellicle strength and thus as potential targets for biofilm inhibition [43, 67].

Bacteria tend to live in mixed-species communities and mixed-species biofilm properties can differ sometimes significantly from single-species. Recently, Yannarell et al. showed in a dual-species biofilm composed by *Bacillus subtilis* and *Pseudomonas agglomerans* that essential matrix

components to form a monoculture biofilm were not required to obtain a wrinkled biofilm when cocultured [75]. Rheological properties of the dual-species biofilm were a combination of both single species biofilms.

The pellicle biofilms can also have different characteristics from biofilms grown in microtiter plates. We have shown previously the role of growth kinetics in the competition for the interface in an environmental dual-species pellicle biofilm using interfacial rheology and microscale analysis [160]. However, despite mixed-species biofilms being predominant in nature, there is a need for a deeper knowledge regarding the interactions between species and the effect on the biofilm development, as most studies have focused on single biofilm models, especially for pellicle biofilms.

In this work we studied the mechanical properties and molecular composition of a dual-species biofilm at the air-liquid interface, composed by the two model organisms *V. cholerae* and *E. coli.* We used interfacial shear rheology to measure the mechanical properties as the pellicle formed at the air-liquid interface and compared the unique viscoelastic profile for each single-species organism to the dual-species biofilms. We analyzed the proteins and pEtN cellulose content in both single and dual-species biofilms to understand the type of interactions between the two bacteria at the air-liquid interface. Using interdisciplinary approaches, we highlight the competition for the interface between the bacteria.

5.2 Methods

5.2.1 Bacterial strains and growth conditions.

A rugose-variant of *V. cholerae* El-Torr A1552 was used along with *E. coli* AR3110 [27], as well as the mutant W3110 Δ*csgBA*(curli deficient). All the strains were grown at 37 °C on Luria-Bertani (LB) agar plate from -80 °C stocks. Overnight cultures were done in LB, shaking at 37 °C. Biofilms assays were perfomed in YESCA broth at 26 °C, from a 1:1000 dilution of overnight culture.

5.2.2 Interfacial rheology

The viscoelastic properties of the biofilms at the air-liquid interface were measured by interfacial shear rheology. The measurements were made with a du Noüy ring geometry – a thin platinum/iridium (Pt/Ir) wire ring – combined to a double-wall ring Teflon flow cell, using a AR-G2 rheometer (TA Instruments), as previously described [67]. Briefly, the flow cell was filled with 10 ml of YESCA media and the overnight culture was added to a dilution of 1:1000. The du Noüy ring geometry was positioned at the air-liquid interface using the instrument software, and was next oscillated at a strain amplitude of γ_0 = 1 % and angular frequency of ω = 0.5 rad/s, in the linear viscoelastic regime. By measuring the stress response obtained from the applied strain, the elastic and viscous moduli were obtained in real-time, as the biofilm forms at the air-liquid interface. Evaporation was compensated by introducing fresh media during the experiment. All experiments were conducted by heating the flow cell at 28°C with a Peltier plate, to have a temperature inside the cell around 26°C. Frequency sweeps were conducted at a strain amplitude of γ_0 = 1 %, in the linear viscoelastic regime, from 0.01 rad/s to 10 rad/s, followed by strain amplitude sweeps at 0.5 rad/s from 0.1 % to 100 %. These last experiments were performed after the time sweep experiments.

5.2.3 Western blot

Western blots were performed to determine the production of curli subunits CsgG and CsgA in single and dual-species pellicle at 48 h. Additionally, the presence of Bap1, a *V. cholerae* protein, was assessed using a bap1-3xHuman influenza hemagglutinin (HA) tag. The experimental procedure was carried out as previously described [159]. Briefly the pellicles were rinsed with 1x Phosphate-buffered saline (PBS) and sonicated to disperse the biofilm community. All samples were diluted to OD_{600} = 1.0 and the pellets were treated with formic acid to dissociate the protein subunits. The samples were resuspended in sodium dodecyl sulfate-polyacrylamide gel electrophoresis (SDS-PAGE) loading buffer. After electrophoresis, proteins were transferred on a PVDF membrane and Western blot analysis were performed. Primary polyclonal anti-rabbit α-csgA and α-csgG (dilution 1:100,000 and 1:5000 respectively) and secondary goat anti-rabbit

antibodies were used to recognize curli units CsgA and CgsG. For Bap1, since the protein was carrying a 3xHA tag, primary mouse monoclonal anti-HA antibodody (Thermofisher, dilution 1:1000) and secondary goat anti-mouse (IgG) antibodies were supplied for Bap1 detection.

5.2.4 Congo Red fluorescence

To assess the presence of amyloid fibrils and pEtN cellulose in the single and dual-species biofilms, pellicles grown in 3 ml of YESCA for 48 h were resuspended in PBS 1x and sonicated. The samples were diluted to OD_{600} = 1.0 and 3 µg/ml of Congo Red were added. Fluorescence was measured using a microplate reader SpectraMax M5 (Molecular Devices) at 525 nm exitation and 610 nm emission. The tests were carried out in biological and technical triplicates and the mean ± SEM (Standard Error of the Mean) was represented.

5.2.5 Bacterial counts

The number of viable bacteria was determined as described previously [160]. Briefly, the pellicles were grown in 3 ml of YESCA in polypropylene tubes for 48 h at 26 °C. They were diluted in 1x PBS and sonicated. Dilutions were plated on selective MacConckey agar to separate the lactose fermenting *E. coli* from the non-lactose fermenting *V. cholerae*, and the plates incubated at 37 °C overnight. All tests were carried out in biological and technical triplicates and the mean ± SEM was represented.

5.2.6 Scanning electron microscopy (SEM)

Scanning electron microscopy was performed on pellicle biofilms to evaluate the microstructure of single and dual-species biofilms. Pellicles were grown at 26 °C in 12-well plates with YESCA for 48 h and then placed on 0.1 % poly-l-lysine coated glass coverslips. As described before [160], pellicles were fixed for 1 h at 4 °C in 2.5 % glutaraldehyde and 4 % formaldehyde, then osmium tetroxide was added for an additional hour. After several rinses with PBS 1x, the pellicles were

dehydrated in 30 %, 50 %, 70 %, 80 %, 90 %, 95 % and 100 % ethanol for 15 min each, and finally dryed with a Critical Point Dryer CPD300 (Leica Biosystems, Concord, ON, Canada). A JEOL JSM 7400 field emission scanning microscope was used with 1.5 kV accelerating voltage for observations.

5.3 Results

5.3.1 Macroscopic morphology of pellicles at the air-liquid interface

Biofilm formation was evaluated by qualitatively analyzing the pellicle macroscopic properties at the air-liquid interface after 48 h of growth at 26 °C (**Fig. 5-1**). The *V. cholerae* biofilm appeared to be a solid opaque, more resistant pellicle while the *E. coli* pellicle was wrinkled, sheet-like and more translucent. The mutant *E. coli* W3110ΔcsgBA did not produce curli nor pEtN cellulose, and no pellicle was observed. The pellicle morphology for the dual-species biofilm with an initial ratio 1:1 was very similar to *V. cholerae* biofilm alone, a thick opaque biofilm. When the initial content of *V. cholerae* was reduced to 0.1 % the pellicle was smoother with microcolonies on top.

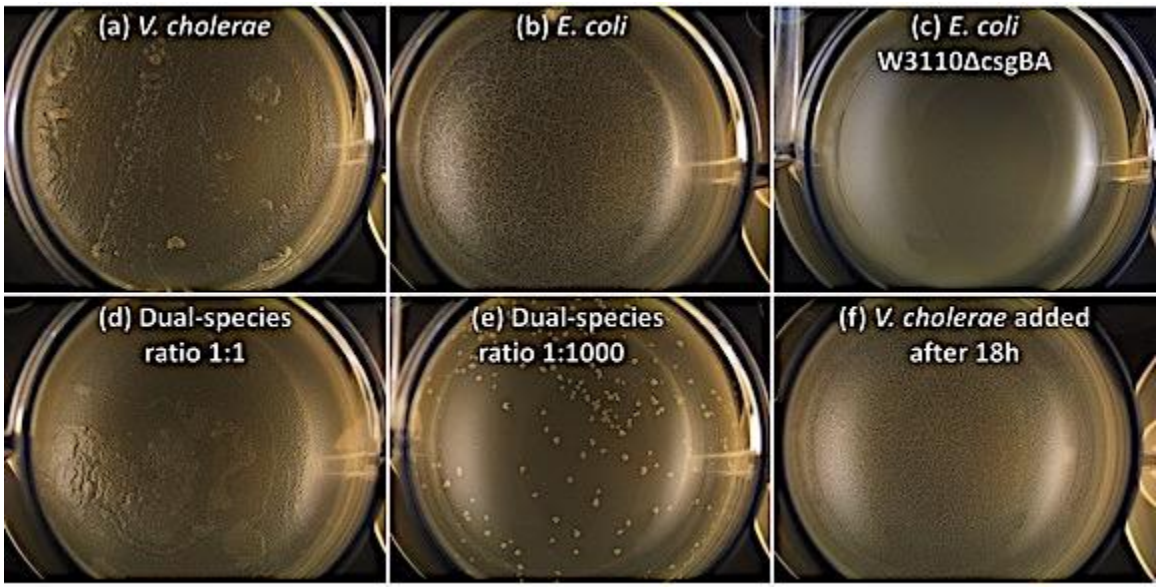

Figure 5-1 Single (a) *V. cholerae*, (b) *E. coli*, (c) *E. coli* W3110ΔcsgBA and dual-species (d) ratio 1:1, (e) ratio 1:1000 (f) *V. cholerae* added after 18 h, pellicles morphology in 24-well plates after 48 h at 26 °C. All the single and dual-species formed a pellicle, apart from the *E. coli* W3110ΔcsgBA (curli-deficient) that did not form a biofilm.

Since *V. cholerae* formed its biofilm about 15 h faster at the air-liquid interface, we hypothesized that *E. coli* would require a head start to be able to colonize the air-liquid interface. The pellicle morphology was then evaluated when *V. cholerae* was added at different delayed times (**Fig. 5-2**). When *V. cholerae* was added after 18 h, in the same initial quantity as *E. coli*, the pellicle morphology exhibited similar wrinkles as *E. coli* alone, indicating the *E. coli* appeared to be able to colonize the air-liquid interface and secrete its ECM when given a head start.

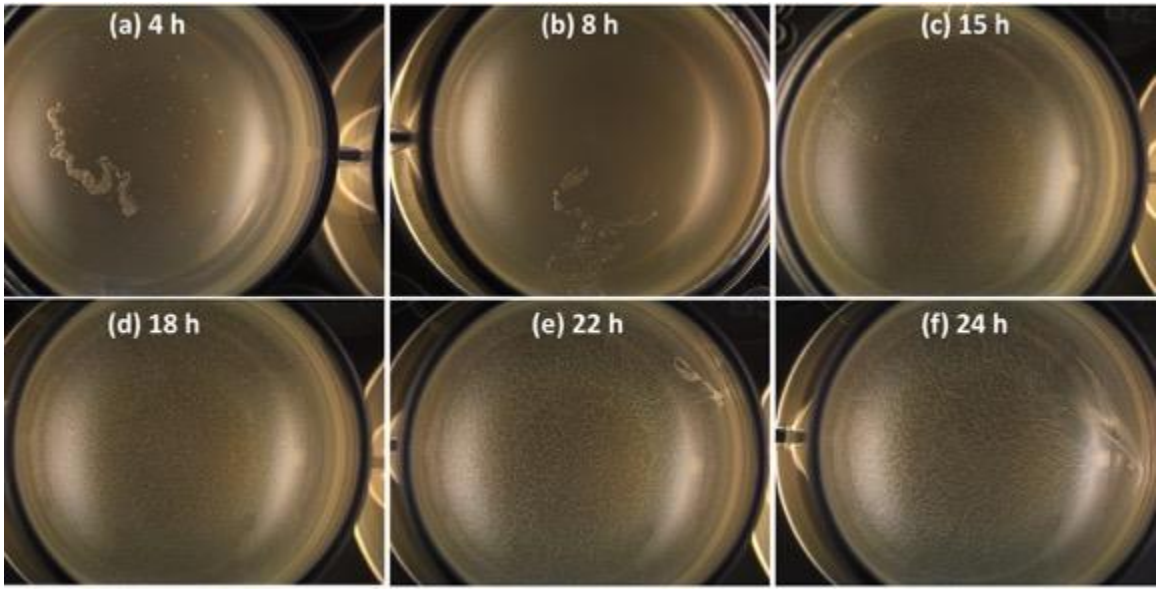

Figure 5-2 Dual-species pellicles morphology in 24-well plates after 48 h at 26 °C where the addition of *V. cholerae* is delayed with respect to *E. coli* by (a) 4 h, (b) 8 h, (c) 15 h, (d) 18 h, (e) 22 h and (c) 24 h, in the same initial quantity as E. coli.

5.3.2 Biofilms rheological properties over time at the air-liquid interface

The interfacial viscoelastic properties were analyzed over the course of the biofilm formation at the air-liquid interface using interfacial rheology. Interfacial rheology proved to be a sensitive technique leading to very reproducible data for each biofilm (**Fig. 5-3**). The interfacial elastic modulus G'_i was higher than the interfacial storage modulus G''_i for both species and the mixed biofilms, indicating a soft solid-like structure (**Fig. S1**). As the ECM components are the main contributors of the mechanical properties of biofilm pellicle, a change in the elastic modulus could indicate a different ECM composition.

The viscoelastic properties of the *E. coli* strain W3110 Δ*csgBA* – a strain not producing the ECM component curli – was used to evaluate the influence of surface active components from the media such as peptides and bacteria, and a plateau was reached during the first 10 h (Fig. 5-3a). The pellicle formed by *V. cholerae* was stronger than that of *E. coli* after 48 h, with a higher elastic modulus of 0.2 Pa.m compared to 0.06 Pa.m for *E. coli*. Under the conditions tested, the *V. cholerae*

elastic modulus started to increase rapidly, as soon as 15 h after inoculation, while it took more than 32 h for *E. coli* to form its pellicle corresponding to the second increase (Fig. 5-3a).

When both bacteria were first inoculated in equal volume quantity initially (ratio 1:1), the viscoelastic profile followed that of *V. cholerae* alone, suggesting that *V. cholerae* could be the main bacteria contributing to the mechanical properties in the dual-species biofilm (Fig. 5-3b). When the initial content of *V. cholerae* was decreased to 0.1% (ratio 1:1000), the mature biofilm elastic modulus was reduced at 48 h to 0.02 Pa.m (Fig. 5-3c). By comparing the pellicle morphologies, it was not possible to determine at this point whether the elastic properties were due to *E. coli* matrix production or a decrease in *V. cholerae*.

To see whether the time required to colonize the interface for each species had a major impact on the dual-species biofilm properties, the addition of *V. cholerae* was delayed by 18 h (Fig. 5-3d). The elastic modulus profile obtained was similar to *E. coli* alone, with the biofilm formation happening around 40 h. This slight delay compared to the *E. coli* single biofilm – happening around 32 h – and the slightly lower G'_i value might indicate that *V. cholerae* still had an influence on the biofilm viscoelastic properties, even when added after 18 h.

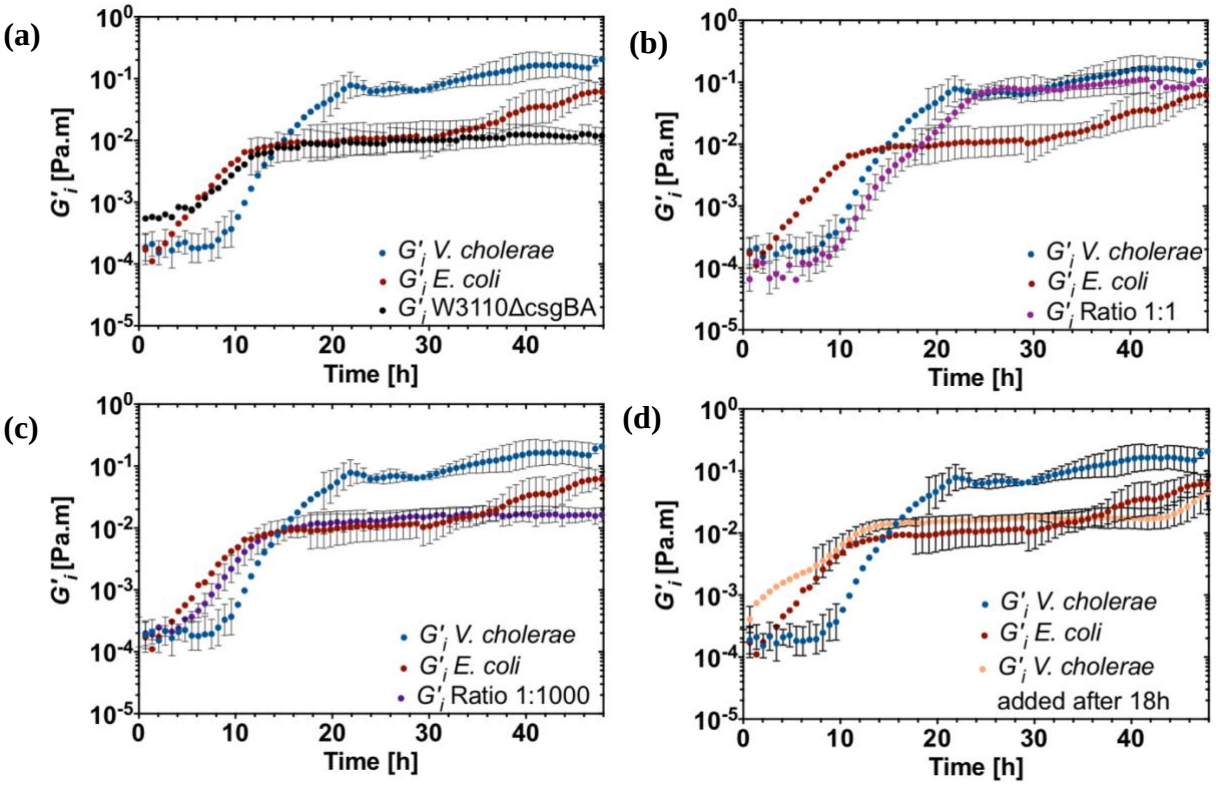

Figure 5-3 Evolution of the interfacial elastic modulus as the biofilms form at the air-liquid interface. The data show the average value of three trials with the error bars. The data compare the single-species biofilm *V. cholerae* (blue) and *E. coli* (red) with (a) W3110 Δ*csgBA*, not producing ECM components (b) dual-species biofilm, ratio 1:1 (c) dual-species biofilm, ratio 1:1000 (d) dual-species biofilm, with *V. cholerae* added after 18 h.

The mature pellicles were subjected to a frequency sweep from 0.01 rad/s to 10 rad/s at γ_0 = 1 %, followed by a strain amplitude sweep from 0.1 % to 100 % at a 0.5 rad/s frequency. The more "solid-like" the biofilm is, the less frequency-dependent is *G'*. Both *E. coli* and *V. cholerae* formed robust elastic networks after 48 h (**Fig. 5-4a**), as well as the dual-species biofilm ratio 1:1. The dual-species ratio 1:1000 and ratio 1:1 with the delayed addition of *V. cholerae* appeared to be less matured pellicles as a stronger frequency-dependence for *G'* was observed, modeled well with a power-law since *G'* could be related to a power of frequency ω (Fig. 5-4a). This behavior is characteristic of a viscoelastic-like structure (and not solely elastic), as it has been previously demonstrated for biofilm systems [43, 69].

The strain amplitude sweep test shows first that the time and frequency sweeps were performed within the linear viscoelastic region for all of the biofilms studied, since the strain used was 1% (Fig. 5-4b). Interestingly, while the interfacial elastic modulus G'_i was higher for *V. cholerae* compared to the *E. coli* biofilm, the breakdown strain was approximately three times lower (10 % versus 30 %). This could be interpreted as stronger interconnections for the *V. cholerae* biofilm network, which leads to a breakdown at a lower strain and a fastest loss of elasticity – as it has been previously observed for complex polymeric structures [161, 162].

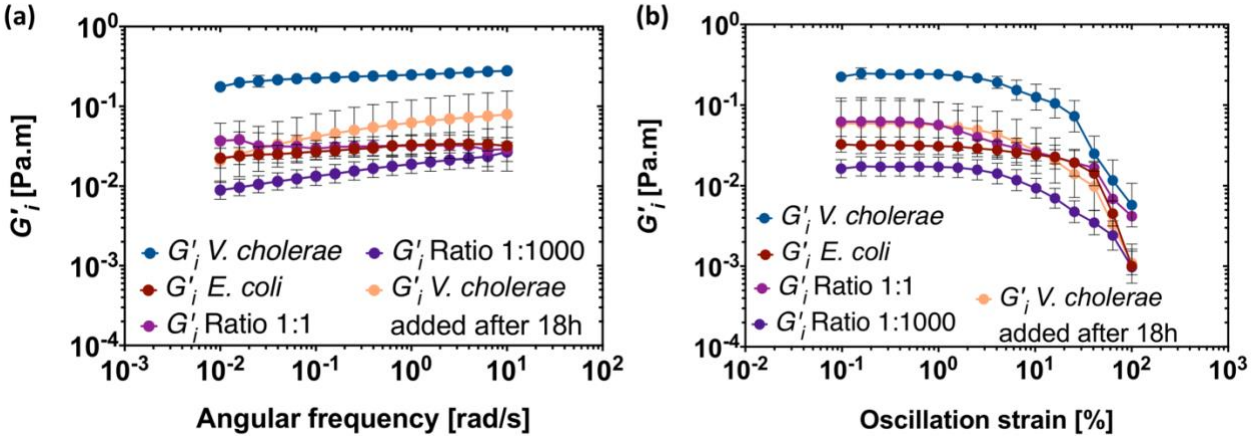

Figure 5-4 (a) Frequency sweep at γ_0 = 1 % strain amplitude, (b) strain amplitude sweep at 0.5 rad/s, performed on mature pellicles after 48 h, at 26 °C.

5.3.3 Microscale biofilm architecture

Scanning electron microscopy (SEM) was performed on mature pellicles to visualize the microstructure for each single and dual-species biofilms (**Fig. 5-5**). Bacteria were embedded within the ECM polymeric network, for both single and multi-species biofilms. The. *E. coli* string-like matrix was clearly visible, for both the single biofilm and after the 18 h delayed addition of *V. cholerae.* The dual-species biofilm morphology was similar to the *V. cholerae* rough coating, with a dense ECM matrix surrounding the *V. cholerae* cells, while few *E. coli* cells were present in the 1:1 ratio. Less ECM material was detected for the dual-species initial ratio 1:1000, which was consistent with the interfacial rheology observations where the elastic moduli was lower for this ratio. Fewer *V. cholerae* cells (curved-shape) were observed when it was added after 18 h,

supporting the hypothesis that once *E. coli* was given time to colonize the interface it was able to create its own network.

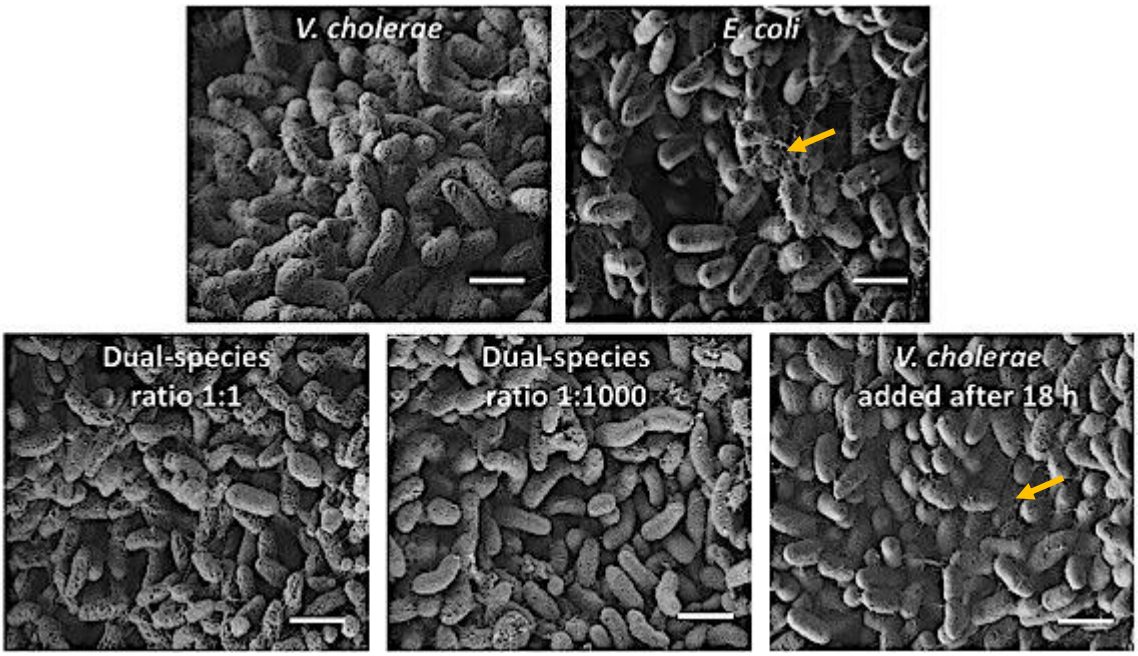

Figure 5-5 Scanning electron microscopy images of single and dual-species pellicles grown at 26°C for 48 h (scale bar, 1µm). The yellow arrow shows a fibril from the *E. coli* matrix.

5.3.4 Detection of major ECM proteins

The protein content in the single and dual-species biofilms were detected and characterized by Western blot analysis. The pellicles were sonicated and treated with formic acid to dissociate the protein monomers. To determine curli levels, secreted by *E. coli*, the subunits CsgA and CsgG were detected using anti-CsgA and anti-CsgG antibodies. In the dual-species biofilm, no curli production was detected even when *Vibrio* was initially present at 0.1% (**Fig. 5-6**). However, when the addition of *V. cholerae* was delayed by 18 h, *E. coli* was able to produce curli – as seen by both CsgA and CsgG subunits were indeed detected in that case, which is in accordance with the rheology results showing similar elastic moduli.

The *V. cholerae* Bap-1 protein plays a major role on the elasticity and pellicle morphology [67]. Bap-1 production was analyzed using an HA-tag antibody. Bap-1 was always produced in the dual-

species biofilm, although less abundant when the *Vibrio* addition was delayed. This is coherent with the interfacial rheology results where the elastic properties of the dual-species biofilm (ratio 1:1) were identical to *V. cholerae* alone.

Thus, even when added in small amount (0.1 %), *V. cholerae* was able to produce Bap-1, whereas the *E. coli* curli subunits CsgA and CsgG production were inhibited. A 18 h head start was necessary for *E. coli* to produce its curli subunits.

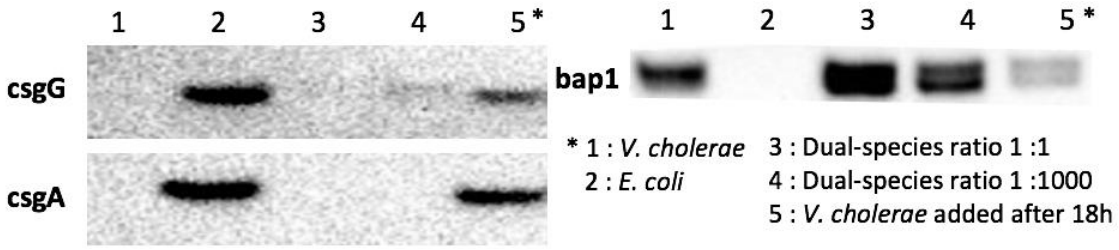

Figure 5-6 Western blot analysis from single and dual-species pellicles at 48 h, on curli (left part) and the protein bap1 (right part).

5.3.5 Cellulose detection with Congo Red fluorescence

Mature pellicles were also stained with Congo Red (CR) after 48 h growth to evaluate the presence of amyloid fibrils and pEtN cellulose. The fluorescence level was measured on sonicated pellicles at 525 nm excitation and 610 nm emission in microtiter plates. The presence of *V. cholerae* did not interfere with the CR fluorescence signal (**Fig. S2**)

Since *V. cholerae* did not produce any pEtN cellulose or amyloid fibers no fluorescence was observed, while for *E. coli* matrix a strong fluorescence signal was detected (**Fig. 5-7**). In the dual-species biofilms, as the *E. coli* initial content increased (ratio 1:1000), more fluorescence was observed although it was only 1/3 of the *E. coli* single-biofilm. For the dual-species biofilms - since curli subunits CsgA and CsgG were not detected by Western Blot analysis, the fluorescence was mostly due to the presence of pEtN cellulose. When *V. cholerae* was added after 18 h, the fluorescence increased to almost half the value for *E. coli* single biofilm. By using fluorescence microscopy (**Fig. S3**), the filamentous sheet-like biofilm network was only observed for *E. coli* single-biofilm alone and for the 18 h delayed addition of *V. cholerae.*

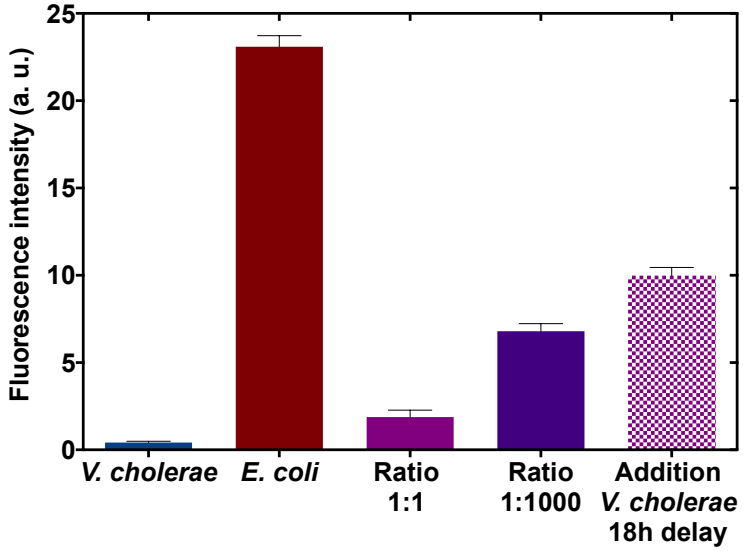

Figure 5-7 Congo Red fluorescence on single and dual-species pellicles at 48 h assessing the presence of curli and pEtN cellulose by quantifying the fluorescence intensity (excitation 525 nm emission 610 nm).

5.3.6 Growth curves for single and co-cultured species

The growth of each species was measured by optical density (OD_{600}) and CFU/ml at selected time points, under the same conditions as the biofilm formation – at 26 °C, standing. The growth curve showed similar rates for each single bacteria during the first 8 h (**Fig. 5-8a**). Then the *V. cholerae* growth increased for the last 16 h, as well as the co-cultured species. Those results were complemented with the CFU/ml at 8 h (Fig. 5-8b) and 24 h (Fig. 5-8c), where the number of bacteria for each species was in the same range of magnitude (10^7 CFU/ml for 8 h and 10^8 for 24 h). The difference observed in the OD_{600} curves could be explained by the aggregates due to the pellicle formation for *V. cholerae* while *E. coli* had not formed a biofilm yet at 24 h.

V. cholerae did not appear to have a strong bactericidal effect on *E. coli,* although a slight decrease was observed at 24 h for *E. coli* when co-cultured – from $2.9x10^8$ to $4.7x10^7$ CFU/ml. Studies have shown the virulence of the *V. cholerae* type 6 secretion system (T6SS) on *E. coli*, in the presence of salt [163]. Since the media used (YESCA) did not contain salt, this mechanism did not have a dramatic impact on *E. coli* growth.

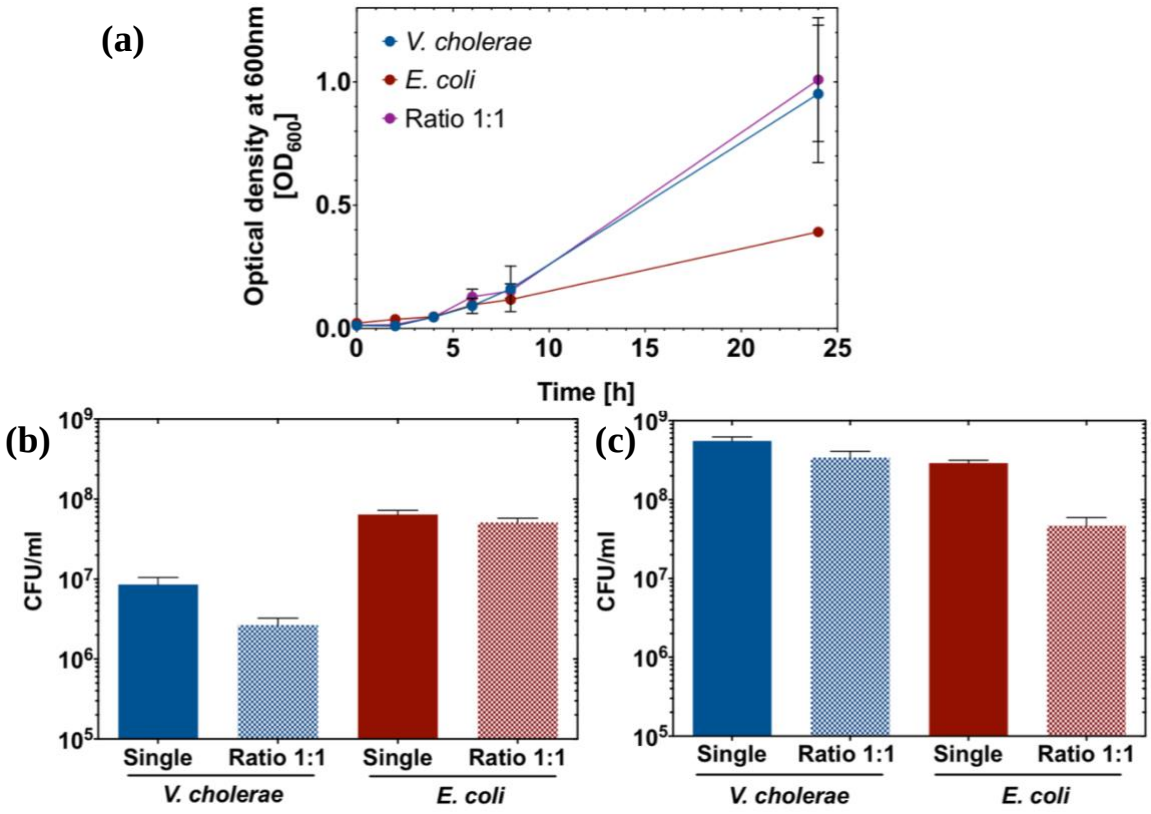

Figure 5-8 Biofilm growth of V.cholerae and E. coli. Overnight cultures were grown for 48 h, under standing culture conditions at 26 °C. The optical density was measured at selected times (a) and the CFU/ml at 8 h (b) and 24 h (c) for single and co-cultured bacteria at an initial ratio 1:1.

5.4 Discussion

In multi-species biofilm, matrix composition is likely to be impacted by competitive or synergetic bacterial interactions. Since the biofilm mass is mainly composed of extracellular polymers exhibiting viscoelastic properties, measuring the biofilm rheological properties over time is essential to have quantitative values on the biofilm development. In this work, we studied a dual-species biofilm composed by two model Gram-negative organisms able to form a pellicle at the air-liquid interface: *V. cholerae* and *E. coli*. From a macroscopic perspective, the dual-species biofilm morphology was very similar to *V. cholerae* alone when both bacteria were added initially in equivalent amounts. This observation was supported by the evolution of the dual-species (ratio 1:1) interfacial elastic moduli, which closely followed that of *V. cholerae* single-species biofilm.

However, when *E. coli* was given an 18 h head start, the macroscopic morphology and mechanical properties were similar to the *E. coli* single-species biofilm. Those real-time measurements led us to hypothesize that *V. cholerae* was the fastest organism to form its pellicle at the air-liquid interface, despite similar planktonic growth rates for both bacteria. *V. cholerae* is one of the fastest bacteria [164, 165], which could explain its ability to colonize the interface and form a biofilm rapidly, as well as the use of bacterial surface structures (outer-membrane proteins, pili, lipopolysaccharides (LPSs), etc.) involved in bacterial adhesion [166].

We subjected the mature pellicles to frequency and strain amplitude sweeps. *E. coli* single-species biofilm was able to withstand larger deformation than *V. cholerae,* despite a lower interfacial elastic moduli. This viscoelastic profile was characteristic of a weaker and flexible interconnected polymeric network. The microstructure observed in SEM and fluorescence microscopy images illustrated that the *E. coli* matrix had a sheet-like aspect due to pEtN cellulose and curli – as it had been previously shown for *E. coli* biofilms [167]. *V. cholerae* single and dual-species biofilms formed stronger networks with high elasticity, from the macroscopic rheological analysis (breakdown at lower strain) and the SEM images showing *V. cholerae* bacteria strongly embedded in a dense ECM matrix.

To separate the contributions from curli and pEtN cellulose in the single *E. coli* and dual-species biofilms, detection of these major ECM proteins were realized by Western blot and fluorescence assays, respectively. The analysis of the pellicle protein composition showed that *E. coli* was only able to produce CsgG and CsgA curli subunits in single-species or when it was given a delay to colonize the air-liquid interface in the dual-species. Even when *V. cholerae* was present at 0.1 % initially (ratio 1:1000), no CsgA was secreted from *E. coli*. However, *V. cholerae* was able to produce Bap1 - one of the major protein responsible for its biofilm elasticity – even when present at only 0.1 % initially, supporting the interfacial rheology results showing that *V. cholerae* is the dominant species due to its fast biofilm formation at the interface. Bacterial analysis of the mature pellicle also showed *V. cholerae* dominated while *E. coli* was present in the bulk rather than at the interface, in the dual-species biofilm ratio 1:1 (**Fig. S4**).

The production of pEtN cellulose, an *E. coli* ECM component, was monitored with CR fluorescence measurements and microscopy and was always detected in the different biofilm mixes. On the contrary, the production of curli, another ECM component, was usually inhibited in

the presence of *V. cholerae* in the dual-species biofilm, even in the presence of a small initial amount of *Vibrio* (0.1 %),. Thus, in the presence of *V. cholera,* curli was secreted only when *E. coli* had an 18 h growth head start. This correlated with the fact that the filamentous matrix was only observed for the *E. coli* single biofilm and when *V. cholerae* was added after 18 h.

Since no bactericidal effect was detected when the bacteria where co-cultured (Fig. 5-8), these results supported the hypothesis that the fastest bacteria producing a biofilm at the interface was the dominant bacteria here, due to factors such as bacterial motility and adhesion.

5.5 Conclusion

In this work, we combined interfacial rheology measurements to follow biofilm formation in real-time with the analysis of some matrix components to apprehend the interactions happening at the interface. We hypothesized that biofilm formation rate at the interface was driving the dual-species final composition, with *V. cholerae* forming the fastest its biofilm being the dominant bacteria. By relating the mechanical properties to the molecular composition of the dual-species biofilm we proposed that *V. cholerae* inhibited the production of curli, even when initially present in small amounts, while *E. coli* still secreted some pEtN cellulose material. Thus our study suggested antagonistic interactions between *V. cholerae* and *E. coli* in the biofilm at the air-liquid interface.

Since the biofilm formation rate appeared to be the major factor impacting the bacterial interactions, investigating the role of bacterial surface components in the initial adhesion might provide further insights into interactions in multispecies communities.

ACKNOWLEDGMENTS: We thank the Electronic Microscopy Platform at Université de Montréal (Dr. Antonio Nanci) for their assistance in electron microscopy analyses.

5.6 Supporting information

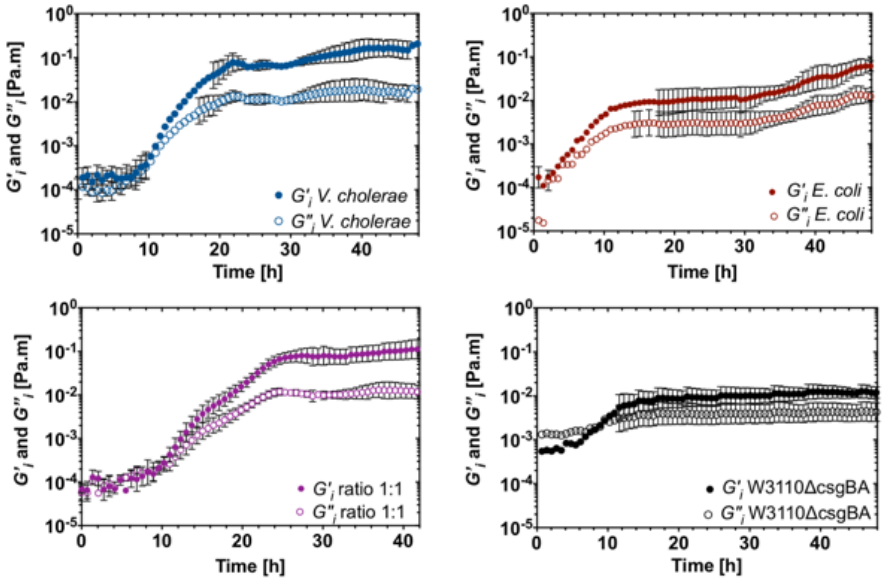

Figure S1 Evolution of the interfacial elastic *G'* (filled symbol) and viscous *G''* (empty symbol) moduli as the biofilms form at the air-liquid interface. The data represent the average value of three trials with the error bars. The data show the biofilms of (a) *V. cholerae* (b) *E. coli* (c) dual-species ratio 1:1 (d) *E. coli* W3110ΔcsgBa (negative control)

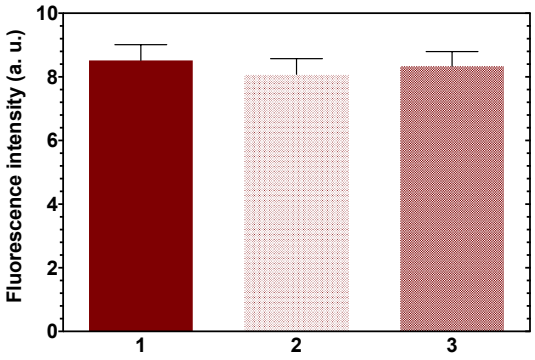

Figure S2 Congo Red fluorescence on *E. coli* pellicle at 48 h (excitation 525 nm emission 610 nm). Pellicles were sonicated and diluted in 1X PBS to OD_{600} 1.0 and 500 µl of the dilution was added to three eppendorfs.

1. 500 µl 1X PBS was added. After 15 min 3 µg/ml Congo Red was mixed.
2. 500 µl of *V. cholerae* pellicle was added. After 15 min 3 µg/ml Congo Red was mixed.
3. 500 µl of *V. cholerae* pellicle was added with 3 µg/ml Congo Red. The mix was left 15 min before measuring the fluorescence

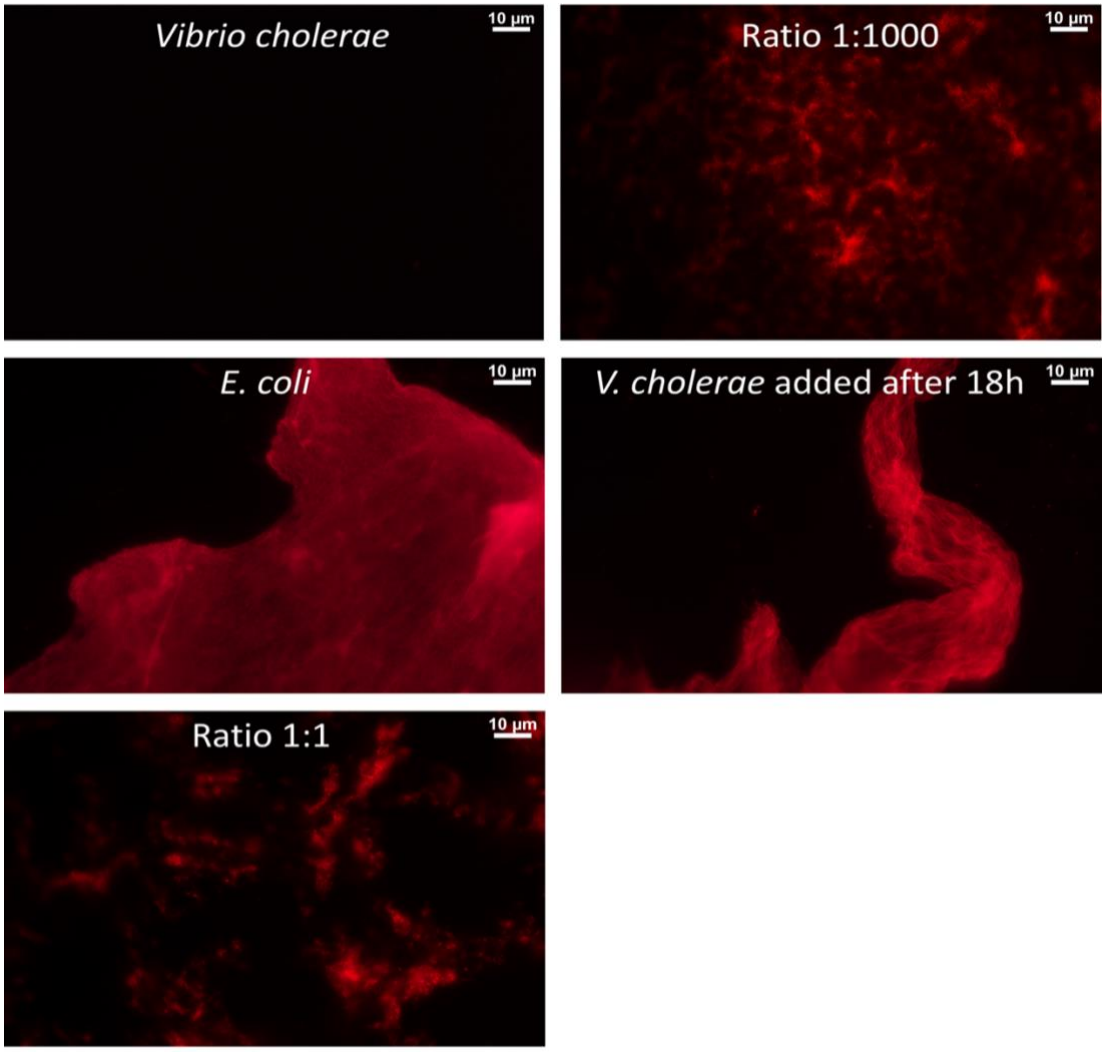

Figure S3 Congo Red fluorescence on pellicles at 48 h assessing the presence of curli and pEtN cellulose by fluorescence microscopy

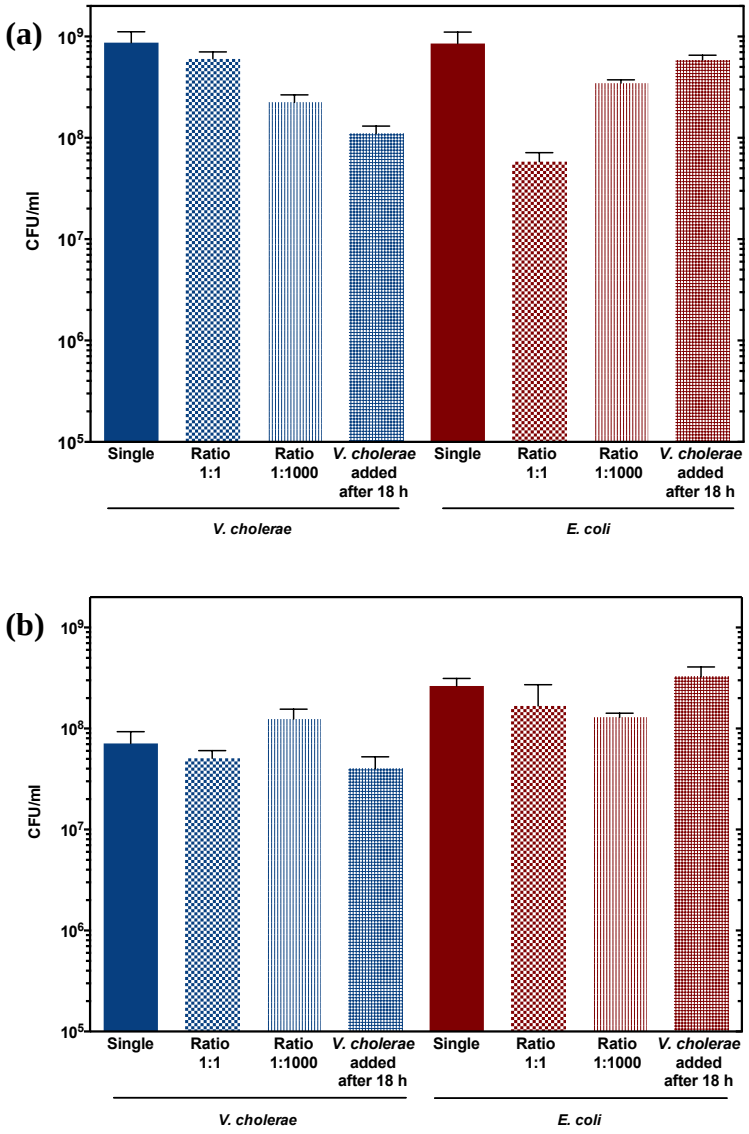

Figure S4 Single and dual-species biofilm bacterial composition at 48 h (a) pellicle (b) bulk. The composition of the mature pellicle biofilm at 48 h was first analyzed by bacterial count – colony forming unit (CFU/ml).

CHAPTER 6 ARTICLE 3: THE POLYMERIC MATRIX COMPOSITION IN VIBRIO CHOLERAE BIOFILM MODULATES THE RESISTANCE TO SILVER NANOPARTICLES PREPARED BY HYDROTHERMAL SYNTHESIS

Authors: Clémence Abriat,[a,b] Olivier Gazil,[a] Marie-Claude Heuzey,[a] France Daigle[b*] and Nick Virgilio[a*]

[a]CREPEC, Department of Chemical Engineering, Polytechnique Montréal, Montréal, Québec, Canada

[b]Department of Microbiology, Infection and Immunology, Université de Montréal, Montréal, Québec, Canada

*Corresponding authors: Nick Virgilio nick.virgilio@polymtl.ca

France Daigle france.daigle@umontreal.ca

Submitted in : *ACS Applied Materials and Interfaces*

GRAPHICAL ABSTRACT

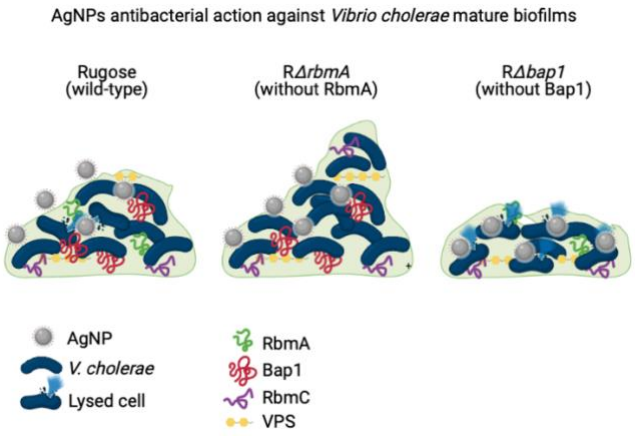

ABSTRACT: Biofilm is the dominant microbial form in nature. These complex microbial communities, in which bacteria are embedded in a self-produced protective polymeric extracellular matrix, display an enhanced resistance to antimicrobials and thus represent a major health challenge. Although nanoparticles have proven to be effective against bacteria, the interactions between nanoparticles and the polymeric biofilm matrix are still unclear. In this work, silver nanoparticles (AgNPs) were used on the pathogen *Vibrio cholerae* mature biofilm and their effects on the biofilm microstructure were evaluated. Bacteria cells within mature biofilms showed an increased tolerance to AgNPs. A concentration nine times higher than for the planktonic cells was required to eliminate the pathogens. Mutant strains not able to form a pellicle biofilm were four times more susceptible to AgNPs than the wild-type strain forming a strong biofilm. Moreover, electron microscopy analysis revealed that AgNPs interacted with the extracellular matrix components and disrupted its microstructure. Finally, two major proteins, Bap1 and RbmA, appeared to mediate the biofilm bacterial resistance to AgNPs. This work highlights the role of the polymeric biofilm matrix composition to its resistance to AgNPs. It underlines how crucial it is to understand and characterize the interactions between nanoparticles and the biofilm matrix, in order to design appropriate metallic nanoparticles efficient against bacterial biofilms.

6.1 Introduction

Bacterial infections represent a growing problem in health care, with the increased appearance of multi-drug resistant pathogenic bacteria [168]. Indeed, over the years, the extensive use of antibiotics has sometimes led bacteria to evolve and develop resistance to the existing antibacterial agents [169]. Moreover, bacteria live predominantly in communities called biofilms, in which they are embedded and protected in a self-produced extracellular matrix (ECM) composed by extracellular polymeric substances (EPS) [114]. Since bacteria within biofilms are protected by their ECM, they are up to 1000 times more resistant than free-floating bacteria – also called planktonic cells, making biofilm-related infections extremely difficult to treat with traditional antibiotics treatments [7, 25]. Lately, there have been very few advances in the development of new classes of antibiotics and thus there is a growing need for new strategies to treat microbial infections [170].

The use of nanoparticles to tackle antibacterial resistance has attracted a strong interest and has been showing promising results. Silver nanoparticles (AgNPs), in particular, have shown exceptional antibacterial performances since they target a wide range of antibacterial mechanisms such as damaging bacterial membrane, the release of toxic silver ions, and the production of reactive oxygen species (ROS) [171-173]. The antibacterial properties of AgNPs depend strongly on their size and shape [107, 108]. Various physical, chemical or biological strategies have been developed and reported to synthesize AgNPs with different sizes and shapes. The chemical synthesis of AgNPs in organic and aqueous media has been predominantly used since it usually provides better control over the morphology and size of AgNPs [101]. However, the use of chemical reducing agents such as sodium borohydride are potentially toxic and unsafe for the environment. Greener synthesis pathways have been explored, such as hydrothermal synthesis with natural polysaccharides that act both as a reductor and as a stabilizing agent against aggregation [103, 104, 174]. Alginate is a natural anionic polysaccharide found in brown algae and some bacterial species. It possesses a number of free carboxyl and hydroxyl groups that are able to reduce Ag^{+} to Ag^{0}, through different synthesis pathways such as gamma irradiation, photochemical reduction and the hydrothermal route [105, 175, 176]. Several research groups have also synthesized silver nanoparticles with catalytic and antibacterial properties by using the cationic polysaccharide chitosan (CS) as a reducing agent and stabilizer [103, 174, 177-179]. Wongpreecha et al. proposed a mechanism where the lone pair electron of oxygen in chitosan reduced Ag^{+} to Ag^{0} under hydrothermal conditions, the Ag nuclei then coalescing into Ag clusters, which merged to form stable AgNPs surrounded by chitosan chains [174]. While those silver nanoparticles have shown good antibacterial properties against a wide range of planktonic bacteria, few studies have been performed to demonstrate their efficiency against mature biofilms, and few have aimed at understanding the interactions between nanoparticles and bacterial biofilms [110]. Choi et al. have shown that bacterial biofilms are four times more resistant to AgNPs than planktonic cells, partially due to the nanoparticles aggregation caused by electrostatic interactions with EPS components and retarded diffusion within the matrix [180]. Indeed, in addition to the ECM acting as a physical barrier, the nanoparticles interact with the EPS components when they are exposed to the biofilm, and those interactions are mainly electrostatic, hydrophobic and steric [111]. These interactions depend on the biofilm physicochemical properties as well as the nanoparticles properties, and they

modulate the antibacterial resistance. As a result, there is a need to deepen the knowledge on how the different biofilm components interact with AgNPs.

Vibrio cholerae is a pathogenic bacteria predominantly found in aquatic environments and capable of forming resilient biofilms displaying higher infectivity than planktonic bacteria [149, 150, 181]. The effect of silver nanocomposites was recently evaluated against *V. cholerae* planktonic cells, surface-attached and pellicle biofilms, and the results showed the susceptibility to antimicrobials was highly dependent on the bacteria lifestyle [182]. However, the role of *V. cholerae* EPS components on its susceptibility to AgNPs has not been investigated, as well as the interactions with nanoparticles occurring within the biofilm matrix.

In this study, we use AgNPs synthesized via a hydrothermal green chemistry process to evaluate the role of *V. cholerae* biofilm matrix composition on the biofilm resistance to AgNPs. Two types of natural biopolymers carrying opposite charges were used as reductors and stabilizers for the nanoparticles, namely alginate and chitosan. Their antibacterial properties were evaluated with antibacterial assays against *V. cholerae* planktonic cells and mature pellicle biofilms. The smooth and rugose-wild type, and four rugose mutant strains unable to produce structural matrix proteins, were used to selectively modify the biofilm extracellular matrix composition. The interactions with EPS components in mature pellicle biofilms were studied by analyzing the impact of the biofilm matrix composition on the bacterial survival when exposed to AgNPs, and the analysis of the biofilm microstructure. By combining these results, we highlight the role of key matrix components on biofilms resistance to AgNPs.

6.2 Experimental section

6.2.1 Silver nanoparticles synthesis and characterization

6.2.1.1 Hydrothermal synthesis

Chitosan (CS) stock solution (0.5% w/v) was prepared by dissolving 0.5 g CS (85% deacetylated, 60 mPa.s for 1% w/v chitosan in 1% w/v acetic acid, BioLog Heppe GmbH) in 0.25% w/v acetic acid and the solution was stirred overnight at room temperature. Sodium alginate stock solution

(2% w/v) was prepared by dissolving 2 g of low viscosity sodium alginate (4-12 mPa.s for 1% w/v alginate in H_2O) (Sigma-Aldrich) in heated distilled water at around 80°C, under constant stirring.

Silver nanoparticles were then synthesized by reducing 1 mM of silver nitrate $AgNO_3$ with the previously prepared 2 % sodium alginate or 0.25 % chitosan solutions, in a hydrothermal autoclave chemical reactor. The reactor was kept at 120 °C and 15 psi for 1 h or 3 h, respectively for particles synthesized with alginate (Alg-AgNPs) and chitosan (CS-AgNPs) (**Figure S1**).

6.2.1.2 Silver nanoparticles characterization

The formation of AgNPs was confirmed by observing the UV-vis spectra acquired with a Nanodrop Spectrophotometer (Thermo Scientific). The size distribution was obtained by measuring the nanoparticles diameters – over 200 particles for Alg-AgNPs and 600 particles for CS-AgNPs, on multiple transmission electron microscopy (TEM) micrographs (Philips Tecnai 12 TEM). High resolution TEM micrographs were acquired with a JEOL JEM-2100F field emission electron microscope at a 200 kV accelerating voltage, and displayed both the nanoparticles morphology and crystallinity through the Selected Area Electron Diffraction (SAED) pattern. The ionic silver and nanoparticle concentrations were determined using a single particle induced coupled plasma mass spectrometer (SP-ICP-MS, Nu AttoM ES, Nu Instruments, U.K). The samples were initially sonicated for 15 min and diluted to approximately 10^5 AgNPs/ml. Finally, the total ionic silver concentration was obtained after acidic digestion of AgNPs with nitric acid for 3 h at 80 °C.

6.2.2 Antibacterial activity of silver nanoparticles

6.2.2.1 Bacterial strains and growth conditions

The antibacterial tests were done with smooth and rugose-variant of V. cholerae El-Tor A1552. Mutants of the rugose-variant lacking the ability to produce the major proteins RbmA (RΔ*rbmA*), Bap1 (RΔ*bap1*), RbmC (RΔ*rbmC*) or all of the three (RΔ*rbmA*Δ*bap1*Δ*rbmC*) were used to control the ECM composition (**Table S1**). All the strains were grown at 37 °C on Luria Bertani (LB) agar plates from -80 °C stocks. Overnight cultures were done in LB, shaking at 37 °C. Biofilms assays were performed in YESCA broth at 26 °C, from a 1:1000 dilution of overnight culture (**Figure S2**). The smooth variant and RΔ*rbmA*Δ*bap1*Δ*rbmC* mutant did not form a pellicle biofilm under the conditions studied, only a ring on the well was observed.

6.2.2.2 Antibacterial activity of AgNPs on planktonic bacteria

The antibacterial activity of AgNPs on planktonic bacteria was evaluated by using the broth dilution method [183] to determine the Minimal Inhibitory Concentration (MIC) and the Minimal Bactericidal Concentration (MBC). Two-fold dilutions of Alg-AgNPs or CS-AgNPs were suspended in YESCA media in 96-well plates. Each well was then inoculated with a bacterial suspension (10^6 CFU/ml) and the plate was incubated at 26 °C for 24 h. The optical density at 600 nm (OD_{600}) was followed over time with a microplate reader (SpectraMax iD3). The well into which no visible growth was detected was considered as the MIC. After 24 h, the wells that did not display any turbidity were plated on LB agar plates and incubated at 37 °C. The dilutions showing no bacterial growth were determined as the MBC.

6.2.2.3 Bacterial viability count in pellicle biofilms

The number of viable bacteria in pellicle biofilms was determined as described previously [160]. Briefly, the pellicles were grown in 24-well plates in 2 ml YESCA for 48 h at 26 °C. The non-adherent cells were then carefully removed and the media was replaced by aqueous suspensions of various concentrations of AgNPs, or deionized water as a negative control. The plates were incubated overnight at 26 °C. The pellicles were then sonicated to disperse the bacterial cells and dilutions were plated onto LB agar to count the living cells. All tests were carried out in biological and technical triplicates and the mean ± Standard Error of the Mean was represented.

6.2.2.4 Scanning electron microscopy (SEM)

Scanning electron microscopy was performed on pellicle biofilms to evaluate their microstructure after exposure to AgNPs. Pellicles were grown at 26 °C in 24-well plates with YESCA for 48 h. They were then treated with different concentrations of AgNPs, or deionized water as a control, for 24 h and then placed on 0.1 % poly-l-lysine coated glass coverslips. As described before [160], the pellicles were next fixed overnight at 4 °C in 2.5 % glutaraldehyde and 4 % formaldehyde. A 1 % osmium tetroxide solution was then added for 1 h at 4°C. After several washes with PBS 1x, the pellicles were dehydrated in ethanol aqueous solutions, and finally dried with a Critical Point Dryer CPD300 (Leica Biosystems, Concord, ON, Canada). An Hitachi Regulus 8220 ultra-high resolution scanning microscope was used at a 1.0 kV accelerating voltage and 10 µA emission

current for observations. High-resolution secondary (SE) and backscattered (BSE) electron detectors were used to image the mature biofilms.

6.3 Results

6.3.1 AgNPs characterization

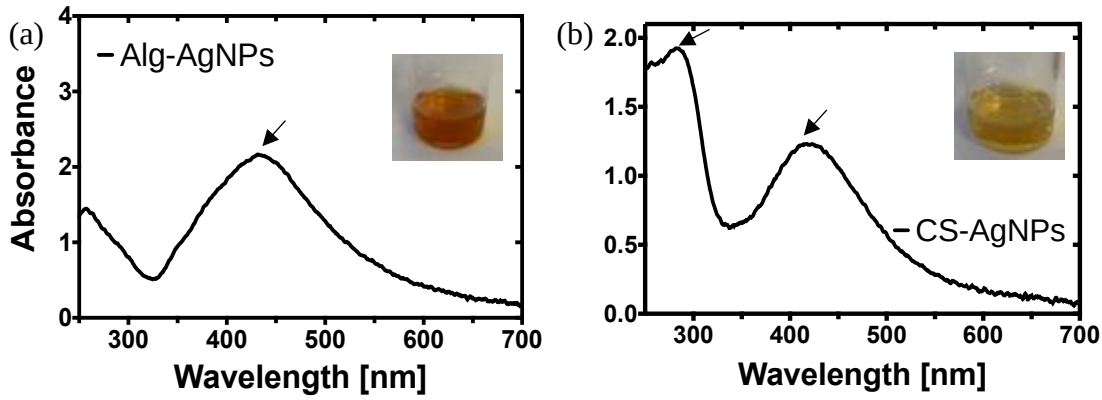

Figure 6-1 UV-vis absorption spectra of (a) Alg-AgNPs and (b) CS-AgNPs synthesized at 120°C under a pressure of 15 psi for 1 h (Alg-AgNPs) and 3 h (CS-AgNPs).

Metallic nanoparticles exhibit a surface plasmon resonance (SPR) due to the collective oscillations of the nanoparticles' free electrons excited by the light wave. The plasmon absorption band is influenced by the size, distribution and morphology of the nanoparticles. The absorption peak observed around 430 nm on the two UV-vis absorption spectra (**Figure 6-1**) indicates the formation of silver nanoparticles for both hydrothermal syntheses using alginate and chitosan. The peak position is characteristic of spherical nanoparticles [184]. For the Alg-AgNPs, the large full width at half maximum (FWHM) of the peak suggests that the nanoparticles might have a broad size distribution, whereas the smaller FWHM observed for CS-AgNPs indicates a narrower size distribution [107].

For the CS-AgNPs, although the peak at 430 nm is well-defined, it is not the dominant one (Figure 6-1b). A second peak around 290 nm is observed, with a higher intensity compared to the AgNPs peak. It is attributed to the still significant presence of the silver precursor, as discussed below,

suggesting that the reduction reaction was incomplete. To verify this hypothesis, a few drops of aqueous $NaBH_4$ were added to reduce the remaining ionic silver in solution. The absorption peak associated with the AgNPs at 430 nm then became the dominant one on the UV spectra (**Figure S3**), indicating a more complete reduction.

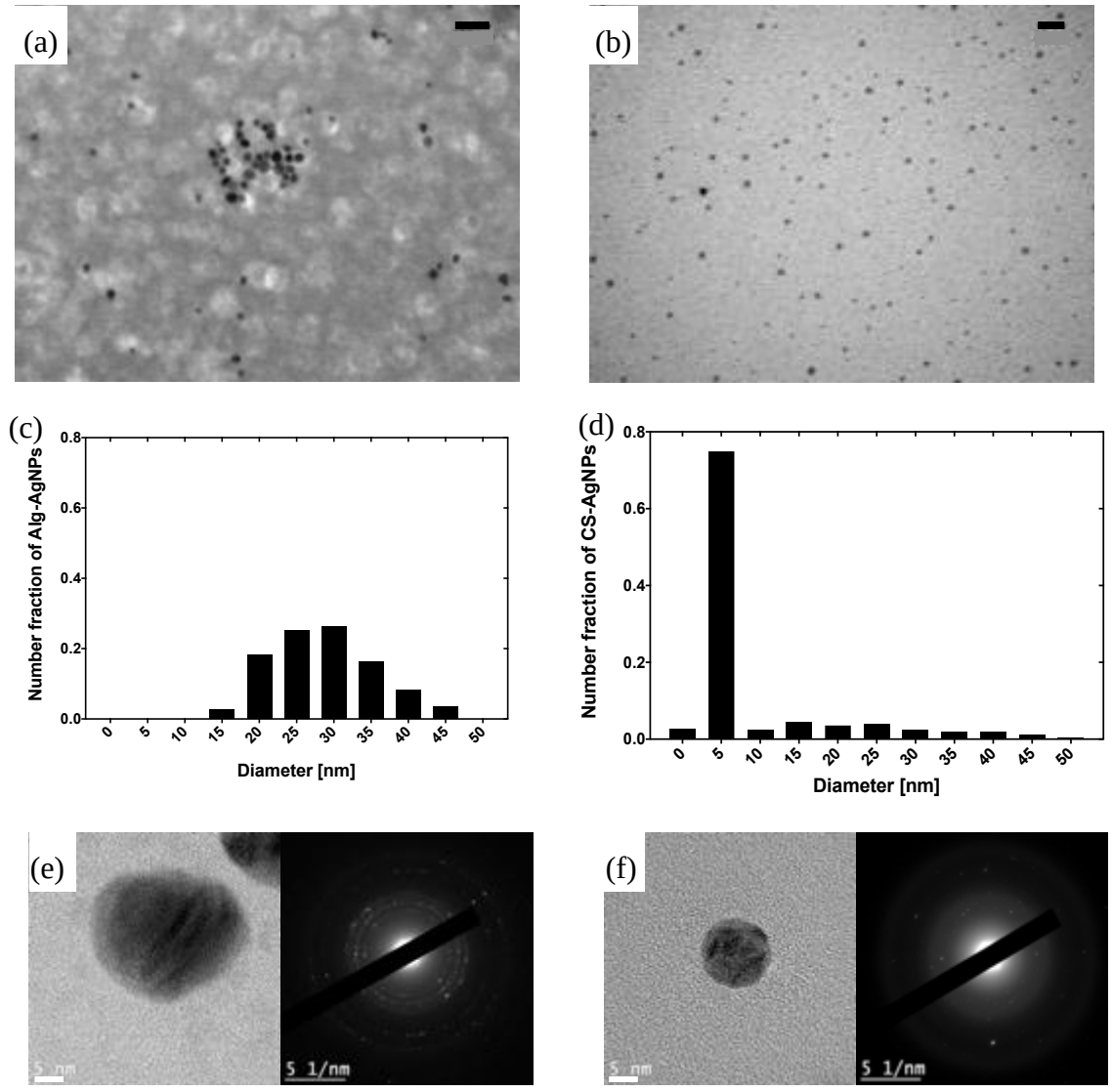

Figure 6-2 TEM images showing (a) Alg-AgNPs and (b) CS-AgNPs, and the associated histograms showing the AgNPs size (diameter) distributions of (c) Alg-AgNPs and (d) CS-AgNPs. High resolution TEM micrographs of (e) Alg-AgNPs and (f) CS-AgNPs, with the corresponding selected area electron diffraction (SAED) patterns.

The size and dispersion state of the AgNPs suspensions were analyzed by TEM (**Figure 6-2**). Spherical and well-dispersed AgNPs are obtained for both hydrothermal syntheses (Figure 6-2a-b). For Alg-AgNPs, as suggested by the UV-vis spectra, the size distribution is broad with an average diameter of around 29 nm, and some aggregation is observed (Figure 6-2a and 6-2c). Very small and well-dispersed nanoparticles are obtained for the chitosan-based synthesis, with most of the CS-AgNPs having a diameter below 5 nm (Figure 6-2b and 6-2d).

High resolution TEM gives further insights on the morphology and crystallinity of the AgNPs (Figure 6-2e-f). Spherical particles are observed for both types of AgNPs, exhibiting high crystallinity as displayed by the clear lattice fringes. The selected area electron diffraction (SAED) patterns confirm the high crystallinity of the synthesized AgNPs, with the diffraction rings indexed as (111), (200), (220) and (311), corresponding to face-centered cubic silver (fcc).

The concentration of nanoparticles and ionic silver, as well as the AgNPs size, were determined by SP-ICPMS (**Table S2**). However, since the lower detection limit is 5 nm, the results obtained for CS-AgNPs are not reliable since small nanoparticles are considered as ionic silver. Instead, the total concentration was obtained after acidic digestion of the nanoparticles suspension, corresponding to the total ionic concentration of the samples. Ideally, the ionic silver plus particle concentrations should be equal to the total concentration. However, there is some adsorption from the nanoparticles inside the instrument. This adsorption is greater with smaller nanoparticles and chitosan appeared to increase this adsorption. As a result, only the total ionic concentration is reported in the following antibacterial analysis.

6.3.2 Antibacterial activity of silver nanoparticles

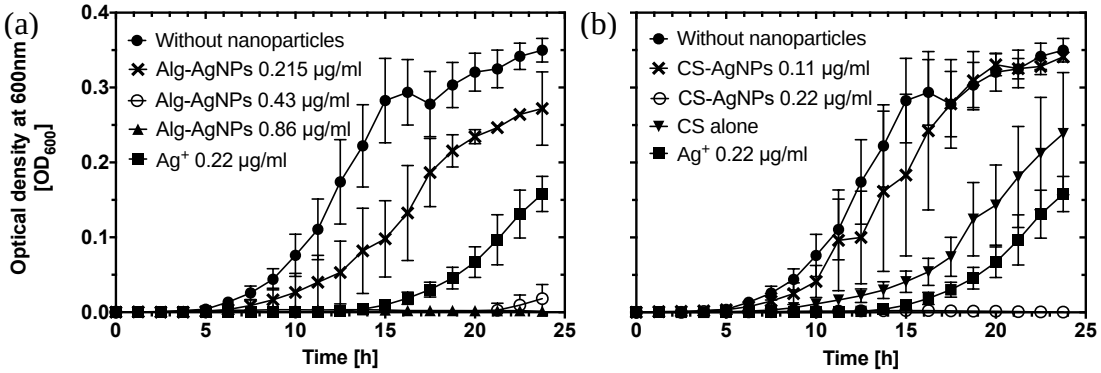

Figure 6-3 Growth kinetics of V. cholerae (wild-type rugose is illustrated) planktonic cells and the antibacterial effect of (a) Alg-AgNPs and (b) CS-AgNPs. The AgNPs concentration corresponds to the total content of silver (nanoparticle and ionic forms) in the suspension.

The AgNPs antibacterial effect on planktonic cells was evaluated by determining the MIC and MBC using the microdilution plate method. AgNPs inoculated with planktonic cells and the bacterial growth was monitored for 24 h by continuously measuring the optical density at 600 nm (OD_{600}). The results for the wild-type rugose variant (**Figure 6-3**) show that both types of AgNPs successfully inhibit bacterial growth during 24 h since bacteria are unable to grow as much as the negative control without nanoparticles. CS-AgNPs are four times more efficient to inhibit bacterial growth. Indeed, their MIC is equal to 0.22 µg/ml (Figure 6-3b), while 0.86 µg/ml of Alg-AgNPs are required to totally inhibit bacterial growth (Figure 6-3a). Chitosan alone – at the same concentration as for CS-AgNPs at 0.22 µg/ml, exhibited an antibacterial action which is only observed in acidic conditions due to the protonation of the chitosan amino groups [185, 186]. At this concentration, it slows down bacteria growth but does not inhibit it. Similarly, ionic silver also reduces bacterial growth at 0.22 µg/ml but is not able to completely inhibit it. Hence, the inhibiting effect observed at 0.22 µg/ml CS-AgNPs can be attributed to the presence of nanoparticles. Alginate alone does not have an effect on bacterial growth (results not shown).

The bactericidal effect of AgNPs was assessed by plating the wells with concentrations higher than the MIC previously determined. The MBC value corresponds to the concentration where no

colony growth is observed on agar. CS-AgNPs demonstrates a higher bactericidal effect with the MBC between 0.22 and 0.44 µg/ml, compared to a concentration in-between 0.86 µg/ml and 1.72 µg/ml for Alg-AgNPs (**Table S3**). No significant difference in the MBC value was observed between the wild-type and mutant strains, in the planktonic state (Table S3). The CS-AgNPs suspension also appears to be more homogenous since the MBC range is smaller than for Alg-AgNPs. This could be due to the homogeneity of the nanoparticles suspension and the presence of residual ionic silver. Moreover, Wongpreecha et al. showed that CS-AgNPs are positively charged at pH < 10, according to their high positive zeta potential superior to 30 mV, so they might adhere better to the negatively charged bacterial membrane [174]. Chitosan alone displays antibacterial properties, as shown above, which could explain their higher efficiency compared to Alg-AgNPs.

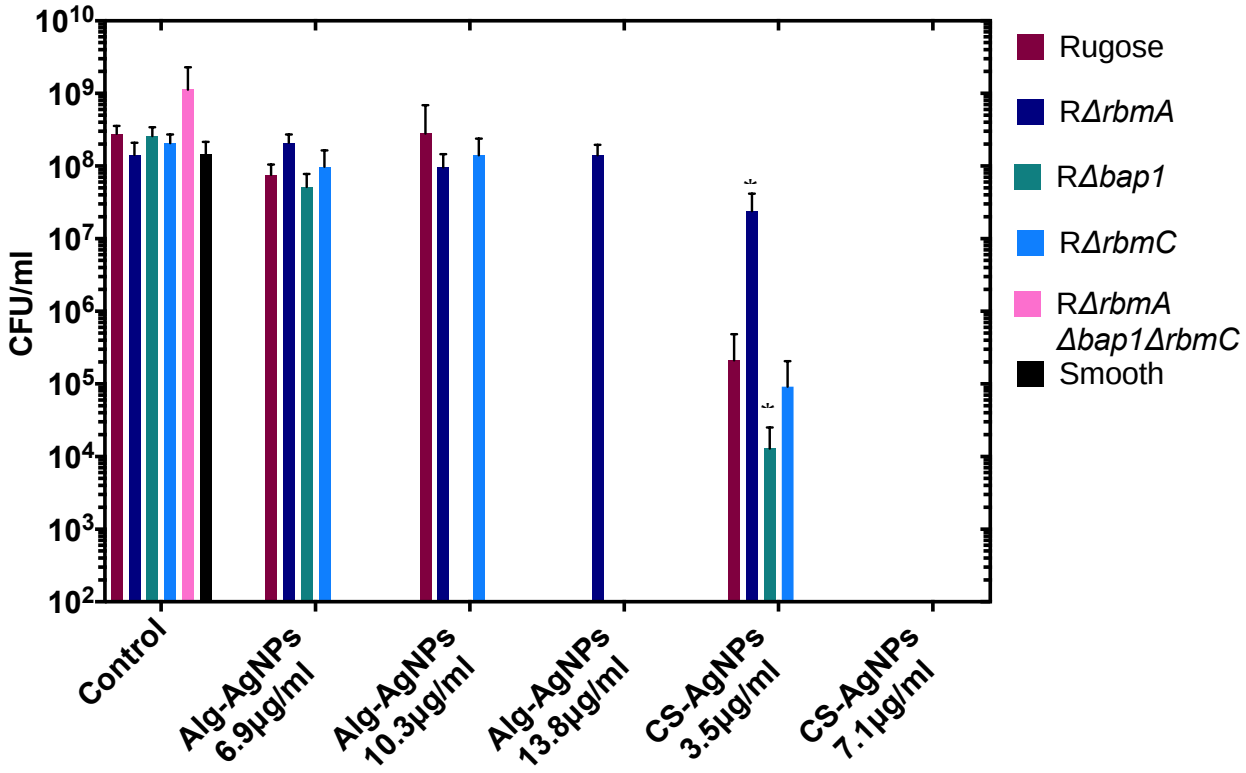

Figure 6-4 Antibacterial effect of AgNPs on mature pellicle biofilms after 24 h treatment. *Statistically significant difference p < 0 .05, compared to the rugose wild-type treated with CS-AgNPs.

The AgNPs antibacterial activity was then assessed on mature pellicle biofilms and the effect of some essential matrix components on bacteria susceptibility was evaluated. The biofilms were exposed to various concentrations of AgNPs and after 48 h the viability of bacteria was measured by counting the number of colony forming units (CFU), as reported in **Figure 6-4**. CS-AgNPs are more efficient than Alg-NPs since 7.1 µg/ml is required to kill the rugose variant, while almost the double of Alg-AgNPs is needed to achieve this result. Non-pellicle formers – the smooth variant and the rugose mutant not producing three major matrix proteins (RΔ*rbma*Δ*bap1*Δ*rbmC*), are more susceptible to both types of AgNPs. Indeed, for those two bacterial strains, Alg-AgNPs and CS-AgNPs eradicate the bacteria within the pellicle at 6.9 µg/ml and 3.5 µg/ml respectively, while twice as much (13.8 µg/ml Alg-AgNPs and 7.1 µg/ml CS-AgNPs) is required to kill bacteria for the wild-type rugose variant producing a strong pellicle. When the protein Bap1 is absent from the matrix (RΔ*bap1*), the bacteria are more easily killed by AgNPs. A significant reduction is already observed for CS-AgNPs at 3.5 µg/ml, while Alg-AgNPs display antibacterial properties at 10.3 µg/ml for this mutant, instead of 13.8 µg/ml for the wild-type rugose. Removing the protein RbmC (RΔ*rbmC*) does not impact the antibacterial resistance of the biofilm: the same concentrations of Alg-AgNPs and CS-AgNPs used for the rugose wild-type are required to kill this mutant.

The mutant not producing the protein RbmA (RΔ*rbmA*) appears to be more resistant to Alg-AgNPs since little effect is observed when the pellicle is exposed to 13.8 µg/ml of Alg-AgNPs – a lethal concentration to all other wild-type and mutants. The CS-AgNPs also has an attenuated antibacterial effect on the RΔ*rbmA* mutant at 3.5 µg/ml, compared to the wild-type variant. However, less variation is observed overall regarding the antibacterial activity of CS-AgNPs between the various *Vibrio* mutants, and they ultimately kill all the bacteria at 7.1 µg/ml. Again, this could be due to the residual content of Ag^+ and smaller nanoparticles size, combined with the positive charges of the chitosan, that penetrate the pellicle more easily and can damage the bacteria.

Although the role of each matrix component is still not fully understood, they clearly appear to play a key role in the pellicle biofilm resistance to silver nanoparticles. Removing structural matrix proteins impacts the activity of AgNPs on fully formed biofilms, either by decreasing (RΔ*rbmA*) or increasing (RΔ*bap1*) their bactericidal properties.

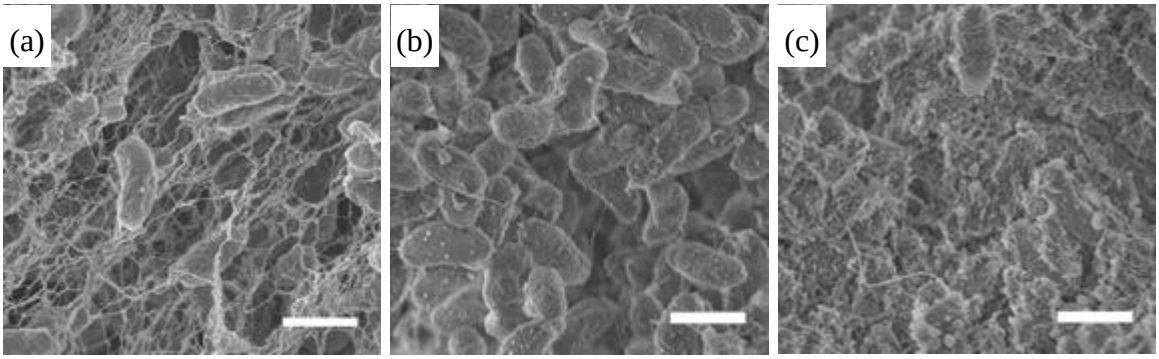

Figure 6-5 Global view of the microstructure of a rugose mature pellicle exposed for 24 h to (a) deionized water as control ; (b) 10.3 µg/ml Alg-AgNPs ; (c) 3.5 µg/ml CS-AgNPs. The scale bar is 1 µm.

The effect of both AgNPs on the rugose mature biofilm microstructure was evaluated by scanning electron microscopy (SEM) (**Figure 6-5**). The rugose pellicle was treated for 24 h with deionized water as a negative control (Fig. 6-5a), 10.3 µg/ml of Alg-AgNPs (Fig. 6-5b) or 3.5 µg/ml of CS-AgNPs (Fig. 6-5c), which are sub-lethal concentrations (see Figure 6-4). In both cases, the biofilm structure appears quite weaker, if not collapsed, when exposed to AgNPs. Most of the extracellular matrix material is not visible anymore after 24 h of AgNPs treatment. This suggests that the nanoparticles interact with the extracellular matrix components by disturbing and/or disrupting the biofilm structure. Moreover, all of the bacterial cells are covered with AgNPs in the case of CS-AgNPs, which again could be due to electrostatic interactions since chitosan is a polymer carrying positive charges at a pH below 6, and thus is more likely to interact with the negatively charged bacterial membrane.

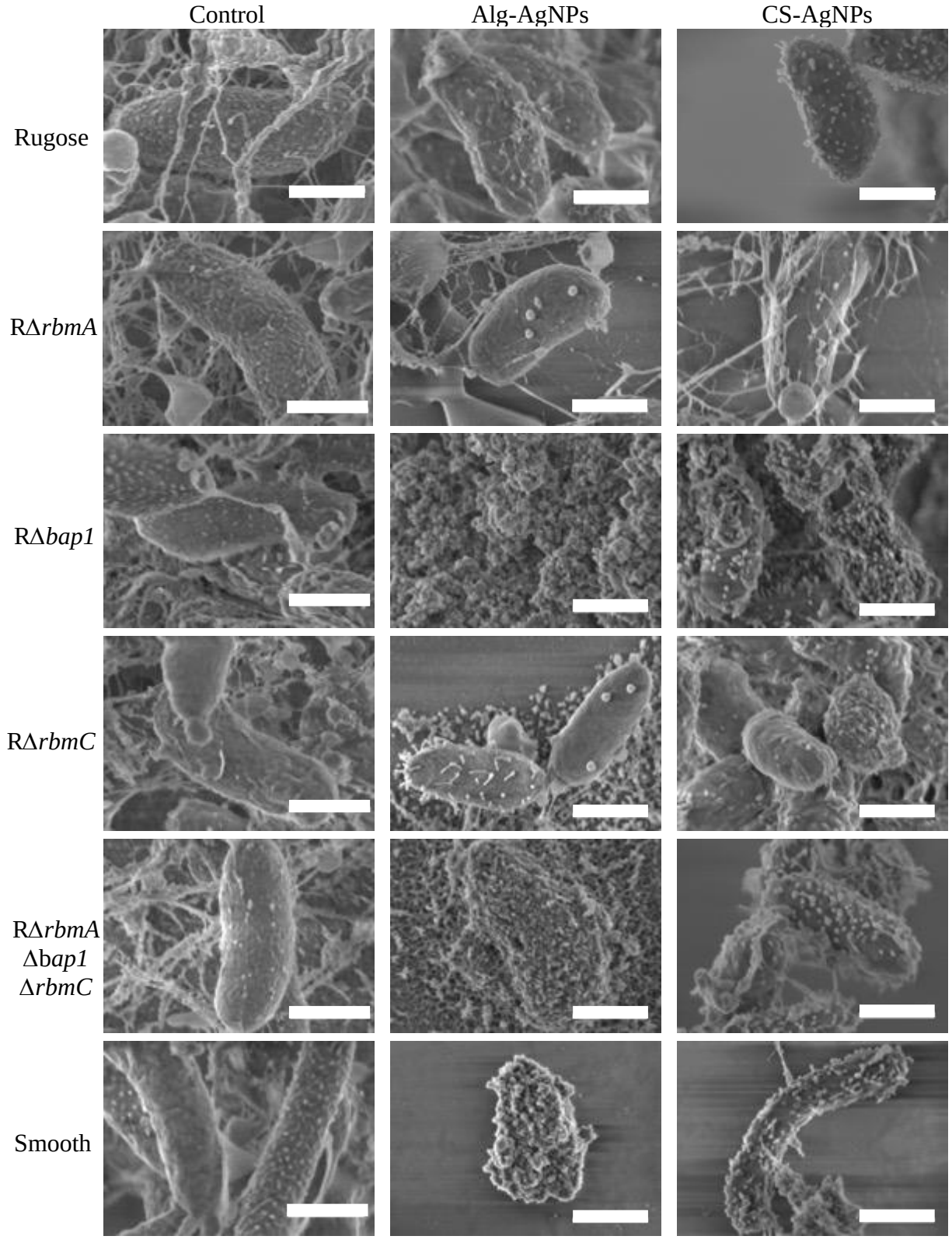
Control
Alg-AgNPs
CS-AgNPs
Rugose
RΔ*rbmA*
RΔ*bap1*
RΔ*rbmC*
RΔ*rbmA*
Δb*ap1*
Δ*rbmC*
Smooth

Figure 6-6 Structural analysis of the mature biofilms of rugose, RΔ*rbmA*, RΔ*bap1*, RΔ*rbmC*, RΔ*rbmA*Δ*bap1*Δ*rbmC* and smooth strains, after treatment with deionized water for the control, Alg-AgNPs or CS-AgNPs, for 24 h. The scale bar is 500 nm.

The impact of AgNPs on the various strains and mutants of bacterial cells embedded in the biofilm's extracellular matrix was also evaluated by SEM (**Figure 6-6** and **Figure S4**). Mature biofilms were exposed to 10.3 µg/ml Alg-AgNPs – a lethal concentration for non-biofilm formers RΔ*rbmA*Δ*bap1*Δ*rbmC* and smooth variant, as well as RΔ*bap1*, according to the CFU/ml values (Figure 6-4). For CS-AgNPs, a concentration of 3.5 µg/ml was used, which is also lethal for non-biofilm formers. As a negative control, biofilms were exposed to deionized water, and the results show that the bacteria cells embedded in the extracellular matrix are undamaged and smooth.

For the non-biofilm formers, both types of AgNPs significantly damage the bacterial morphology and debris from cell lysis are observed, demonstrating the antibacterial properties of AgNPs. Biofilm-formers bacteria are able to retain their morphological integrity when exposed to Alg-AgNPs – except for the weak biofilm formed by RΔ*bap1*, supporting the hypothesis that the extracellular matrix plays a crucial role in the bacteria protection to AgNPs. Few Alg-AgNPs are observed on the bacterial cells of those biofilm-formers, confirming the role of the biofilm matrix as a physical barrier against larger nanoparticles.

All bacterial strains exposed to CS-AgNPs appear to be covered by small nanoparticles. Moreover, bacteria display crenelated surfaces suggesting membrane damages and demonstrating the antibacterial activity of CS-AgNPs. Clearly, CS-AgNPs appear to have a more efficient antibacterial effect across the different bacterial strains compared to Alg-AgNPs.

6.4 Discussion

Bacteria living in biofilms exhibit a greater resistance to antimicrobials. Metallic nanoparticles, and more specifically silver nanoparticles (AgNPs), have demonstrated a promising effectiveness in killing bacteria within biofilms [187, 188]. When AgNPs are in contact with biofilms, they interact with the EPS components (i.e. proteins, polysaccharides, lipids, etc.) via various forces

(i.e. electrostatic, hydrophobic, Van der Waals, etc.), which influence their diffusion within the biofilm [189]. Thus, the biofilm composition and chemistry are important factors mitigating the AgNPs antibacterial action.

CS-AgNPs exhibit a higher antibacterial activity against planktonic *V. cholerae* bacteria, with only 0.22 µg/ml required to inhibit bacterial growth, while 0.86 µg/ml of Alg-AgNPs is necessary. It can be explained first by the smaller and more homogeneous size of CS-AgNPs compared to Alg-AgNPs, since it was demonstrated previously that smaller nanoparticles have enhanced antibacterial efficiency [107]. Moreover, chitosan also possesses antibacterial properties and is positively charged, which increases the interactions with the negatively charged bacterial cells and thus the antibacterial efficiency of CS-AgNPs.

While no significant difference is observed with non-biofilm formers in the planktonic study (Table S3), the production and composition of EPS plays an important role in the antibacterial resistance in the biofilm formers. Mature pellicle biofilms show an increased tolerance to AgNPs compared to planktonic cells, as it was also observed in previous studies [180]. In addition, non-biofilm formers (RΔ*rbmA*Δ*bap1*Δ*rbmC* and smooth) are more susceptible to both types of AgNPs. By looking at the microstructure of the biofilms, the ECM organization is severely altered after exposition to AgNPs, indicating that AgNPs interact with EPS.

In particular, the protein Bap1 contributes to the biofilm resistance to AgNPs since when Bap1 was removed (RΔ*bap1*) the mature biofilm was much more susceptible to AgNPs than the rugose wild-type, and the microstructure collapsed after the AgNPs addition. This protein is known for its role in biofilm hydrophobicity, mechanical strength and resistance to antimicrobial peptides [67, 190]. In contrast, another protein, RbmA, had an interesting role in mediating *V. cholerae* biofilm susceptibility to AgNPs. The biofilm tolerance to AgNPs increased when this protein, responsible for cell-cell adhesion and biofilm integrity [191], was removed (RΔ*rbmA*). This suggests that when RbmA is absent from the biofilm, other matrix components could interact with AgNPs and reduce their antibacterial activity. The effect of those matrix proteins on the biofilm resistance to AgNPs was less pronounced with CS-AgNPs compared to Alg-AgNPs, which could be due to the residual concentration of ionic silver present in the suspension as well as chitosan, both known for their antibacterial properties. Moreover, CS-AgNPs had overall a higher antibacterial effect on all the strains, with the combined action of AgNPs, the chitosan and ionic silver present in the suspension.

Those results demonstrate the important role of the interactions occurring between the ECM components and the AgNPs on their bactericidal efficiency. The antibacterial activity of AgNPs against fully formed biofilms was amplified or reduced by removing specific structural proteins from the ECM. Thus, a better understanding of the interactions between the ECM components and nanoparticles is required to design appropriate nanoparticles with the highest bactericidal activity.

6.5 Conclusion

V. cholerae mature biofilms were exposed to AgNPs, synthesized via a green chemistry process using either alginate or chitosan biopolymers as reductors and stabilizers. Both types of AgNPs successfully exhibited antibacterial activity against biofilms, although the biofilm matrix offered an increased protection compared to planktonic cells. AgNPs interacted with the biofilm matrix and were able to disrupt or destroy the microstructure of established biofilms. The nature of the interactions and the antibacterial effect depended on the chemical properties of both the biofilm matrix and nanoparticles. Structural matrix proteins Bap1 and RbmA had a major impact on the overall bactericidal activity of AgNPs.

Altogether, those results highlighted the role of the biofilm composition in the antibacterial resistance to AgNPs. Understanding the interactions between nanoparticles and the biofilm matrix is crucial to modulate the nanoparticles properties in order to maximize their antibacterial activity. Future work will aim to understand the role of RbmA in *V. cholerae* biofilm susceptibility to AgNPs, as well as deepening the understanding of the molecular origin of the biofilms resistance mechanisms to nanoparticles in order to design appropriate antibacterial strategies.

ACKNOWLEDGEMENTS: We thank the Electronic Microscopy Platform at Université de Montréal (Prof. Antonio Nanci and Aurélien Fouillen) for their assistance in electron microscopy analyses, and the *Centre de Caractérisation Microscopique des Matériaux* (CM2) (Prof. Gilles L'Espérance and Jean-Philippe Masse) at Polytechnique Montreal for access to the high resolution TEM. We thank Prof. Kevin Wilkinson and Nesrine Amiri (Université de Montréal) for the use of the SP-ICPMS equipment.

6.6 Supporting information

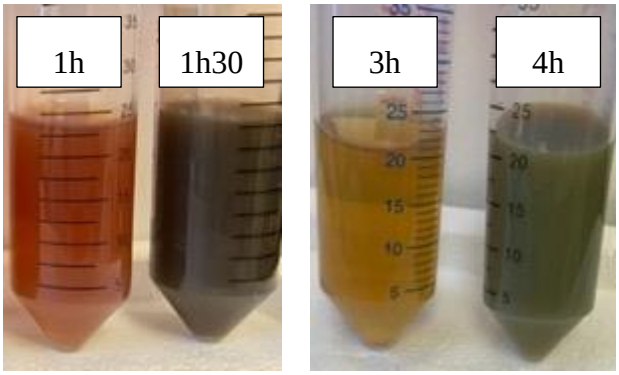

Alg-AgNPs CS-AgNPs

Figure S1 effect of time of AgNPs hydrothermal synthesis

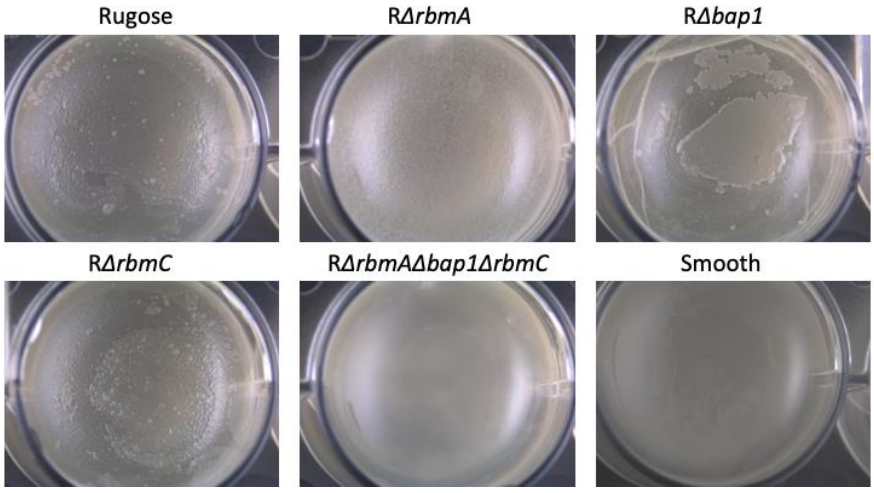

Figure S2 Pellicle morphology in 24-well plates after 48 h at 26 °C.

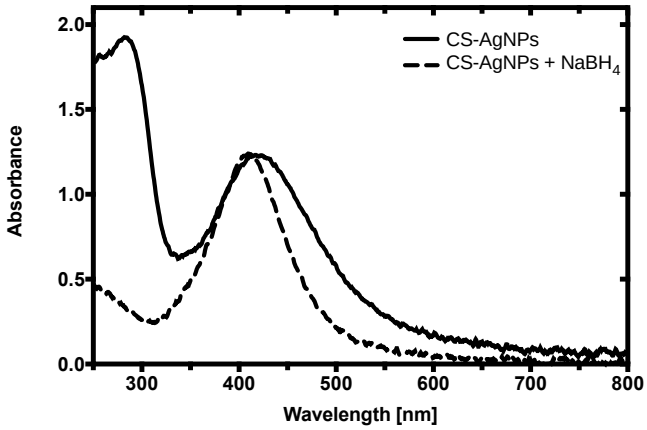

Figure S3 UV-vis spectra showing the reduction of the remaining $AgNO_3$ in the CS-AgNPs suspension.

Table S1 *V. cholerae* strains used in this study

Strain	**Description**
Rugose	*Vibrio cholerae* O1 El Tor A1552R, rugose wild-type variant[192]
RΔ*rbmA*	Rugose-variant unable to produce matrix protein RbmA[67]
RΔ*bap1*	Rugose-variant unable to produce matrix protein Bap1[67]
RΔ*rbmC*	Rugose-variant unable to produce matrix protein RbmC[67]
RΔ*rbmA*Δ*bap1*Δ*rbmC*	Rugose-variant unable to produce matrix proteins RbmA, Bap1 and RbmC[67]
Smooth	*Vibrio cholerae* O1 El Tor A1552, smooth wild-type variant[193]

Table S2 AgNPs size and concentration (ICP-MS)

Sample	**Size (nm)**	**Ionic concentration (µg/ml)**	**Particle concentration (µg/ml)**	**Total concentration after acidic digestion (µg/ml)**
Alg-AgNPs	19.7±5.3	3.5±0.4	26.2±0.8	27.6±0.6
CS-AgNPs	19.4±7.8	4.3±0.5	2.3±0.1	28.3±0.2

The ionic concentration corresponds to the silver ionic content, the particle concentration to the nanoparticles concentration.

Table S3 Minimal bactericidal concentration (MBC)

Bacterial strain	**Alg-AgNPs (µg/ml)**	**CS-AgNPs (µg/ml)**
Rugose	0.86 - 1.72	0.22 - 0.44
RΔ*rbmA*	0.86 - 1.72	0.22 - 0.44
RΔ*bap1*	0.43 - 1.72	0.22 - 0.44
RΔ*rbmC*	0.43 - 1.72	0.44
RΔ*rbmA*Δ*bap1*Δ*rbmC*	0.86 - 1.72	0.44
Smooth	0.86 - 1.72	0.44

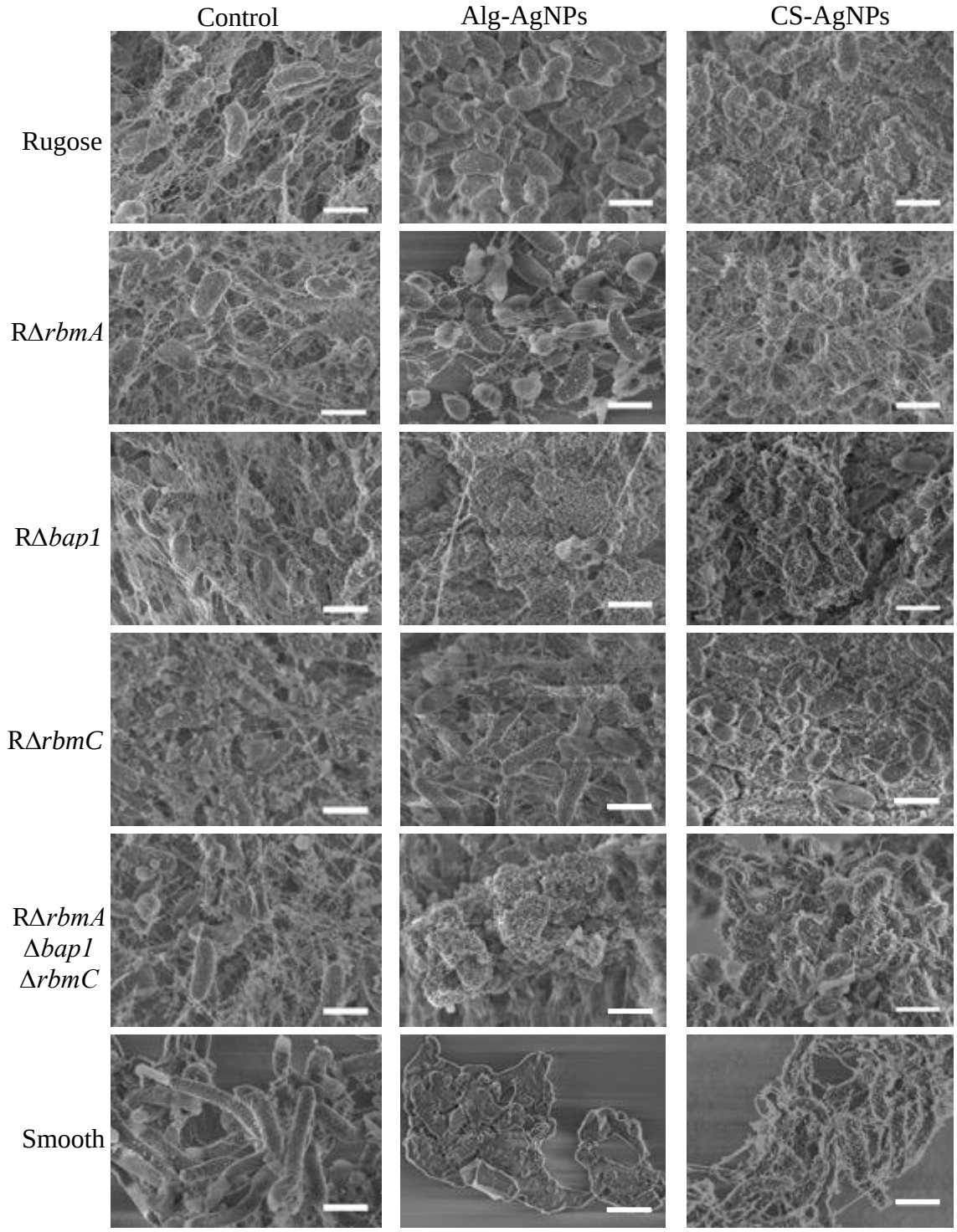

Figure S4 Global view of the microstructure of the mature biofilms of rugose, RΔ*rbmA*, RΔ*bap1*, RΔ*rbmC*, RΔ*rbmA*Δ*bap1*Δ*rbmC* and smooth strains, after treatment with deionized water for the control, Alg-AgNPs or CS-AgNPs, for 24 h. The scale bar is 1 µm.

CHAPTER 7 GENERAL DISCUSSION

Bacteria predominantly live in mixed-species communities and those inter-species interactions modify the biofilms physicochemical properties. Biofilms are generally characterized *in vitro* with a single-specie model and using traditional microbiological techniques at specific time-points.

Interfacial rheology is a unique tool which quantitatively follows the biofilm growth in real-time. In this work, we used two interfacial rheology setups to quantitatively measure the viscoelastic properties of dual-species biofilms over time. The first interfacial rheology system from Anton-Paar consisted of an interfacial shear cell made of glass, with a stainless steel external cover and the bicone geometry positioned at the air-liquid interface. This geometry has a large contact area with the subphase, making it less sensitive compared to other geometries. For example, it was recently demonstrated that the bicone geometry is not sensitive enough to measure weak fatty alcohol interfaces, however this stiffer geometry is appropriate to obtain high moduli associated with stronger interfaces [64]. In this work, this geometry was not sensitive enough to the efficiently capture in a reproducible manner the bacterial and protein adsorption at the interface during the first couple of hours of testing. Moreover, during this time frame, the setup was extremely sensitive to the environmental vibrations, making it difficult to obtain reproducible results for this first adsorption phase. However, once the solid biofilm started to form and attached itself to the bicone, the setup successfully measured reproducible viscoelastic moduli for mature biofilms and unique trends in the viscoelastic profiles for each individual species were unraveled. The closed steel and glass flow cell allowed good control of the temperature (30 °C) over the experimental time period. Evaporation is a concern when performing extended interfacial rheology measurements, since the surface should remain stable and flat to accurately measure the interfacial rheological properties. To avoid any evaporation and improve the homogeneity of the media inside the flow cell, a heating lamp was placed outside to heat the cover.

The second interfacial rheological setup employed in this work was a double-wall ring flow cell combined with a du Noüy ring. The flow cell was made of Teflon, thus the temperature could not be precisely set and controlled. Since the experiments were conducted at 26 °C, it did not greatly influence the measurements. The evaporation was also controlled with the injection of fresh media and the removal of any excess media with a vacuum system. The du Noüy ring allowed precise and

reproducible measurements especially at the beginning of the biofilm formation, unlike the bicone. Moreover, this interfacial rheology setup was isolated from external vibrations with an anti-vibration table, which reduced variations in the measurements. Since both interfacial rheology setups were used with biological samples, the environment was kept as sterile as possible, with a cleaning protocol carefully established. The bicone geometry required a more thorough sterilization compared to the du Noüy ring that was sterilized using a flame. Since the flow cell combined with the bicone was closed and autoclavable, it reduced the contamination risks compared to the double-wall ring flow cell setup.

Bacteria are sensitive to environmental changes, such as the chemical composition of the media or the temperature. While studying dual-species bacterial biofilms is a step closer to more realistic conditions, specific environmental growth conditions were chosen as a model in order to study the interactions between the two bacterial species. *Bacillus licheniformis* and *Pseudomonas fluorescens* are two environmental bacteria and thus likely to coexist together in the environment. Their interactions were analyzed in this work at 30 °C, however the competition observed could be very different if the temperature changed. For example *P. fluorescens* does not form a pellicle biofilm at 37 °C, while *B. licheniformis* forms a strong pellicle in a short timeframe. On the other hand, decreasing the temperature to 25 °C slows down considerably the formation of pellicle for *B. licheniformis*. Furthermore, the temperature can influence the extracellular matrix composition, for example at a temperature above 30 °C, *Escherichia coli* is not able to produce curli, while its production is inhibited in the presence of *Vibrio cholerae* at 26 °C. The media composition has also a great influence on the interspecies interactions: in the presence of salt, *Vibrio cholerae* can activate a predatory mechanism (type VI) against other bacterial species such as *Escherichia coli*. The media YESCA did not contain any salt, thus only the competition for the interface was observed. Thus, in this work controlled environmental conditions (temperature and media) were used in order to apprehend and unravel the competition between two bacterial species for the interface. A new interfacial exchange cell will allow a quantitative study of the effect of environmental changes, such as temperature, media composition, on multi-species biofilms properties in the future.

The effects of environmental changes on the biofilm composition is crucial to develop appropriate antimicrobial strategies. Indeed, the biofilm polymeric matrix acts as a protective barrier and the

antibacterial silver nanoparticles used in this work interacted with proteins and polysaccharides present in *V. cholerae* matrix. Those interactions change the antibacterial activity of the silver nanoparticles by either making them more efficient in killing bacteria within the biofilm or reducing their antibacterial activity. In addition to environmental conditions, the biofilm matrix composition is also subjected to the bacteria specific strain. Within a same bacterial specie, different variants might produce different biopolymers in the matrix. For example, the *V. cholerae* smooth variant secretes reduced amount of the polysaccharide VPS, which affects its ability to form pellicle biofilms and thus decreases its resistance to AgNPs compared to the rugose variant. In the case of multi-species biofilms, additional interactions might occur, with other matrix components involved which could also modify the antibacterial activity of nanoparticles. Antibacterial treatments have to address the complex chemistry of the extracellular matrix biofilms which changes with the environment and the bacterial species involved.

CHAPTER 8 CONCLUSION AND RECOMMENDATIONS

8.1 Conclusions

The aim of this research was to characterize and establish the interdependence between the viscoelastic properties and composition of dual-species biofilms at the air-liquid interface, and to investigate the role of the polymeric matrix in the antimicrobial resistance. Although the biofilms viscoelastic properties have been increasingly studied over the past two decades, few researches have focused on biofilms involving multiple species. Interfacial rheology has been recognized as a quantitative and innovative method to measure in real-time the viscoelastic properties of pellicle biofilms as they form.

In a first step, a model environmental dual-species biofilm was chosen to develop and adapt the interfacial rheology technique for multispecies biofilms. The real-time quantitative rheological properties of *P. fluorescens* and *B. licheniformis* biofilm were related to the microstructure and microbiological composition of the mature pellicle. Those findings demonstrated that the biofilm growth rate was a major factor in the dual-species biofilm composition, with the dominant bacteria *P. fluorescens* being the fastest colonizer under the conditions studied. After reaching a first equilibrium at 48 h, the dual-species biofilm reached its maturation at 72 h and the bacteria *B. licheniformis* was able to increase its contribution to the dual-species biofilm bacterial population in the final 72 h. Those results highlighted the importance of real-time quantitative measurements of the biofilm viscoelastic properties to unravel the interspecies competition for the interface, driven by the planktonic growth factor. While microbiological and rheological analysis of the mature dual-species biofilm at 72 h showed that both bacteria were equally present, it was not possible to determine whether *B. licheniformis* was also contributing to the viscoelastic properties since the ECM composition was not analyzed.

In a second phase, a dual-species system was chosen to incorporate the pathogenic bacteria *V. cholerae* to a co-culture with the well-known Gram-negative *E. coli.* The interfacial rheological measurements showed that the dual-species biofilm elastic and viscous moduli followed the *V. cholerae* single-species rheological behavior. Combined with macroscopic biofilm morphology, this suggested that *V. cholerae* might be the dominant bacteria. When *V. cholerae* was added 18 h

after *E. coli*, the biofilm properties were instead similar to the *E. coli* single-species biofilm, which led to hypothesize that the biofilm formation rate was a major factor in the bacteria competitive interactions, since *V. cholerae* formed a biofilm at the air-liquid interface faster than *E. coli*. The analysis of key matrix components was performed to evaluate the impact of interspecies interactions on the extracellular matrix composition. Detection of the main matrix proteins – realized by Western blot assays, showed that *V. cholerae* inhibited the production of curli from *E. coli*, even when this pathogen was initially added in less than 0.1%. Only when *E. coli* was given an 18 h head start on *V. cholerae*, was it able to secrete curli. However, fluorescence analysis revealed that *E. coli* was able to produce its other main matrix component, pEtN cellulose, in the presence of *V. cholerae.* Western blot analysis also demonstrated that *V. cholerae* was able to produce its protein Bap1 in the dual-species biofilm, responsible for the viscoelastic properties, even when the bacteria was initially present at 0.1%. The molecular analysis of the extracellular matrix supported the interfacial rheology results showing that *V. cholerae* was the dominant species due to its fast biofilm formation at the interface. Those results established the relationship between the mechanical properties and molecular biofilm matrix composition of a dual-species biofilm pathogenic model. Antagonistic interactions dictated the dual-species biofilm matrix composition at the air-liquid interface, with *V. cholerae* inhibiting *E. coli* production of a key protein.

Finally, an antibacterial strategy was developed against *V. cholerae* biofilms. Two types of silver nanoparticles, synthesized via a green hydrothermal process with either alginate or chitosan, two natural and oppositely charged polysaccharides, were used against *V. cholerae* mature pellicles. The extracellular matrix protected bacteria against AgNPs, with non-biofilm formers being more susceptible to both types of AgNPs. Overall chitosan-stabilized silver nanoparticles (CS-AgNPs) were almost four times more efficient against *V. cholerae* biofilms compared to alginate-stabilized nanoparticles (Alg-AgNPs). This higher antibacterial activity could be explained first by their smaller size and the presence of ionic silver in the suspension, known to contribute to the antibacterial properties. Moreover, since the bacterial membrane was negatively charged, as well as other matrix polymers, the positively charged CS-AgNPs likely interacted more with the biofilm components. Those interactions were further investigated by individually removing some major matrix components and the influence of the extracellular matrix polymeric composition on the biofilm resistance to AgNPs was assessed. Two major proteins in particular, Bap1 and RbmA, had

a major impact on the AgNPs antibacterial activity, by either improving or decreasing it. Altogether, those results demonstrate that the interactions between the biofilm and the antibacterial nanoparticles are mediated by the biofilm polymeric composition and the nanoparticles surface chemistry.

8.2 Original contributions

The original contributions of this research are the following:

1. Adapting the interfacial rheology methodology for dual-species biofilms, using both the bicone and the du Noüy geometries, for environmental and pathogenic models.
2. Demonstrating that planktonic growth governs the competitive interactions in *P. fluorescens* and *B. licheniformis* environmental dual-species biofilm.
3. Establishing that the biofilm growth rate is a major factor impacting the bacterial interactions in *V. cholerae* and *E. coli* pellicle biofilms.
4. Demonstrating that *V. cholerae* inhibits the production of the essential *E. coli* matrix component curli, displaying thus antagonistic interactions in the biofilm at the air-liquid interface.
5. Confirming that the biofilm resistance to AgNPs depends on *V. cholerae* biofilm's polymeric matrix composition, as well as the chemical properties of AgNPs.

8.3 Recommendations

This multidisciplinary research projects provides an extensive mechanical and microstructural insights of dual-species pellicle biofilms, as well as the role of the polymeric matrix in the resistance to antimicrobials. Future studies should include:

1. As observed in the *V. cholerae* biofilm, removing key matrix proteins modified the overall bacterial resistance to antimicrobials. A deeper analysis of the interactions between the matrix components and the nanoparticles would be required to understand the role of each protein in the overall bacterial resistance. The protein RbmA especially appears to be of great importance and its interactions with nanoparticles should be investigated. Moreover,

the overall biofilm chemical composition needs to be determined to target appropriate matrix components to destroy established biofilms.

2. Biofilms are heterogenous structures. Thus characterizing the mechanical and composition on a more microscopic level would bring important knowledge required to prevent or disturb biofilms formation, using microrheology or microfluidics. For example, the role of bacterial surface components such as fimbriae in the first adhesion might provide insights into the interactions in multispecies biofilms.
3. Since the biofilm composition depends on the chemical composition of the environment as well as some physiological parameters such as the temperature or pH, evaluating the impact of such changes on the biofilm properties would be crucial to develop appropriate antimicrobial treatments.
4. In this work, dual-species biofilms were used as a model to establish some of the interspecies interactions. To improve the model and have more realistic conditions, additional species should be added to the system.
5. Antimicrobials were used on mature single-specie biofilms. The next step would be to apply them on multi-species biofilms and test the resistance of the heterogenous community. In addition to that, it would be pertinent to inject those antimicrobials at different stages of the biofilm development.
6. Bacteria are social microorganisms and they use quorum-sensing to communicate. In addition to lethal antimicrobials such as silver nanoparticles, it would be pertinent to apply anti-quorum molecules to prevent multi-species biofilm formation for example.

REFERENCES

[1] H.-C. Flemming and S. Wuertz, "Bacteria and archaea on Earth and their abundance in biofilms," *Nature Reviews Microbiology,* vol. 17, no. 4, pp. 247-260, 2019/04/01 2019, doi: 10.1038/s41579-019-0158-9.

[2] "Antony van Leeuwenhoek and his “Little Animals”: being some Account of the Father of Protozoology and Bacteriology and his Multifarious Discoveries in these Disciplines," *Nature,* vol. 130, no. 3288, pp. 679-680, 1932/11/01 1932, doi: 10.1038/130679a0.

[3] J. W. Costerton, G. G. Geesey, and K. J. Cheng, "How Bacteria Stick," *Scientific American,* vol. 238, no. 1, pp. 86-95, 1978/01 1978, doi: 10.1038/scientificamerican0178-86.

[4] L. Yang, Y. Liu, H. Wu, N. Høiby, S. Molin, and Z. j. Song, "Current understanding of multi-species biofilms," *International Journal of Oral Science,* vol. 3, no. 2, pp. 74-81, 2011/04 2011, doi: 10.4248/ijos11027.

[5] S. Elias and E. Banin, "Multi-species biofilms: living with friendly neighbors," *FEMS Microbiol Rev,* vol. 36, no. 5, pp. 990-1004, Sep 2012, doi: 10.1111/j.1574-6976.2012.00325.x.

[6] (2002). *RESEARCH ON MICROBIAL BIOFILMS*. [Online] Available: https://grants.nih.gov/grants/guide/pa-files/PA-03-047.html

[7] D. Davies, "Understanding biofilm resistance to antibacterial agents," *Nature Reviews Drug Discovery,* vol. 2, no. 2, pp. 114-122, 2003/02 2003, doi: 10.1038/nrd1008.

[8] I. W. Sutherland, "Biofilm exopolysaccharides: a strong and sticky framework," *Microbiology,* vol. 147, no. 1, pp. 3-9, 2001/01/01 2001, doi: 10.1099/00221287-147-1-3.

[9] A. R. M. Coates, G. Halls, and Y. Hu, "Novel classes of antibiotics or more of the same?," *British Journal of Pharmacology,* https://doi.org/10.1111/j.1476-5381.2011.01250.x vol. 163, no. 1, pp. 184-194, 2011/05/01 2011, doi: https://doi.org/10.1111/j.1476-5381.2011.01250.x.

[10] R. M. Klevens *et al.*, "Estimating Health Care-Associated Infections and Deaths in U.S. Hospitals, 2002," *Public Health Reports,* vol. 122, no. 2, pp. 160-166, 2007/03/01 2007, doi: 10.1177/003335490712200205.

[11] R. M. Donlan, "Biofilms: microbial life on surfaces," *Emerg Infect Dis,* vol. 8, no. 9, pp. 881-90, Sep 2002, doi: 10.3201/eid0809.020063.

[12] M. Kostakioti, M. Hadjifrangiskou, and S. J. Hultgren, "Bacterial biofilms: development, dispersal, and therapeutic strategies in the dawn of the postantibiotic era," *Cold Spring Harb Perspect Med,* vol. 3, no. 4, p. a010306, Apr 1 2013, doi: 10.1101/cshperspect.a010306.

[13] Harbron R.S. and K. C.A., "Aspects of Cell Adhesion.," in *In: Melo L.F., Bott T.R., Bernardo C.A. (eds) Fouling Science and Technology.*, vol. 145. NATO ASI Series (Series E: Applied Sciences): Springer, Dordrecht, 1988, pp. 125-140.

[14] C. Beloin, A. Roux, and J. M. Ghigo, "*Escherichia coli* biofilms," *Curr Top Microbiol Immunol,* vol. 322, pp. 249-89, 2008, doi: 10.1007/978-3-540-75418-3_12.

[15] G. A. O'Toole and R. Kolter, "Flagellar and twitching motility are necessary for *Pseudomonas aeruginosa* biofilm development," *Mol Microbiol,* vol. 30, no. 2, pp. 295-304, Oct 1998, doi: 10.1046/j.1365-2958.1998.01062.x.

[16] P. Watnick and R. Kolter, "Biofilm, City of Microbes," *Journal of Bacteriology,* vol. 182, no. 10, p. 2675, 2000, doi: 10.1128/JB.182.10.2675-2679.2000.

[17] P. I. Watnick and R. Kolter, "Steps in the development of a *Vibrio cholerae* El Tor biofilm," *Mol Microbiol,* vol. 34, no. 3, pp. 586-95, Nov 1999, doi: 10.1046/j.1365-2958.1999.01624.x.

[18] P. S. Stewart and M. J. Franklin, "Physiological heterogeneity in biofilms," *Nature Reviews Microbiology,* vol. 6, no. 3, pp. 199-210, 2008/03/01 2008, doi: 10.1038/nrmicro1838.

[19] R. T. Vasudevan, "Biofilms: Microbial Cities of Scientific Significance," *J Microbiol Exp.,* vol. 1, no. 3, pp. 84-98, 2014, doi: 10.15406/jmen.2014.01.00014.

[20] H.-C. Flemming and J. Wingender, "The biofilm matrix," *Nature Reviews Microbiology,* 2010/08/02 2010, doi: 10.1038/nrmicro2415.

[21] E. Karatan and P. Watnick, "Signals, regulatory networks, and materials that build and break bacterial biofilms," *Microbiol Mol Biol Rev,* vol. 73, no. 2, pp. 310-47, Jun 2009, doi: 10.1128/MMBR.00041-08.

[22] M. Otto, "Staphylococcal Infections: Mechanisms of Biofilm Maturation and Detachment as Critical Determinants of Pathogenicity," *Annual Review of Medicine,* vol. 64, no. 1, pp. 175-188, 2013/01/14 2013, doi: 10.1146/annurev-med-042711-140023.

[23] R. D. Monds and G. A. O'Toole, "The developmental model of microbial biofilms: ten years of a paradigm up for review," *Trends in Microbiology,* vol. 17, no. 2, pp. 73-87, 2009/02/01/ 2009, doi: https://doi.org/10.1016/j.tim.2008.11.001.

[24] K. Lewis, "Persister cells," *Annu Rev Microbiol,* vol. 64, pp. 357-72, 2010, doi: 10.1146/annurev.micro.112408.134306.

[25] H. Anwar, M. K. Dasgupta, and J. W. Costerton, "Testing the susceptibility of bacteria in biofilms to antibacterial agents," *Antimicrob Agents Chemother,* vol. 34, no. 11, pp. 2043-6, Nov 1990, doi: 10.1128/aac.34.11.2043.

[26] H. C. Flemming, T. R. Neu, and D. J. Wozniak, "The EPS matrix: the "house of biofilm cells"," *J Bacteriol,* vol. 189, no. 22, pp. 7945-7, Nov 2007, doi: 10.1128/JB.00858-07.

[27] D. O. Serra, A. M. Richter, and R. Hengge, "Cellulose as an architectural element in spatially structured *Escherichia coli* biofilms," *Journal of Bacteriology,* vol. 195, no. 24, p. 5540, 2013, doi: 10.1128/JB.00946-13.

[28] S. S. Branda, F. Chu, D. B. Kearns, R. Losick, and R. Kolter, "A major protein component of the *Bacillus subtilis* biofilm matrix," *Mol Microbiol,* vol. 59, no. 4, pp. 1229-38, Feb 2006, doi: 10.1111/j.1365-2958.2005.05020.x.

[29] B. Frølund, R. Palmgren, K. Keiding, and P. H. Nielsen, "Extraction of extracellular polymers from activated sludge using a cation exchange resin," *Water Research,* vol. 30,

no. 8, pp. 1749-1758, 1996/08/01/ 1996, doi: https://doi.org/10.1016/0043-1354(95)00323-1.

[30] J. Wingender, M. Strathmann, A. Rode, A. Leis, and H. C. Flemming, "Isolation and biochemical characterization of extracellular polymeric substances from *Pseudomonas aeruginosa*," *Methods Enzymol,* vol. 336, pp. 302-14, 2001, doi: 10.1016/s0076-6879(01)36597-7.

[31] K. M. Colvin *et al.*, "The pel polysaccharide can serve a structural and protective role in the biofilm matrix of *Pseudomonas aeruginosa*," *PLoS Pathog,* vol. 7, no. 1, p. e1001264, Jan 27 2011, doi: 10.1371/journal.ppat.1001264.

[32] P. N. Danese, L. A. Pratt, and R. Kolter, "Exopolysaccharide Production Is Required for Development of *Escherichia coli* K-12 Biofilm Architecture," *Journal of Bacteriology,* vol. 182, no. 12, p. 3593, 2000, doi: 10.1128/JB.182.12.3593-3596.2000.

[33] I. Lasa and J. R. Penades, "Bap: a family of surface proteins involved in biofilm formation," *Res Microbiol,* vol. 157, no. 2, pp. 99-107, Mar 2006, doi: 10.1016/j.resmic.2005.11.003.

[34] E. Erskine, C. E. MacPhee, and N. R. Stanley-Wall, "Functional Amyloid and Other Protein Fibers in the Biofilm Matrix," *J Mol Biol,* vol. 430, no. 20, pp. 3642-3656, Oct 12 2018, doi: 10.1016/j.jmb.2018.07.026.

[35] C. B. Whitchurch, "Extracellular DNA Required for Bacterial Biofilm Formation," *Science,* vol. 295, no. 5559, pp. 1487-1487, 2002/02/22 2002, doi: 10.1126/science.295.5559.1487.

[36] A. L. Spoering and M. S. Gilmore, "Quorum sensing and DNA release in bacterial biofilms," *Current Opinion in Microbiology,* vol. 9, no. 2, pp. 133-137, 2006/04 2006, doi: 10.1016/j.mib.2006.02.004.

[37] Q. Wei and L. Ma, "Biofilm Matrix and Its Regulation in *Pseudomonas aeruginosa*," *International Journal of Molecular Sciences,* vol. 14, no. 10, pp. 20983-21005, 2013/10/18 2013, doi: 10.3390/ijms141020983.

[38] F. HC., "Why Microorganisms Live in Biofilms and the Problem of Biofouling.," in *Flemming HC., Murthy P.S., Venkatesan R., Cooksey K. Marine and Industrial Biofouling.*, vol. 4, B. Springer, Heidelberg Ed., no. Springer Series on Biofilms,), 2009.

[39] R. S. Wotton and T. M. Preston, "Surface Films: Areas of Water Bodies That Are Often Overlooked," *BioScience,* vol. 55, no. 2, pp. 137-145, 2005, doi: 10.1641/0006-3568(2005)055[0137:SFAOWB]2.0.CO;2.

[40] C. Hung *et al.*, "*Escherichia coli* biofilms have an organized and complex extracellular matrix structure," *mBio,* vol. 4, no. 5, pp. e00645-13, Sep 10 2013, doi: 10.1128/mBio.00645-13.

[41] M. N. Yap, C. H. Yang, J. D. Barak, C. E. Jahn, and A. O. Charkowski, "The Erwinia chrysanthemi type III secretion system is required for multicellular behavior," *J Bacteriol,* vol. 187, no. 2, pp. 639-48, Jan 2005, doi: 10.1128/JB.187.2.639-648.2005.

[42] K. L. Visick, K. P. Quirke, and S. M. McEwen, "Arabinose induces pellicle formation by Vibrio fischeri," *Appl Environ Microbiol,* vol. 79, no. 6, pp. 2069-80, Mar 2013, doi: 10.1128/AEM.03526-12.

[43] C. Wu, Ji Y. Lim, Gerald G. Fuller, and L. Cegelski, "Quantitative analysis of amyloid-Integrated biofilms formed by uropathogenic *Escherichia coli* at the air-liquid interface," *Biophysical Journal,* vol. 103, no. 3, pp. 464-471, 2012/08 2012, doi: 10.1016/j.bpj.2012.06.049.

[44] J. Armitano, V. Méjean, and C. Jourlin-Castelli, "Gram-negative bacteria can also form pellicles," *Environmental Microbiology Reports,* vol. 6, no. 6, pp. 534-544, 2014/12/01 2014, doi: 10.1111/1758-2229.12171.

[45] A. J. Spiers, J. Bohannon, S. M. Gehrig, and P. B. Rainey, "Biofilm formation at the air-liquid interface by the *Pseudomonas fluorescens* SBW25 wrinkly spreader requires an acetylated form of cellulose," *Molecular Microbiology,* vol. 50, no. 1, pp. 15-27, 2003/08/14 2003, doi: 10.1046/j.1365-2958.2003.03670.x.

[46] K. Scher, E. Kesselman, E. Shimoni, and S. Yaron, "Morphological analysis of young and old pellicles of *Salmonella* Typhimurium," *Biofouling,* vol. 23, no. 5-6, pp. 385-94, 2007, doi: 10.1080/08927010701648265.

[47] F. H. Yildiz and G. K. Schoolnik, "*Vibrio cholerae* O1 El Tor: identification of a gene cluster required for the rugose colony type, exopolysaccharide production, chlorine resistance, and biofilm formation," *Proc Natl Acad Sci U S A,* vol. 96, no. 7, pp. 4028-33, Mar 30 1999, doi: 10.1073/pnas.96.7.4028.

[48] S. Paytubi, C. Cansado, C. Madrid, and C. Balsalobre, "Nutrient Composition Promotes Switching between Pellicle and Bottom Biofilm in *Salmonella*," *Frontiers in Microbiology,* 10.3389/fmicb.2017.02160 vol. 8, p. 2160, 2017. [Online]. Available: https://www.frontiersin.org/article/10.3389/fmicb.2017.02160.

[49] I. Pastar *et al.*, "Interactions of methicillin resistant *Staphylococcus aureus* USA300 and *Pseudomonas aeruginosa* in polymicrobial wound infection," *PLoS One,* vol. 8, no. 2, p. e56846, 2013, doi: 10.1371/journal.pone.0056846.

[50] C. A. Fux, J. W. Costerton, P. S. Stewart, and P. Stoodley, "Survival strategies of infectious biofilms," *Trends Microbiol,* vol. 13, no. 1, pp. 34-40, Jan 2005, doi: 10.1016/j.tim.2004.11.010.

[51] S. K. Filoche, S. A. Anderson, and C. H. Sissons, "Biofilm growth of *Lactobacillus* species is promoted by *Actinomyces* species and *Streptococcus* mutans," *Oral Microbiology and Immunology,* vol. 19, no. 5, pp. 322-326, 2004/10 2004, doi: 10.1111/j.1399-302x.2004.00164.x.

[52] E. J. Stewart *et al.*, "Effect of Antimicrobial and Physical Treatments on Growth of Multispecies *Staphylococcal* Biofilms," *Applied and Environmental Microbiology,* vol. 83, no. 12, pp. e03483-16, 2017/04/14 2017, doi: 10.1128/aem.03483-16.

[53] A. Khare and S. Tavazoie, "Multifactorial Competition and Resistance in a Two-Species Bacterial System," *PLOS Genetics,* vol. 11, no. 12, p. e1005715, 2015/12/08 2015, doi: 10.1371/journal.pgen.1005715.

[54] L. C. M. Antunes and R. B. R. Ferreira, "Intercellular communication in bacteria," *Critical Reviews in Microbiology,* vol. 35, no. 2, pp. 69-80, 2009/03/20 2009, doi: 10.1080/10408410902733946.

[55] E. S. Gloag, S. Fabbri, D. J. Wozniak, and P. Stoodley, "Biofilm mechanics: Implications in infection and survival," *Biofilm*, vol. 2, p. 100017, 2020/12/01/ 2020, doi: https://doi.org/10.1016/j.bioflm.2019.100017.

[56] I. Klapper, C. J. Rupp, R. Cargo, B. Purvedorj, and P. Stoodley, "Viscoelastic fluid description of bacterial biofilm material properties," *Biotechnol Bioeng*, vol. 80, no. 3, pp. 289-96, Nov 5 2002, doi: 10.1002/bit.10376.

[57] Y. Liu and J.-H. Tay, "The essential role of hydrodynamic shear force in the formation of biofilm and granular sludge," *Water Research*, vol. 36, no. 7, pp. 1653-1665, 2002/04/01/ 2002, doi: https://doi.org/10.1016/S0043-1354(01)00379-7.

[58] C. S. Laspidou and B. E. Rittmann, "Modeling the development of biofilm density including active bacteria, inert biomass, and extracellular polymeric substances," *Water Research*, vol. 38, no. 14, pp. 3349-3361, 2004/08/01/ 2004, doi: https://doi.org/10.1016/j.watres.2004.04.037.

[59] P. Stoodley, I. Dodds, J. D. Boyle, and H. M. Lappin-Scott, "Influence of hydrodynamics and nutrients on biofilm structure," *J Appl Microbiol*, vol. 85 Suppl 1, pp. 19S-28S, Dec 1998, doi: 10.1111/j.1365-2672.1998.tb05279.x.

[60] B. W. Peterson, H. C. van der Mei, J. Sjollema, H. J. Busscher, and P. K. Sharma, "A Distinguishable Role of eDNA in the Viscoelastic Relaxation of Biofilms," *mBio*, vol. 4, no. 5, pp. e00497-13, 2013, doi: 10.1128/mBio.00497-13.

[61] K. Kovach *et al.*, "Evolutionary adaptations of biofilms infecting cystic fibrosis lungs promote mechanical toughness by adjusting polysaccharide production," *npj Biofilms and Microbiomes*, vol. 3, no. 1, p. 1, 2017/01/23 2017, doi: 10.1038/s41522-016-0007-9.

[62] J. Yan *et al.*, "Bacterial Biofilm Material Properties Enable Removal and Transfer by Capillary Peeling," *Advanced Materials*, vol. 30, no. 46, p. 1804153, 2018/11/01 2018, doi: 10.1002/adma.201804153.

[63] S. G. V. Charlton *et al.*, "Regulating, Measuring, and Modeling the Viscoelasticity of Bacterial Biofilms," *Journal of Bacteriology*, vol. 201, no. 18, pp. e00101-19, 2019, doi: 10.1128/JB.00101-19.

[64] D. Renggli, A. Alicke, R. H. Ewoldt, and J. Vermant, "Operating windows for oscillatory interfacial shear rheology," *Journal of Rheology*, vol. 64, no. 1, pp. 141-160, 2020/01/01 2019, doi: 10.1122/1.5130620.

[65] S. Vandebril, A. Franck, G. G. Fuller, P. Moldenaers, and J. Vermant, "A double wall-ring geometry for interfacial shear rheometry," *Rheologica Acta*, vol. 49, no. 2, pp. 131-144, 2010/02/01 2010, doi: 10.1007/s00397-009-0407-3.

[66] P. Erni, P. Fischer, E. J. Windhab, V. Kusnezov, H. Stettin, and J. Läuger, "Stress- and strain-controlled measurements of interfacial shear viscosity and viscoelasticity at liquid/liquid and gas/liquid interfaces," *Review of Scientific Instruments*, vol. 74, no. 11, pp. 4916-4924, 2003/11/01 2003, doi: 10.1063/1.1614433.

[67] Emily C. Hollenbeck, Jiunn C. N. Fong, Ji Y. Lim, Fitnat H. Yildiz, Gerald G. Fuller, and L. Cegelski, "Molecular determinants of mechanical properties of *V. cholerae* biofilms

at the air-liquid interface," *Biophysical Journal,* vol. 107, no. 10, pp. 2245-2252, 2014/11 2014, doi: 10.1016/j.bpj.2014.10.015.

[68] L. Qi and G. F. Christopher, "Role of Flagella, Type IV Pili, Biosurfactants, and Extracellular Polymeric Substance Polysaccharides on the Formation of Pellicles by *Pseudomonas aeruginosa*," *Langmuir,* vol. 35, no. 15, pp. 5294-5304, 2019/04/16 2019, doi: 10.1021/acs.langmuir.9b00271.

[69] P. A. Rühs, L. Böni, G. G. Fuller, R. F. Inglis, and P. Fischer, "In-situ quantification of the interfacial rheological response of bacterial biofilms to environmental stimuli," *PLoS ONE,* vol. 8, no. 11, p. e78524, 2013/11/11 2013, doi: 10.1371/journal.pone.0078524.

[70] O. Galy, P. Latour-Lambert, K. Zrelli, J.-M. Ghigo, C. Beloin, and N. Henry, "Mapping of Bacterial Biofilm Local Mechanics by Magnetic Microparticle Actuation," *Biophysical Journal,* vol. 103, no. 6, pp. 1400-1408, 2012/09/19/ 2012, doi: https://doi.org/10.1016/j.bpj.2012.07.001.

[71] S. S. Rogers, C. van der Walle, and T. A. Waigh, "Microrheology of Bacterial Biofilms In Vitro: *Staphylococcus aureus* and *Pseudomonas aeruginosa*," *Langmuir,* vol. 24, no. 23, pp. 13549-13555, 2008/12/02 2008, doi: 10.1021/la802442d.

[72] B. W. Towler, C. J. Rupp, A. B. Cunningham, and P. Stoodley, "Viscoelastic Properties of a Mixed Culture Biofilm from Rheometer Creep Analysis," *Biofouling,* vol. 19, no. 5, pp. 279-285, 2003/10/01 2003, doi: 10.1080/0892701031000152470.

[73] L. Pavlovsky, J. G. Younger, and M. J. Solomon, "In situ rheology of *Staphylococcus epidermidis* bacterial biofilms," *Soft Matter,* 10.1039/C2SM27005F vol. 9, no. 1, pp. 122-131, 2013, doi: 10.1039/C2SM27005F.

[74] O. Lieleg, M. Caldara, R. Baumgärtel, and K. Ribbeck, "Mechanical robustness of Pseudomonasaeruginosa biofilms," *Soft Matter,* 10.1039/C0SM01467B vol. 7, no. 7, pp. 3307-3314, 2011, doi: 10.1039/C0SM01467B.

[75] S. M. Yannarell, G. M. Grandchamp, S. Y. Chen, K. E. Daniels, and E. A. Shank, "A dual-species biofilm with emergent mechanical and protective properties," *Journal of Bacteriology,* vol. 201, no. 18, pp. e00670-18, 2019, doi: 10.1128/JB.00670-18.

[76] P. Stoodley, R. Cargo, C. J. Rupp, S. Wilson, and I. Klapper, "Biofilm material properties as related to shear-induced deformation and detachment phenomena," *Journal of Industrial Microbiology and Biotechnology,* vol. 29, no. 6, pp. 361-367, 2002/12/01 2002, doi: 10.1038/sj.jim.7000282.

[77] N. Kandemir, W. Vollmer, N. S. Jakubovics, and J. Chen, "Mechanical interactions between bacteria and hydrogels," *Scientific Reports,* vol. 8, no. 1, p. 10893, 2018/07/18 2018, doi: 10.1038/s41598-018-29269-x.

[78] R. T. Rozenbaum, H. C. van der Mei, W. Woudstra, E. D. de Jong, H. J. Busscher, and P. K. Sharma, "Role of Viscoelasticity in Bacterial Killing by Antimicrobials in Differently Grown *Pseudomonas aeruginosa* Biofilms," *Antimicrobial Agents and Chemotherapy,* vol. 63, no. 4, pp. e01972-18, 2019, doi: 10.1128/AAC.01972-18.

[79] A. Allen, O. Habimana, and E. Casey, "The effects of extrinsic factors on the structural and mechanical properties of *Pseudomonas fluorescens* biofilms: A combined study of nutrient concentrations and shear conditions," *Colloids and Surfaces B: Biointerfaces,* vol. 165, pp. 127-134, 2018/05/01/ 2018, doi: https://doi.org/10.1016/j.colsurfb.2018.02.035.

[80] S. Yu, Q. Wei, T. Zhao, Y. Guo, and L. Z. Ma, "A Survival Strategy for *Pseudomonas aeruginosa* That Uses Exopolysaccharides To Sequester and Store Iron To Stimulate Psl-Dependent Biofilm Formation," *Appl Environ Microbiol,* vol. 82, no. 21, pp. 6403-6413, Nov 1 2016, doi: 10.1128/AEM.01307-16.

[81] W. L. Jones, M. P. Sutton, L. McKittrick, and P. S. Stewart, "Chemical and antimicrobial treatments change the viscoelastic properties of bacterial biofilms," *Biofouling,* vol. 27, no. 2, pp. 207-215, 2011/01/27 2011, doi: 10.1080/08927014.2011.554977.

[82] N. Rodgers and A. Murdaugh, "Chlorhexidine-induced elastic and adhesive changes of *Escherichia coli* cells within a biofilm," *Biointerphases,* vol. 11, no. 3, p. 031011, 2016/09/01 2016, doi: 10.1116/1.4962265.

[83] J. O'Neill, "Review on Antimicrobial Resistance Antimicrobial Resistance: Tackling a crisis for the health and wealth of nations," 2014. [Online]. Available: https://amr-review.org/sites/default/files/AMR%20Review%20Paper%20-%20Tackling%20a%20crisis%20for%20the%20health%20and%20wealth%20of%20nations_1.pdf

[84] M. N. Alekshun and S. B. Levy, "Molecular Mechanisms of Antibacterial Multidrug Resistance," *Cell,* vol. 128, no. 6, pp. 1037-1050, 2007/03/23/ 2007, doi: https://doi.org/10.1016/j.cell.2007.03.004.

[85] P. Fernandes and E. Martens, "Antibiotics in late clinical development," *Biochem Pharmacol,* vol. 133, pp. 152-163, Jun 1 2017, doi: 10.1016/j.bcp.2016.09.025.

[86] N. Niño-Martínez, M. F. Salas Orozco, G.-A. Martínez-Castañón, F. Torres Méndez, and F. Ruiz, "Molecular Mechanisms of Bacterial Resistance to Metal and Metal Oxide Nanoparticles," *International Journal of Molecular Sciences,* vol. 20, no. 11, 2019, doi: 10.3390/ijms20112808.

[87] G. Navale, M. Thripuranthaka, D. Late, and S. Shinde, "Antimicrobial Activity of ZnO Nanoparticles against Pathogenic Bacteria and Fungi.," *JSM Nanotechnology & Nanomedicine* vol. 3, no. 1, p. 1033, 2015.

[88] H. Rokbani, F. Daigle, and A. Ajji, "Combined Effect of Ultrasound Stimulations and Autoclaving on the Enhancement of Antibacterial Activity of ZnO and SiO2/ZnO Nanoparticles," *Nanomaterials,* vol. 8, no. 3, 2018, doi: 10.3390/nano8030129.

[89] Y. Zhang, T. P. Shareena Dasari, H. Deng, and H. Yu, "Antimicrobial Activity of Gold Nanoparticles and Ionic Gold," *J Environ Sci Health C Environ Carcinog Ecotoxicol Rev,* vol. 33, no. 3, pp. 286-327, 2015, doi: 10.1080/10590501.2015.1055161.

[90] S. Shaikh *et al.*, "Mechanistic Insights into the Antimicrobial Actions of Metallic Nanoparticles and Their Implications for Multidrug Resistance," (in eng), *International journal of molecular sciences,* vol. 20, no. 10, p. 2468, 2019, doi: 10.3390/ijms20102468.

[91] M. Chamundeeswari *et al.*, "Preparation, characterization and evaluation of a biopolymeric gold nanocomposite with antimicrobial activity," *Biotechnol Appl Biochem,* vol. 55, no. 1, pp. 29-35, Jan 25 2010, doi: 10.1042/BA20090198.

[92] H. J. Johnston, G. Hutchison, F. M. Christensen, S. Peters, S. Hankin, and V. Stone, "A review of the in vivo and in vitro toxicity of silver and gold particulates: particle attributes and biological mechanisms responsible for the observed toxicity," *Crit Rev Toxicol,* vol. 40, no. 4, pp. 328-46, Apr 2010, doi: 10.3109/10408440903453074.

[93] E. Sánchez-López *et al.*, "Metal-Based Nanoparticles as Antimicrobial Agents: An Overview," *Nanomaterials (Basel),* vol. 10, no. 2, p. 292, 2020, doi: 10.3390/nano10020292.

[94] M. Li, L. Zhu, and D. Lin, "Toxicity of ZnO nanoparticles to *Escherichia coli*: mechanism and the influence of medium components," *Environ Sci Technol,* vol. 45, no. 5, pp. 1977-83, Mar 1 2011, doi: 10.1021/es102624t.

[95] A. Lipovsky, Y. Nitzan, A. Gedanken, and R. Lubart, "Antifungal activity of ZnO nanoparticles--the role of ROS mediated cell injury," *Nanotechnology,* vol. 22, no. 10, p. 105101, Mar 11 2011, doi: 10.1088/0957-4484/22/10/105101.

[96] X. Jiang, L. Yang, P. Liu, X. Li, and J. Shen, "The photocatalytic and antibacterial activities of neodymium and iodine doped TiO(2) nanoparticles," *Colloids Surf B Biointerfaces,* vol. 79, no. 1, pp. 69-74, Aug 1 2010, doi: 10.1016/j.colsurfb.2010.03.031.

[97] P. Liu, W. Duan, Q. Wang, and X. Li, "The damage of outer membrane of *Escherichia coli* in the presence of TiO2 combined with UV light," *Colloids Surf B Biointerfaces,* vol. 78, no. 2, pp. 171-6, Jul 1 2010, doi: 10.1016/j.colsurfb.2010.02.024.

[98] P. Wu, R. Xie, K. Imlay, and J. K. Shang, "Visible-light-induced bactericidal activity of titanium dioxide codoped with nitrogen and silver," *Environ Sci Technol,* vol. 44, no. 18, pp. 6992-7, Sep 15 2010, doi: 10.1021/es101343c.

[99] X. Chen and H. J. Schluesener, "Nanosilver: a nanoproduct in medical application," (in eng), no. 0378-4274 (Print).

[100] J. Polte *et al.*, "Formation Mechanism of Colloidal Silver Nanoparticles: Analogies and Differences to the Growth of Gold Nanoparticles," *ACS Nano,* vol. 6, no. 7, pp. 5791-5802, 2012/07/24 2012, doi: 10.1021/nn301724z.

[101] S. Iravani, H. Korbekandi, S. V. Mirmohammadi, and B. Zolfaghari, "Synthesis of silver nanoparticles: chemical, physical and biological methods," (in eng), *Res Pharm Sci,* vol. 9, no. 6, pp. 385-406, Nov-Dec 2014. [Online]. Available: https://pubmed.ncbi.nlm.nih.gov/26339255

https://www.ncbi.nlm.nih.gov/pmc/articles/PMC4326978/.

[102] T. C. Dakal, A. Kumar, R. S. Majumdar, and V. Yadav, "Mechanistic Basis of Antimicrobial Actions of Silver Nanoparticles," (in eng), no. 1664-302X (Print).

[103] M. Venkatesham, D. Ayodhya, A. Madhusudhan, N. Veera Babu, and G. Veerabhadram, "A novel green one-step synthesis of silver nanoparticles using chitosan: catalytic activity

and antimicrobial studies," *Applied Nanoscience,* vol. 4, no. 1, pp. 113-119, 2014/01/01 2014, doi: 10.1007/s13204-012-0180-y.

[104] N. Vigneshwaran, R. P. Nachane, R. H. Balasubramanya, and P. V. Varadarajan, "A novel one-pot 'green' synthesis of stable silver nanoparticles using soluble starch," *Carbohydrate Research,* vol. 341, no. 12, pp. 2012-2018, 2006/09/04/ 2006, doi: https://doi.org/10.1016/j.carres.2006.04.042.

[105] J. Yang and J. Pan, "Hydrothermal synthesis of silver nanoparticles by sodium alginate and their applications in surface-enhanced Raman scattering and catalysis," *Acta Materialia,* vol. 60, no. 12, pp. 4753-4758, 2012/07/01/ 2012, doi: https://doi.org/10.1016/j.actamat.2012.05.037.

[106] S. V. Kumar, A. A.-O. Bafana, P. Pawar, A. Rahman, S. A. Dahoumane, and C. A.-O. Jeffryes, "High conversion synthesis of <10 nm starch-stabilized silver nanoparticles using microwave technology," (in eng), no. 2045-2322 (Electronic).

[107] S. Agnihotri, S. Mukherji, and S. Mukherji, "Size-controlled silver nanoparticles synthesized over the range 5–100 nm using the same protocol and their antibacterial efficacy," *RSC Advances,* 10.1039/C3RA44507K vol. 4, no. 8, pp. 3974-3983, 2014, doi: 10.1039/C3RA44507K.

[108] S. Pal, Y. K. Tak, and J. M. Song, "Does the Antibacterial Activity of Silver Nanoparticles Depend on the Shape of the Nanoparticle? A Study of the Gram-Negative Bacterium *Escherichia coli*," *Applied and Environmental Microbiology,* vol. 73, no. 6, p. 1712, 2007, doi: 10.1128/AEM.02218-06.

[109] A. Abbaszadegan *et al.*, "The Effect of Charge at the Surface of Silver Nanoparticles on Antimicrobial Activity against Gram-Positive and Gram-Negative Bacteria: A Preliminary Study," *Journal of Nanomaterials,* vol. 2015, p. 720654, 2015/02/15 2015, doi: 10.1155/2015/720654.

[110] S. Fulaz, S. Vitale, L. Quinn, and E. Casey, "Nanoparticle–Biofilm Interactions: The Role of the EPS Matrix," *Trends in Microbiology,* vol. 27, no. 11, pp. 915-926, 2019/11/01/ 2019, doi: https://doi.org/10.1016/j.tim.2019.07.004.

[111] A. S. Joshi, P. Singh, and I. Mijakovic, "Interactions of Gold and Silver Nanoparticles with Bacterial Biofilms: Molecular Interactions behind Inhibition and Resistance," (in eng), *International journal of molecular sciences,* vol. 21, no. 20, p. 7658, 2020, doi: 10.3390/ijms21207658.

[112] A. M. El Badawy, R. G. Silva, B. Morris, K. G. Scheckel, M. T. Suidan, and T. M. Tolaymat, "Surface charge-dependent toxicity of silver nanoparticles," *Environ Sci Technol,* vol. 45, no. 1, pp. 283-7, Jan 1 2011, doi: 10.1021/es1034188.

[113] M. R. Mitzel and N. Tufenkji, "Transport of Industrial PVP-Stabilized Silver Nanoparticles in Saturated Quartz Sand Coated with *Pseudomonas aeruginosa* PAO1 Biofilm of Variable Age," *Environmental Science & Technology,* vol. 48, no. 5, pp. 2715-2723, 2014/03/04 2014, doi: 10.1021/es404598v.

[114] H.-C. Flemming, J. Wingender, U. Szewzyk, P. Steinberg, S. A. Rice, and S. Kjelleberg, "Biofilms: an emergent form of bacterial life," *Nature Reviews Microbiology*, vol. 14, no. 9, pp. 563-575, 2016/08/11 2016, doi: 10.1038/nrmicro.2016.94.

[115] N. Høiby, "Recent advances in the treatment of *Pseudomonas aeruginosa* infections in cystic fibrosis," *BMC Medicine*, vol. 9, no. 1, p. 32, 2011/04/04 2011, doi: 10.1186/1741-7015-9-32.

[116] N. Høiby, T. Bjarnsholt, M. Givskov, S. Molin, and O. Ciofu, "Antibiotic resistance of bacterial biofilms," *International Journal of Antimicrobial Agents*, vol. 35, no. 4, pp. 322-332, 2010/04/01/ 2010, doi: https://doi.org/10.1016/j.ijantimicag.2009.12.011.

[117] H. Wu, C. Moser, H.-Z. Wang, N. Høiby, and Z.-J. Song, "Strategies for combating bacterial biofilm infections," *International Journal of Oral Science*, vol. 7, no. 1, pp. 1-7, 2015/03/01 2015, doi: 10.1038/ijos.2014.65.

[118] M. D. Rodney, "Biofilms and Device-Associated Infections," *Emerging Infectious Disease journal*, vol. 7, no. 2, p. 277, 2001, doi: 10.3201/eid0702.700277.

[119] L. Percival Steven, E. Hill Katja, W. Williams David, J. Hooper Samuel, W. Thomas Dave, and W. Costerton John, "A review of the scientific evidence for biofilms in wounds," *Wound Repair and Regeneration*, vol. 20, no. 5, pp. 647-657, 2012/09/01 2012, doi: 10.1111/j.1524-475X.2012.00836.x.

[120] N. Høiby, O. Ciofu, and T. Bjarnsholt, "*Pseudomonas aeruginosa* biofilms in cystic fibrosis," *Future Microbiology*, vol. 5, no. 11, pp. 1663-1674, 2010/11/01 2010, doi: 10.2217/fmb.10.125.

[121] V. Lazarova, J. Perera, M. Bowen, and P. Sheilds, "Application of aerated biofilters for production of high quality water for industrial reuse in West Basin," *Water Science and Technology*, vol. 41, no. 4-5, p. 417, 2000. [Online]. Available: http://wst.iwaponline.com/content/41/4-5/417.abstract.

[122] P. S. Majumder and S. K. Gupta, "Hybrid reactor for priority pollutant nitrobenzene removal," *Water Research*, vol. 37, no. 18, pp. 4331-4336, 2003/11/01/ 2003, doi: https://doi.org/10.1016/S0043-1354(03)00436-6.

[123] K. G. Ho, A. I. Pometto, P. N. Hinz, and A. Demirci, "Nutrient leaching and end product accumulation in plastic composite supports for L-(+)-lactic Acid biofilm fermentation," *Applied and Environmental Microbiology*, vol. 63, no. 7, pp. 2524-2532, 1997. [Online]. Available: http://aem.asm.org/content/63/7/2524.abstract.

[124] A. Demirci, A. L. Pometto Iii, and K. L. G. Ho, "Ethanol production by *Saccharomyces cerevisiae* in biofilm reactors," *Journal of Industrial Microbiology and Biotechnology*, vol. 19, no. 4, pp. 299-304, 1997/10/01 1997, doi: 10.1038/sj.jim.2900464.

[125] S. S. Branda, J. E. González-Pastor, S. Ben-Yehuda, R. Losick, and R. Kolter, "Fruiting body formation by *Bacillus subtilis*," *Proceedings of the National Academy of Sciences*, 10.1073/pnas.191384198 vol. 98, no. 20, p. 11621, 2001. [Online]. Available: http://www.pnas.org/content/98/20/11621.abstract.

[126] H. Vlamakis, Y. Chai, P. Beauregard, R. Losick, and R. Kolter, "Sticking together: building a biofilm the *Bacillus subtilis* way," *Nature Reviews Microbiology*, Review Article vol. 11, p. 157, 01/28/online 2013, doi: 10.1038/nrmicro2960

https://www.nature.com/articles/nrmicro2960#supplementary-information.

[127] S. S. Branda, Å. Vik, L. Friedman, and R. Kolter, "Biofilms: the matrix revisited," *Trends in Microbiology*, vol. 13, no. 1, pp. 20-26, 2005/01/01/ 2005, doi: https://doi.org/10.1016/j.tim.2004.11.006.

[128] M. Marvasi, P. T. Visscher, and L. Casillas Martinez, "Exopolymeric substances (EPS) from *Bacillus subtilis* : polymers and genes encoding their synthesis," *FEMS Microbiology Letters*, vol. 313, no. 1, pp. 1-9, 2010, doi: 10.1111/j.1574-6968.2010.02085.x.

[129] S. M. Cutting, "*Bacillus* probiotics," *Food Microbiology*, vol. 28, no. 2, pp. 214-220, 2011/04 2011, doi: 10.1016/j.fm.2010.03.007.

[130] R. Pasvolsky, V. Zakin, I. Ostrova, and M. Shemesh, "Butyric acid released during milk lipolysis triggers biofilm formation of *Bacillus* species," *International Journal of Food Microbiology*, vol. 181, pp. 19-27, 2014/07 2014, doi: 10.1016/j.ijfoodmicro.2014.04.013.

[131] D. Kalogridou-Vassiliadou, "Biochemical activities of *Bacillus* species isolated from flat sour evaporated milk," (in eng), no. 0022-0302 (Print).

[132] I. Randrianjatovo-Gbalou, P. Rouquette, D. Lefebvre, E. Girbal-Neuhauser, and C. E. Marcato-Romain, "In situ analysis of *Bacillus licheniformis* biofilms: amyloid-like polymers and eDNA are involved in the adherence and aggregation of the extracellular matrix," *Journal of Applied Microbiology*, vol. 122, no. 5, pp. 1262-1274, 2017/04/11 2017, doi: 10.1111/jam.13423.

[133] M. M. Baum *et al.*, "Characterization of structures in biofilms formed by a *Pseudomonas fluorescens* isolated from soil," *BMC Microbiology*, vol. 9, no. 1, p. 103, 2009, doi: 10.1186/1471-2180-9-103.

[134] C. Rossi, C. Chaves-López, A. Serio, E. Goffredo, B. T. C. Goga, and A. Paparella, "Influence of Incubation Conditions on Biofilm Formation by *Pseudomonas Fluorescens* Isolated from Dairy Products and Dairy Manufacturing Plants," *Italian journal of food safety*, vol. 5, no. 3, pp. 5793-5793, 2016, doi: 10.4081/ijfs.2016.5793.

[135] K. W. K. Lee, S. Periasamy, M. Mukherjee, C. Xie, S. Kjelleberg, and S. A. Rice, "Biofilm development and enhanced stress resistance of a model, mixed-species community biofilm," *The Isme Journal*, Original Article vol. 8, p. 894, 10/24/online 2013, doi: 10.1038/ismej.2013.194

https://www.nature.com/articles/ismej2013194#supplementary-information.

[136] M. Burmølle, J. S. Webb, D. Rao, L. H. Hansen, S. J. Sørensen, and S. Kjelleberg, "Enhanced Biofilm Formation and Increased Resistance to Antimicrobial Agents and Bacterial Invasion Are Caused by Synergistic Interactions in Multispecies Biofilms," *Applied and Environmental Microbiology*, 10.1128/AEM.03022-05 vol. 72, no. 6, pp. 3916-3923, 2006. [Online]. Available: http://aem.asm.org/content/72/6/3916.abstractN2.

[137] A. Ternström, A. M. Lindberg, and G. Molin, "Classification of the spoilage flora of raw and pasteurized bovine milk, with special reference to *Pseudomonas* and *Bacillus*," *Journal of Applied Bacteriology,* vol. 75, no. 1, pp. 25-34, 1993/07/01 1993, doi: 10.1111/j.1365-2672.1993.tb03403.x.

[138] J. C. Ribeiro Júnior, A. M. de Oliveira, F. d. G. Silva, R. Tamanini, A. L. M. de Oliveira, and V. Beloti, "The main spoilage-related psychrotrophic bacteria in refrigerated raw milk," *Journal of Dairy Science,* vol. 101, no. 1, pp. 75-83, 2018, doi: 10.3168/jds.2017-13069.

[139] J. D. G. McPhee, M.W. , "Pseudomonas spp.," in *Encyclopedia of Dairy Sciences* vol. 4, H. Roginski, Fuquay W.J., Fox, F.P., Ed., ed: Academic Press, 2002, pp. 2340-2350.

[140] V. Domingue Gauthier, "Inhibition du pathogène des salmonidés *Saprolegnia parasitica* par des bactéries aquatiques," Maître ès sciences (M.Sc) Electronic Thesis or Dissertation, Département de microbiologie et immunologie, Université de Montréal, 2013. [Online]. Available: http://hdl.handle.net/1866/10042

[141] W. Ma *et al.*, "*Bacillus subtilis* biofilm development in the presence of soil clay minerals and iron oxides," *npj Biofilms and Microbiomes,* vol. 3, no. 1, p. 4, 2017/02/09 2017, doi: 10.1038/s41522-017-0013-6.

[142] S. Branda Steven, F. Chu, B. Kearns Daniel, R. Losick, and R. Kolter, "A major protein component of the *Bacillus subtilis* biofilm matrix," *Molecular Microbiology,* vol. 59, no. 4, pp. 1229-1238, 2006/02/01 2005, doi: 10.1111/j.1365-2958.2005.05020.x.

[143] G. T. Kim, G. Webster, J. W. T. Wimpenny, B. H. Kim, H. J. Kim, and A. J. Weightman, "Bacterial community structure, compartmentalization and activity in a microbial fuel cell," *Journal of Applied Microbiology,* vol. 101, no. 3, pp. 698-710, 2006/09/01 2006, doi: 10.1111/j.1365-2672.2006.02923.x.

[144] S.-M. Nguyen-Mau, S.-Y. Oh, V. J. Kern, D. M. Missiakas, and O. Schneewind, "Secretion Genes as Determinants of *Bacillus anthracis* Chain Length," *Journal of Bacteriology,* 10.1128/JB.00384-12 vol. 194, no. 15, pp. 3841-3850, 2012. [Online]. Available: http://jb.asm.org/content/194/15/3841.abstractN2.

[145] T. Hölscher *et al.*, "Motility, Chemotaxis and Aerotaxis Contribute to Competitiveness during Bacterial Pellicle Biofilm Development," (in eng), *J Mol Biol,* vol. 427, no. 23, pp. 3695-3708, 2015/11// 2015, doi: 10.1016/j.jmb.2015.06.014.

[146] Y. M. Bar-On and R. Milo, "Towards a quantitative view of the global ubiquity of biofilms," *Nature Reviews Microbiology,* vol. 17, no. 4, pp. 199-200, 2019/04/01 2019, doi: 10.1038/s41579-019-0162-0.

[147] J. B. Kaper, J. G. Morris, and M. M. Levine, "Cholera," *Clinical Microbiology Reviews,* vol. 8, no. 1, pp. 48-86, 1995, doi: 10.1128/CMR.8.1.48.

[148] A. J. Silva and J. A. Benitez, "*Vibrio cholerae* biofilms and cholera pathogenesis," *PLOS Neglected Tropical Diseases,* vol. 10, no. 2, p. e0004330, 2016, doi: 10.1371/journal.pntd.0004330.

[149] K. L. Cottingham, D. A. Chiavelli, and R. K. Taylor, "Environmental microbe and human pathogen: the ecology and microbiology of *Vibrio cholerae*," *Frontiers in Ecology and the*

Environment, vol. 1, no. 2, pp. 80-86, 2003/03/01 2003, doi: 10.1890/1540-9295(2003)001[0080:EMAHPT]2.0.CO;2.

[150] M. Alam *et al.*, "Viable but nonculturable *Vibrio cholerae* O1 in biofilms in the aquatic environment and their role in cholera transmission," *Proceedings of the National Academy of Sciences,* vol. 104, no. 45, p. 17801, 2007, doi: 10.1073/pnas.0705599104.

[151] A. Huq *et al.*, "Detection of *Vibrio cholerae* O1 in the aquatic environment by fluorescent-monoclonal antibody and culture methods," *Applied and Environmental Microbiology,* vol. 56, no. 8, pp. 2370-2373, 1990. [Online]. Available: http://aem.asm.org/content/56/8/2370.abstract.

[152] A. Fasano *et al.*, "*Vibrio cholerae* produces a second enterotoxin, which affects intestinal tight junctions," *Proceedings of the National Academy of Sciences,* vol. 88, no. 12, pp. 5242-5246, 1991, doi: 10.1073/pnas.88.12.5242.

[153] K. Kierek and P. I. Watnick, "Environmental determinants of *Vibrio cholerae* biofilm development," *Applied and Environmental Microbiology,* vol. 69, no. 9, pp. 5079-5088, 2003, doi: 10.1128/AEM.69.9.5079-5088.2003.

[154] A. D. Tischler and A. Camilli, "Cyclic diguanylate (c-di-GMP) regulates *Vibrio cholerae* biofilm formation," *Molecular Microbiology,* vol. 53, no. 3, pp. 857-869, 2004/08/01 2004, doi: 10.1111/j.1365-2958.2004.04155.x.

[155] J. Fong, K. Syed, K. Klose, and F. Yildiz, "Role of *Vibrio* polysaccharide (vps) genes in VPS production, biofilm formation and *Vibrio cholerae* pathogenesis," (in eng), vol. 156, no. 9, pp. 2757-69, doi: 10.1099/mic.0.040196-0.

[156] D. L. MacIntyre, S. T. Miyata, M. Kitaoka, and S. Pukatzki, "The *Vibrio cholerae* type VI secretion system displays antimicrobial properties," *Proceedings of the National Academy of Sciences,* vol. 107, no. 45, p. 19520, 2010, doi: 10.1073/pnas.1012931107.

[157] O. Besharova, V. M. Suchanek, R. Hartmann, K. Drescher, and V. Sourjik, "Diversification of gene expression during formation of static submerged biofilms by *Escherichia coli*," (in eng), *Frontiers in microbiology,* vol. 7, no. 1568, 2016, doi: 10.3389/fmicb.2016.01568.

[158] W. Thongsomboon, D. O. Serra, A. Possling, C. Hadjineophytou, R. Hengge, and L. Cegelski, "Phosphoethanolamine cellulose: A naturally produced chemically modified cellulose," *Science,* vol. 359, no. 6373, pp. 334-338, 2018, doi: 10.1126/science.aao4096.

[159] C. Wu, J. Lim, G. Fuller, and L. Cegelski, "Disruption of *Escherichia coli* amyloid-integrated biofilm formation at the air-liquid interface by a polysorbate surfactant," (in eng), no. 29, pp. 920-926, doi: 10.1021/la304710k.

[160] C. Abriat, N. Virgilio, M.-C. Heuzey, and F. Daigle, "Microbiological and real-time mechanical analysis of *Bacillus licheniformis* and *Pseudomonas fluorescens* dual-species biofilm," *Microbiology,* vol. 165, no. 7, pp. 747-756, 2019, doi: doi:10.1099/mic.0.000819.

[161] M. R. Kamal and V. Khoshkava, "Effect of cellulose nanocrystals (CNC) on rheological and mechanical properties and crystallization behavior of PLA/CNC nanocomposites," *Carbohydrate Polymers,* vol. 123, pp. 105-114, 2015/06/05/ 2015, doi: https://doi.org/10.1016/j.carbpol.2015.01.012.

[162] D. Khaidapova, E. Milanovskiy, and E. Shein, "Rheological properties of different minerals and clay soils," *Eurasian Journal of Soil Science,* vol. 4, no. 3, pp. 198-202, Jul 2015 2015, doi: 10.18393/ejss.2015.3.198-202.

[163] T. Ishikawa *et al.*, "Pathoadaptive conditional regulation of the type VI secretion system in *Vibrio cholerae* O1 strains," (in eng), *Infect Immun,* vol. 80, no. 2, pp. 575-584, 2012, doi: 10.1128/IAI.05510-11.

[164] S. Kojima, K. Yamamoto, I. Kawagishi, and M. Homma, "The polar flagellar motor of *Vibrio cholerae* is driven by an Na+ motive force," *Journal of Bacteriology,* vol. 181, no. 6, pp. 1927-1930, 1999. [Online]. Available: http://jb.asm.org/content/181/6/1927.abstract.

[165] A. S. Utada *et al.*, "*Vibrio cholerae* use pili and flagella synergistically to effect motility switching and conditional surface attachment," (in eng), *Nat Commun,* vol. 5, no. 4913, 2014, doi: 10.1038/ncomms5913.

[166] P. C. Bogino, M. d. l. M. Oliva, F. G. Sorroche, and W. Giordano, "The role of bacterial biofilms and surface components in plant-bacterial associations," (in eng), *International journal of molecular sciences,* vol. 14, no. 8, pp. 15838-15859, 2013, doi: 10.3390/ijms140815838.

[167] E. S. Lim, O. K. Koo, M.-J. Kim, and J.-S. Kim, "Bio-enzymes for inhibition and elimination of *Escherichia coli* O157:H7 biofilm and their synergistic effect with sodium hypochlorite," *Scientific Reports,* vol. 9, no. 1, p. 9920, 2019/07/09 2019, doi: 10.1038/s41598-019-46363-w.

[168] "RESEARCH ON MICROBIAL BIOFILMS: PA-03-047," *Journal of Investigative Medicine,* vol. 51, no. 3, pp. 162-163, 2003/05 2003, doi: 10.1097/00042871-200305000-00024.

[169] A. S. Lynch and G. T. Robertson, "Bacterial and Fungal Biofilm Infections," *Annual Review of Medicine,* vol. 59, no. 1, pp. 415-428, 2008/02/01 2008, doi: 10.1146/annurev.med.59.110106.132000.

[170] M. A. Fischbach and C. T. Walsh, "Antibiotics for Emerging Pathogens," *Science,* vol. 325, no. 5944, p. 1089, 2009, doi: 10.1126/science.1176667.

[171] J. R. Morones *et al.*, "The bactericidal effect of silver nanoparticles," *Nanotechnology,* vol. 16, no. 10, pp. 2346-2353, 2005/08/26 2005, doi: 10.1088/0957-4484/16/10/059.

[172] J. S. Kim *et al.*, "Antimicrobial effects of silver nanoparticles," *Nanomedicine: Nanotechnology, Biology and Medicine,* vol. 3, no. 1, pp. 95-101, 2007/03/01/ 2007, doi: https://doi.org/10.1016/j.nano.2006.12.001.

[173] M. K. Rai, S. D. Deshmukh, A. P. Ingle, and A. K. Gade, "Silver nanoparticles: the powerful nanoweapon against multidrug-resistant bacteria," *Journal of Applied Microbiology,* https://doi.org/10.1111/j.1365-2672.2012.05253.x vol. 112, no. 5, pp. 841-852, 2012/05/01 2012, doi: https://doi.org/10.1111/j.1365-2672.2012.05253.x.

[174] J. Wongpreecha, D. Polpanich, T. Suteewong, C. Kaewsaneha, and P. Tangboriboonrat, "One-pot, large-scale green synthesis of silver nanoparticles-chitosan with enhanced

antibacterial activity and low cytotoxicity," *Carbohydrate Polymers*, vol. 199, pp. 641-648, 2018/11/01/ 2018, doi: https://doi.org/10.1016/j.carbpol.2018.07.039.

[175] Y. Liu, S. Chen, L. Zhong, and G. Wu, "Preparation of high-stable silver nanoparticle dispersion by using sodium alginate as a stabilizer under gamma radiation," *Radiation Physics and Chemistry*, vol. 78, no. 4, pp. 251-255, 2009/04/01/ 2009, doi: https://doi.org/10.1016/j.radphyschem.2009.01.003.

[176] S. Saha, A. Pal, S. Kundu, S. Basu, and T. Pal, "Photochemical Green Synthesis of Calcium-Alginate-Stabilized Ag and Au Nanoparticles and Their Catalytic Application to 4-Nitrophenol Reduction," *Langmuir*, vol. 26, no. 4, pp. 2885-2893, 2010/02/16 2010, doi: 10.1021/la902950x.

[177] L. Biao *et al.*, "Synthesis, characterization and antibacterial study on the chitosan-functionalized Ag nanoparticles," *Materials Science and Engineering: C*, vol. 76, pp. 73-80, 2017/07/01/ 2017, doi: https://doi.org/10.1016/j.msec.2017.02.154.

[178] H. Huang, Q. Yuan, and X. Yang, "Preparation and characterization of metal–chitosan nanocomposites," *Colloids and Surfaces B: Biointerfaces*, vol. 39, no. 1, pp. 31-37, 2004/11/25/ 2004, doi: https://doi.org/10.1016/j.colsurfb.2004.08.014.

[179] G. López-Carballo, L. Higueras, R. Gavara, and P. Hernández-Muñoz, "Silver Ions Release from Antibacterial Chitosan Films Containing in Situ Generated Silver Nanoparticles," *Journal of Agricultural and Food Chemistry*, vol. 61, no. 1, pp. 260-267, 2013/01/09 2013, doi: 10.1021/jf304006y.

[180] O. Choi, C.-P. Yu, G. Esteban Fernández, and Z. Hu, "Interactions of nanosilver with *Escherichia coli* cells in planktonic and biofilm cultures," *Water Research*, vol. 44, no. 20, pp. 6095-6103, 2010/12/01/ 2010, doi: https://doi.org/10.1016/j.watres.2010.06.069.

[181] S. M. Faruque *et al.*, "Transmissibility of cholera: In vivo-formed biofilms and their relationship to infectivity and persistence in the environment," *Proceedings of the National Academy of Sciences*, vol. 103, no. 16, p. 6350, 2006, doi: 10.1073/pnas.0601277103.

[182] A. Meza-Villezcas, A. L. Gallego-Hernández, F. H. Yildiz, O. E. Jaime-Acuña, O. Raymond-Herrera, and A. Huerta-Saquero, "Effect of antimicrobial nanocomposites on *Vibrio cholerae* lifestyles: Pellicle biofilm, planktonic and surface-attached biofilm," *PLOS ONE*, vol. 14, no. 6, p. e0217869, 2019, doi: 10.1371/journal.pone.0217869.

[183] I. Wiegand, K. Hilpert, and R. E. W. Hancock, "Agar and broth dilution methods to determine the minimal inhibitory concentration (MIC) of antimicrobial substances," *Nature Protocols*, vol. 3, no. 2, pp. 163-175, 2008/02/01 2008, doi: 10.1038/nprot.2007.521.

[184] C. Noguez, "Optical properties of isolated and supported metal nanoparticles," *Optical Materials*, vol. 27, no. 7, pp. 1204-1211, 2005/04/01/ 2005, doi: https://doi.org/10.1016/j.optmat.2004.11.012.

[185] N. Ardila, F. Daigle, M.-C. Heuzey, and A. Ajji, "Effect of Chitosan Physical Form on Its Antibacterial Activity Against Pathogenic Bacteria," *Journal of Food Science*, https://doi.org/10.1111/1750-3841.13635 vol. 82, no. 3, pp. 679-686, 2017/03/01 2017, doi: https://doi.org/10.1111/1750-3841.13635.

[186] M. Rinaudc, G. Pavlov, and J. Desbrières, "Solubilization of Chitosan in Strong Acid Medium," *International Journal of Polymer Analysis and Characterization*, vol. 5, no. 3, pp. 267-276, 1999/06/01 1999, doi: 10.1080/10236669908009742.

[187] Y. K. Mohanta, K. Biswas, S. K. Jena, A. Hashem, E. F. Abd_Allah, and T. K. Mohanta, "Anti-biofilm and Antibacterial Activities of Silver Nanoparticles Synthesized by the Reducing Activity of Phytoconstituents Present in the Indian Medicinal Plants," *Frontiers in Microbiology*, 10.3389/fmicb.2020.01143 vol. 11, p. 1143, 2020. [Online]. Available: https://www.frontiersin.org/article/10.3389/fmicb.2020.01143.

[188] F. Martinez-Gutierrez *et al.*, "Anti-biofilm activity of silver nanoparticles against different microorganisms," *Biofouling*, vol. 29, no. 6, pp. 651-660, 2013/07/01 2013, doi: 10.1080/08927014.2013.794225.

[189] K. Ikuma, A. W. Decho, and B. L. T. Lau, "When nanoparticles meet biofilms-interactions guiding the environmental fate and accumulation of nanoparticles," (in eng), *Frontiers in microbiology*, vol. 6, pp. 591-591, 2015, doi: 10.3389/fmicb.2015.00591.

[190] M. Duperthuy, A. E. Sjöström, D. Sabharwal, F. Damghani, B. E. Uhlin, and S. N. Wai, "Role of the *Vibrio cholerae* matrix protein Bap1 in cross-resistance to antimicrobial peptides," (in eng), *PLoS pathogens*, vol. 9, no. 10, pp. e1003620-e1003620, 2013, doi: 10.1371/journal.ppat.1003620.

[191] K. M. Giglio, J. C. Fong, F. H. Yildiz, and H. Sondermann, "Structural Basis for Biofilm Formation via the *Vibrio cholerae* Matrix Protein RbmA," *Journal of Bacteriology*, vol. 195, no. 14, p. 3277, 2013, doi: 10.1128/JB.00374-13.

[192] F. H. Yildiz, N. A. Dolganov, and G. K. Schoolnik, "VpsR, a Member of the Response Regulators of the Two-Component Regulatory Systems, Is Required for Expression of vps Biosynthesis Genes and EPS(ETr)-Associated Phenotypes in *Vibrio cholerae* O1 El Tor," *J Bacteriol*, vol. 183, no. 5, pp. 1716-26, Mar 2001, doi: 10.1128/JB.183.5.1716-1726.2001.

[193] A. Allué-Guardia, M. Echazarreta, S. S. K. Koenig, K. E. Klose, and M. Eppinger, "Closed Genome Sequence of *Vibrio cholerae* O1 El Tor Inaba Strain A1552," *Genome Announcements*, vol. 6, no. 9, pp. e00098-18, 2018, doi: 10.1128/genomeA.00098-18.